Reaction synthesis, hybrid & intensified techniques assisted efficient process synthesis

by

Shuang Xu

A dissertation submitted to the Graduate Faculty of
Auburn University
in partial fulfillment of the
requirements for the Degree of
Doctor of Philosophy

Auburn, Alabama
December 12, 2023

Keywords: Reaction pathways, innovative separation, process synthesis, optimization

Copyright 2023 by Shuang Xu

Approved by

Mario R. Eden, Chair, Joe T. and Billie Carole McMillan Professor of Chemical Engineering, Auburn University
Selen Cremaschi, Co-chair, B. Redd & Susan W. Redd Endowed Eminent Scholar Chair Professor of Chemical Engineering, Auburn University
Anjan K. Tula, Assistant Professor of Control Science and Engineering, Zhejiang University
Michael Howard, Assistant Professor of Chemical Engineering, Auburn University
Chris Kieslich, Assistant Professor of Chemical Engineering, Auburn University

Abstract

Process synthesis is a crucial aspect of sustainable process design, aiming to identify efficient interconnections among various unit operations to convert raw materials into products. However, existing research predominantly focuses on downstream separation without considering the upstream reaction pathway selection and the application of innovative separation techniques. This dissertation addresses this gap by analyzing the process performance of selected innovative separation techniques and integrating them into process synthesis, thereby identifying optimal reaction pathways and novel process configurations for the entire process system, from reaction to separation.

Two approaches were used to solve the synthesis problem. The first approach employed a decomposed synthesis approach, where the problem is decomposed into three sub-problems: generation/selection of reaction pathways, generation/selection of separation configurations, and results analysis. To address the generation/selection of reaction pathways, the reaction synthesis tool ASKCOS was utilized to generate potential feasible pathways based on given reactants or products. Selection criteria, encompassing reaction performance, and reactant/product properties (such as reaction enthalpy, toxicity, profitability, and ease of separation), were proposed for pathway screening and selection. The selected top pathways were then subjected to the generation of separation configurations using a thermodynamic insight-based method. Feasible separation techniques were identified based on component thermodynamic properties.

To identify the optimal solvent for azeotrope mixture separation, a solvent evaluation method was introduced. A validation model based on derivative-free optimization (DFO) was developed to validate the solvent selection results, demonstrating the effectiveness of the developed solvent selection model for agent-based distillation. Furthermore, prior to integrating

advanced separation techniques into the configurations, a hybrid distillation design was performed to evaluate the performance of these techniques using the developed DFO model. Results showed that applying hybrid distillation to separate azeotrope mixtures could reduce solvent usage and process energy cost, thereby enhancing overall process sustainability. However, the effectiveness of hybrid distillation, such as distillation membrane/adsorption, strongly depends on the membrane/adsorbent separation abilities. Hybrid design results for simple mixtures indicated potential benefits in terms of reducing separation energy cost and/or improving process throughput. The proposed solvent selection model and hybrid distillation design contribute to a better understanding of innovative separation techniques and assist the generation/selection of process configurations. Subsequently, rigorous simulation and life-cycle analysis were performed to analyze the selected process flowsheets. By comparing utility cost, capital cost, carbon footprint, and global warming potential (GWP) among different processes, the optimal sustainable process flowsheet was determined.

The second approach involved optimization, which simultaneously determined the optimal pathway and flowsheet instead of solving sub-problems step-by-step. A modified generalized distillation network optimization model, considering different reaction pathways and process carbon emissions, was employed and integrated with additional thermodynamic databases to determine the optimal process route. By inputting a list of potential reaction pathways and their corresponding conversion rate/selectivity, the optimization model extracted thermodynamic data from the database and performed optimization for multi-step reaction pathways, starting from raw materials and intermediates to the final product. Therefore, the optimal process route was determined by comparing the objective values of each pathway.

Acknowledgements

First and foremost, I would like to express my deepest appreciation and gratitude to my advisors, Dr. Mario Eden, Dr. Selen Cremaschi and Dr. Anjan Tula, for their persistent support, mentorship, and guidance. They have generously shared their knowledge and experience, helping me navigate through challenges and significantly contributing to my academic growth. I am truly grateful for their patience, encouragement, and belief in my abilities throughout this challenging journey.

I would also like to thank Dr. Michael Howard and Dr. Chris Kieslich for their valuable advice and constructive feedback to improve my research work. Additionally, I would like to express my gratitude to Dr. Brian Via for serving as my university reader, providing valuable input and guidance. Furthermore, I would like to thank all my colleagues at Auburn University for their shared experience and intellectual discussions. Their support and inspiration have motivated me to strive for excellence, and I am grateful for the privilege of working alongside them.

I would like to express my heartfelt appreciation for my aunt, Shiqiong Xu, who has gone above and beyond to uplift a boy from a small village, providing opportunities and opening doors to a brighter future. I am also fortunate to have collaborated with Dr. Teng Zhou and Dr. Kevin McBride, who have opened the doors of academia for me. Their mentorship has been instrumental in shaping my journey and fueling my passion for research and scholarship.

I would like to thank my partner Dr. Wenjuan Zhou, for her patience and unwavering emotional support during the challenging times I have faced throughout my journey. Her love, understanding, and encouragement have been an incredible source of strength, and I am profoundly

grateful for her presence in my life. Finally, I would like to thank my mother and father for their selfless love and support throughout this process.

Table of Contents

List of Tables

List of Figures

Chapter 1 – **Introduction**

Reducing the environmental impact of chemical production has become a critical objective due to carbon emission regulations and the challenges posed by the carbon market. Process synthesis, which aims to identify the optimal interconnections of different unit operations for reaction and multicomponent separation (Westerberg, 2004), is an important approach for sustainable design. In general, chemical production in the process industry involves a series of reactions and downstream separations to produce various chemical products. Thus, various feasible configurations can be generated based on different reaction pathways, separation techniques, and separation sequences, and the selected options significantly influence the overall process cost and sustainability. One can improve process sustainability by solving different subsystem synthesis problems, for example, reaction synthesis (Agnihotri and Motard, 1980), identifying better reaction pathways; separation system synthesis (Hendry et al., 1973), optimizing the separation network; heat exchanger networks synthesis (Hohmann Jr, 1971), improving the process heat efficiency; reactor networks optimization (Nishida et al., 1981), optimizing the configuration of chemical reactors, etc. As pointed out by Nishida et al. (1981), to develop an efficient process, it is not enough to solely identify an efficient reaction path. Product separation, capital investment, raw materials cost, etc., weigh very heavily in the final decision. Therefore, to systematic synthesize the entire chemical production process including reaction, separation and energy-transfer equipment, it is essential to integrate all the subsystem problems.

The existing body of research on process synthesis algorithms primarily concentrates on identifying economically viable and sustainable processes that convert a fixed raw material to the target product using conventional unit operations. However, for raw material utilization/chemical production problems, various feasible reaction pathways, which can convert the same raw

materials into a number of different products or a number of different raw materials into the same target product, are available. For example, Kongpanna et al. (2015) summarized seven process routes for dimethyl carbonate (DMC) production. Moo-Young (2019) reviewed five multistep reaction processes for 1,4-butanediol (BDO) production, utilizing different raw materials or types of reaction. In this case, to identify the sustainable process route for DMC and BDO production, one has to extend the process synthesis algorithm by considering different feasible reaction pathways.

Additionally, there is a growing trend in the research community to explore innovative separation techniques and integrate advanced separation technologies into process synthesis methodologies to enhance overall process performance and further optimize the identified processes. Malone and Doherty (2000) reported that the well-known Eastman Kodak reactive distillation process leads to five times lower investment and energy usage than traditional design. The reverse flow reactor, which periodically changes the feed flow direction, could improve catalyst stability and reduce the reactor's utility cost (Tian et al., 2018). The dividing wall column could achieve 20-30% lower capital costs than conventional tower designs (Bhargava and Sharma, 2019). A hybrid distillation-membrane process can save up to 30% of energy costs in the ethylene/ethane separation system (Caballero et al., 2009). These reported promising results also suggest the need for incorporating advanced separation technologies into the separation techniques' search space in the early stage of process synthesis so that more sustainable and economical process flowsheets can be generated.

1.1 Objectives

This dissertation will:

(1) Optimize and evaluate the hybrid distillation process, including extractive distillation and hybrid distillation membrane/adsorption processes.

(2) Develop an integrated process synthesis framework to identify the optimal process route for raw material utilization and chemical production.

(3) Develop an optimization framework for simultaneous reaction pathway selection and downstream separation network optimization.

1.2 Organization

The dissertation is organized as follows. Chapter 2 presents a review of the relevant literature. Section 2.1 reviews the reaction synthesis, including the definition and developed approaches for solving reaction synthesis problems. Section 2.2 provides an overview of the process synthesis methods, and Section 2.3 goes over recently developed innovative separation techniques. Chapter 3 presents the work for analyzing the process performance of hybrid distillation separation, including a short-cut model for preliminary optimal solvent selection for extractive distillation and a following optimal conceptual design for hybrid distillation membrane/adsorption processes. Chapter 4 describes the proposed integrated framework for process synthesis, involving reactions and separation synthesis for generating reaction pathways and innovative process alternatives. Section 4.1 discusses the algorithm for generating and screening potential feasible reaction pathways. Section 4.2 introduces the separation synthesis algorithm, which identifies feasible separation techniques and generates and ranks feasible separation process alternatives. The innovative separation techniques and their feasibility criteria are included in Section 4.3. Section 4.4 lists the detailed step-by-step explanation and results for case studies. Chapter 5 presents the simultaneous optimization framework for reaction pathway selection and optimal sustainable

separation network determination. Finally, Chapter 6 summarizes the achievement of the dissertation work and provides future directions for this project.

Note that parts of the contributions described in this dissertation have been previously published in one journal papers (Xu et al., 2023a) and four conference papers (Xu et al., 2023b, 2022b, 2022a, 2021).

Chapter 2 – **Literature Review**

2.1 Reaction Synthesis

Reaction synthesis, searching for reaction paths to produce a given product (retrosynthesis) or utilize a given raw material (forward synthesis), was initially developed to assist the research of organic chemistry and the pharmaceutical industry. Generally, to automate the generation of reaction paths, one has to solve two critical problems, representation of chemical bonds, number of different atoms and charge distribution, etc., for chemical molecules, and generation of feasible reaction pathways. Three approaches, which have different types of molecule representation and reaction path generation strategies, have been presented: 1) the logic-centered approach, 2) the direct-association approach, and 3) the data-driven approach.

2.1.1 Logic-centered Approach

The logic-centered approaches (CICLOPS, EROS, MATCHEM) (Ugi et al., 1970) utilize a block diagonal matrix, which contains the information of atoms, connectivity, and the number of chemical bonds, to represent a chemical molecule. And a chemical reaction occurs by transforming the matrix with a reaction matrix (operator). In this way, different reaction alternatives can be generated by changing the form of the operator. The other method (Hendrickson, 1975a, 1975b, 1971) also applies the mentioned chemical representation method but further particularly highlights the classification of different carbon atoms based on the types of carbon bond forms with other atoms. During a reaction, sixteen identified operators, which can transform carbon atom from its initial reactant state to the final product sate, are used to predict the potential reaction paths. The CHIRP program (Agnihotri and Motard, 1980) uses a similar method, but a screening strategy based on Gibbs free energy is applied for identifying the most thermodynamically feasible reaction alternatives.

2.1.2 Direct Associative Approach

A well-known direct associative approach is the LHASA (Logic and Heuristics Applied to Synthetic Analysis) program (Corey, 1971; Corey et al., 1974), which allows communication between man and computer. It uses a set of connection tables to represent the chemical structure, including the number of attachments, charge, the valence of the atom and the atom type, etc. Different reaction precursors/intermediates can be generated by using predefined chemical transformations. This program takes advantage of man-computer interaction to adjust the flow of analysis, but the predefined template reactions do not allow for generating innovative reaction paths. The program SYNCHEM (Gelernter et al., 1977) uses a similar algorithm to generate alternative reaction paths, and the screening techniques based on artificial intelligence are applied to select the 'best' pathways. Similar to the LHASA program, the CAMEO (Computer-Assisted Mechanistic Evaluation of Organic Reactions) (Salatin and Jorgensen, 1980) program uses complex connection tables to represent the chemical molecules. And the reaction pathways, derived from fundamental reaction mechanisms, are predicted by analyzing the structure-reactivity relationships of nucleophilic and electrophilic sites. The SECS (Simulation and Evaluation of Chemical Synthesis) (Wipke et al., 1978) program borrows the LHASA program's basic algorithm. It is also a man-computer interactive system in which prescribed appropriate transforms are applied to generate the precursor of the target. The REACT program (Govind and Powers, 1981) pioneered the automation of generating chemical reaction paths from a chemical engineering perspective. It replaces the connection matrix of chemical molecules with a computationally efficient linear numerical representation, facilitating automated analysis and identification of reaction routes. Multiple alternative reaction routes can be identified by analyzing various functional groups and matching functional substructures. The program incorporates a heuristic weighting score to reduce

the search space during path generation. The SOPHIA (System for organic reaction prediction by heuristic approach) (Satoh and Funatsu, 1995) program combines different numerical lists, which have the information of molecules' atoms, bonds, and structural characteristics, to represent chemical molecules. Thus, it could predict various reaction paths based on the analysis of potential reactive functional groups.

2.1.3 Data-driven Approach

The data-driven approach has been extensively studied over the past decades, coinciding with the advancement of machine learning techniques. Generally, the input chemical molecules are converted into molecular descriptors, containing the atomic information, number of neighboring atoms and types of chemical bonds, etc. Then the developed machine learning classification method (deep neural network) could read the input information and identify the associated reaction rules. Kayala et al. (2011, 2012) presented a machine learning algorithm for filtering the reaction site and ranking the results, which uses graph-based representations of molecules. In this algorithm, the reaction is treated as an interaction between a donor and an acceptor orbital. Wei et al. (2016) presented a neural network algorithm to predict the outcome of reactions based on reactant fingerprints with a limiting number of reaction types. Segler and Waller (2017a, 2017b) described two approaches for reaction path prediction. One is a knowledge-graph approach that uses a known reaction database to search the possible products by giving exactly two reactants. The other approach is based on neural networks that predict the most probable transformation rules for the input molecules. Coley et al. (2017) further developed a machine learning algorithm, including a forward reaction enumeration by applying reaction templates and a neural network-based scoring model for candidate ranking. Coley et al. (2018) also studied the opportunity of machine learning in the area of synthesis planning, including both retrosynthesis

and forward synthesis. The developed software package ASKCOS is free to access. Based on this model, Gao et al. (2020) formulated the retrosynthesis problem as a mixed-integer nonlinear programming (MINLP) model to identify the optimal reaction path for a given medicine product.

2.2 Process Synthesis

The current research focus of process synthesis refers to the optimal design of the process flowsheet, especially for the separation section, involving the identification and selection of separation techniques and configurations for multicomponent separation. The objective of process synthesis is to identify sustainable and economic processes that satisfy the design specifications, such as product purity, energy efficiency, and yield. The general mathematical formulation can be presented as

$$Min/max\ Z\ =\ f(x,y) \tag{2.1}$$
$$s.t.h(x,y)\ =\ 0 \tag{2.2}$$
$$g(x,y) \leq\ 0 \tag{2.3}$$
$$x\epsilon X, y \in \{0,1\} \tag{2.4}$$

Where $f(x,y)$ denotes the objective function such as capital/operational cost and process profit. $h(x,y)$ denotes the process mass and energy balance constraints. $g(x,y)$ denotes the process design specifications.

There are two typical process synthesis problems: 1) identifying an improvement of existing facilities (retrofitting), and 2) finding a completely new process flowsheet. Researchers have proposed several approaches to solve retrofit and new design problems by selecting the best sequence of unit operations, using new separation technologies, optimizing the process operating conditions, etc. These approaches can broadly be classified into three types: 1) heuristics or knowledge-based methods. 2) mathematical optimization methods, and 3) hybrid methods.

Siirola et al. (1971) first developed a computerized process flowsheet generator based on a set of combination rules of experience, insights, and engineering knowledge (data). Seader and Westerberg (1977) further improved the previous method by applying evolutionary modification rules for the initial flowsheet to generate process alternatives. Nath and Motard (1981) extended this approach by involving more evolutionary rules, and it was used not only for simple distillation but also for agent-based distillation. Nadgir and Liu (1983) proposed an improved systematic heuristic synthesis method to generate the initial sequence of multicomponent separations. Due to the fact that the separation in the process industry cannot achieve an ideally sharp split, Cheng and Liu (1988) proposed a simple heuristic method for the synthesis of sloppy multicomponent separation tasks. Liu et al. (1990) further extended the work and programmed it into an expert system called PROLOG. Pajula et al. (2001) presented the case-based reasoning (CBR) approach to expand its application range. This approach solves new problems by retrieval, adaptation, revising, and retaining the old designs. These developed methods evaluate the process alternatives based on the conflict and overlapping of defined heuristic rules. However, Modi and Westerberg (1992) introduced an evaluation function based on Underwood's method for ideal behaving distillation separations. Floquet et al. (1994) developed a fuzzy rule-based approach to quantify the qualitative terms ("large", "high", "appropriate") of the heuristic rules. In addition to heuristic rules, researchers also developed thermodynamic insights-based methods for solving process synthesis problems. Jaksland et al. (1995) proposed thermodynamic rules for a wide range of separation techniques, which can be applied to identify feasible separation techniques. Another thermodynamic insight-based methods was developed (Gani and Bek-Pedersen, 2000; Tsirlin et al., 2009, 2007; Tsirlin and Sukin, 2014) and applied for downstream separation synthesis. Fox et

al. (2013) and Sempuga et al. (2010) developed a method for the entire process synthesis based on thermodynamic properties, such as enthalpy and Gibbs free energy.

Besides heuristic rule-based process synthesis approaches, one can mathematically formulate the process/separation superstructure (Figure 1) and find the optimal processing structure by minimizing/maximizing a pre-defined cost/profit objective function (refer to Equation 2.1 – 2.4). This approach has been successfully applied to the processes' subsystem synthesis, such as the synthesis of distillation column sequencing (Grossmann, 1990), optimization of complex reactor networks (Kokossis, 1990; Kokossis and Floudas, 1994), and heat exchange networks (Floudas et al., 1986; Yee et al., 1990; Yee and Grossmann, 1990). Grossmann and Daichendt (1996) reviewed the optimization-based approach for process synthesis, in which they discussed different formulations (MINLP, MILP, NLP) based on the problem type. Different approaches have been proposed to generate and solve the resulting mathematical programming models, e.g., generalized disjunctive programming model (Raman and Grossmann, 1994) and outer-approximation (Duran and Grossmann, 1986), respectively. A review of the developed approaches was presented by Grossmann (2002). The main advantage of mathematical programming based approaches is its simultaneous optimization of process structure and process operating conditions. However, it is usually limited to moderately sized problems because of the computational complexity associated with the resulting problem with many integer variables and nonlinear equations.

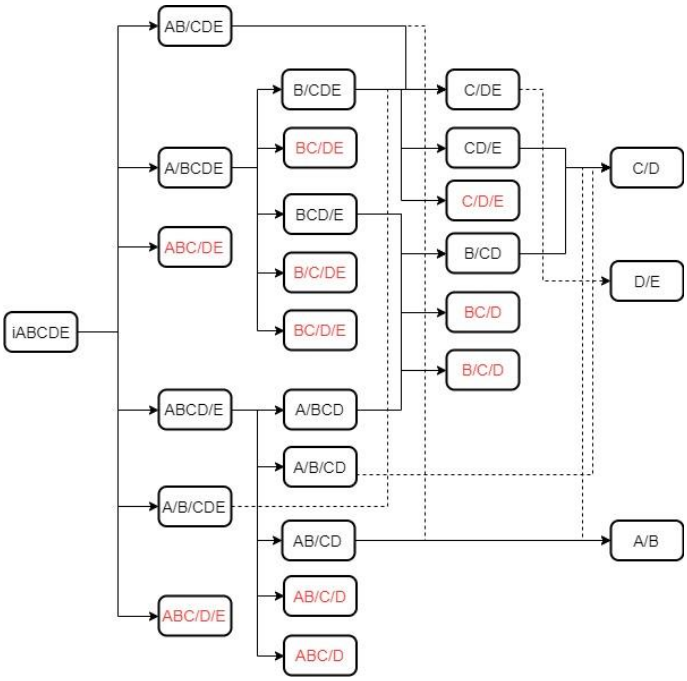

Figure 1. Separation superstructure of multicomponent system.

Hybrid methods combine different approaches into one method to solve the synthesis problem. Lu and Motard (1985) first proposed a hybrid process synthesis method by using linear programming techniques to generate the preliminary process flowsheet. And the preliminary flowsheet is further optimized based on a heuristic-evolutionary approach. Mizsey and Fonyo (1990) introduced a hybrid approach to the process synthesis problem. This approach uses a hierarchical design strategy to create and screen process alternatives based on heuristics, short-cut models, and simple estimations of the total costs. The results are then further verified and improved by applying three defined algorithms, i.e., user-driven synthesis technique, bounding strategy, and algorithmic methods. Hostrup et al. (2001) proposed an integrated approach, which first uses thermodynamic insight for pre-analysis. Then the generated flowsheet superstructure is solved through an MINLP formulation to generate the optimum flowsheet. d'Anterroches and Gani (2005) presented a framework for computer-aided flowsheet design (CAFD) based on the concept of group contribution. In this approach, the process alternatives are represented as the selection and

combination of different processing units, analogous to functional groups within a molecule. A software package ProCAFD was further developed based on this method (Tula et al., 2015).

2.3 Developed Hybrid and Intensified Technologies

2.3.1 Hybrid Techniques

Analysis of the column entropy shows that the distillation has low thermodynamic efficiency: from 18% in air separation to 12% in crude units and about 5% for ethylene and propylene production (Kiss, 2014). This low efficiency implies that there is a potential to significantly improve process efficiency. One of the promising advanced solutions, hybrid distillation, which integrates the distillation with other low energy-consuming separation units like membranes, adsorption, and crystallization, has been proposed and widely investigated over the decades. The hybrid distillation membrane (HDM) technique is one of the most used hybrid separation techniques in the process industry. Pressly and Ng (1998) gave a systematic classification of distillation-membrane hybrid configurations, which is based on three types of mixtures: tangent pinch or azeotrope near a pure component (type I), azeotrope at an intermediate concentration (type II), and system with overall low relative volatility (type III). In general, for mixture types I, II, and III, the task of the membrane within the overall process is final polishing, overcoming separation restriction, and concentration enhancement, respectively. Lipnizki et al. (1999) reviewed pervaporation-based distillation processes, including azeotrope mixtures of ethanol/water, dimethyl acetate/water, dimethyl carbonate/methanol, methyl isobutyl ketone/water, and benzene/cyclohexane. Various economic comparisons have shown that a pervaporation-based hybrid process can be economically competitive compared to conventional separation processes or pervaporation alone. However, achieving economic viability requires highly efficient and low-cost membranes, as well as optimal process design. To design the hybrid distillation membrane

systems, Moganti et al. (1994) determined the optimal membrane position by minimizing the column stages. The results suggested that locating the membrane close to the feed position of the column for enhancing the column feed composition could achieve a reduction of at least 25% in tray numbers. Pettersen and Lien (1995) introduced an algebraic membrane permeation model to analyze the design trade-off in hybrid systems, such as column duty versus membrane selectivity, and membrane area versus distillate pressure/composition. Bausa and Marquardt (2000) proposed a short-cut method to assist in designing multicomponent hybrid systems with the aim of determining the minimum energy demand, optimal side-stream composition, and minimum membrane surface area. Kookos (2003) presented a rigorous mixed-integer nonlinear programming (MINLP) model to determine the optimal membrane position, column stages, operating pressure, etc., by minimizing the system's annualized cost. This optimization model was applied to the propylene/propane separation case study. Szitkai et al. (2002) also developed an MINLP model to optimally design the ethanol/water hybrid separation system by minimizing the process annualized cost, but a regression model was applied to fit the solutions of differential equations for membrane modules. Compared to an existing process, the optimal design and operating parameters, such as column stages, feed location, reflux ratio, and number of membrane sections and modules, were identified, which leads to 12% savings in total annual cost. Eliceche et al. (2002) determined the operating conditions for the hybrid distillation system for separating azeotrope methanol/methyl tert-butyl ether azeotrope mixture by performing rigorous process simulation (HYSYS) at different conditions. Caballero et al. (2009) proposed a two-stage approach for ethylene/ethane hybrid system retrofitting design where a short-cut model is first applied for preliminary trade-off analysis. Then, an MINLP model that integrates process simulator and

hollow fiber membrane permeation model was used to determine the optimal operating parameters like membrane position, area, selectivity, and operating pressure.

In the hybrid distillation adsorption system, the adsorption unit was initially applied to bypass the distillation azeotropic point or pre-separation of the distillation feed stream. Thus, adsorption-distillation has been studied to separate close boiling or azeotrope mixture such as propane/propylene (Kumar et al., 1992) and isopropanol/water (Mujiburohman et al., 2006). Researchers also discovered that the adsorption could act as a final separation step for distillate/bottom product purification (distillation-adsorption). Ghosh et al. (1993) applied this concept to propane/propylene separation. They found that a high selectivity adsorbent is necessary to satisfy the product purity requirement. Tula et al. (2019) investigated the distillation adsorption hybrid for methanol/water separation and showed that it could save 40% energy costs. A modeling approach for the distillation adsorption process is proposed by Ritter et al. (2012). This approach includes two parts. Based on the "black box" model of adsorption, the first part is applied for a preliminary assessment. The second part, based on the rigorous adsorption model, is used to verify the results.

Hybrid distillation crystallization provides a feasible way to overcome the limitation imposed by distillation and crystallization. In particular, the distillation can be used to cross the eutectic barrier that limits the separation of crystallization; likewise, the crystallization can be used to overcome the azeotrope barrier that restricts the distillation separation. Depending on the requirement of additional solvents for crystallization, the two most commonly used hybrid systems are distillation/solvent crystallization and distillation/melt crystallization. Berry and Ng (1997) presented a general systematic method for synthesizing the distillation/melt crystallization. The design and optimization approaches have been investigated by many researchers (Beierling et al.,

2014; Franke et al., 2008; Marquardt et al., 2008; Micovic et al., 2013). Distillation/melt crystallization has been used for different separation systems, such as monomeric methylene diphenyl diisocyanate (MDI) isomers (Stefanski and Fassler, 2002) and m-xylene recovery (Stepanski and Haller, 2000), etc.

Conventional pressure-swing distillation and solvent/entrainer based distillation are also treated as hybrid distillation techniques. Two distillation columns that operate at different pressures are used to separate the pressure sensitive azeotrope mixtures. It has been investigated in many separation systems, such as acetone/chloroform (Luyben, 2013), isobutyl alcohol/isobutyl acetate (Munoz et al., 2006), bioethanol (Mulia-Soto and Flores-Tlacuahuac, 2011), and toluene/1-butanol (Qasim et al., 2016), etc. A comprehensive overview of pressure-swing distillation separation was presented by Liang et al. (2017). The solvent/entrainer based distillation utilizes a third component to destroy/alter the azeotrope point. Separation systems, such as ethanol/water, ethanol/benzene, tetrahydrofuran/ethanol, etc. (Gerbaud et al., 2019), have been investigated. Babi and Gani (2014) presented an overview and generalized selection rules for hybrid distillation. Skiborowski et al. (2013) introduced a conceptual design algorithm for hybrid distillation techniques, where hybrid processes are designed based on four steps, including generation of hybrid processes, screening with short-cut models, optimization of the conceptual model, and optimization of rigorous mathematical models.

Hybrid separation techniques are not limited to hybrid distillation. Researchers also investigated other hybrid separation techniques such as membrane crystallization, membrane extraction, membrane absorption, membrane chromatography, pressure-swing adsorption, and simulated moving bed adsorption.

In the membrane-crystallization process, the membrane assists in creating the supersaturated solution, in which crystals can nucleate and grow. For instance, with the continuous removal of solvent from the solutions by a membrane (gas/liquid or liquid/liquid), the solute concentration will increase and eventually be supersaturated. As a result, the membrane acts as physical support, facilitating the crystals' nucleation and growth after changing temperature and/or composition (Chabanon et al., 2016). Membrane crystallization has been investigated in the separation processes such as recovering minerals from water (Pramanik et al., 2016), manufacturing pharmaceuticals (Drioli et al., 2011), etc. Due to the formation of crystals on the membrane surface, it may cause fouling, which may affect the membrane permeability.

The membrane-extraction techniques have been widely applied in environmental, food, and industrial analysis. The membrane provides a physical barrier for the analyte component, which permeates the membrane and is extracted by an acceptor phase (Pawliszyn, 2012). Similarly, the membrane-absorption also uses the membrane as a physical barrier between the gas and liquid phase. It has unique advantages compared to the conventional absorption process, such as operational flexibility (independent control of gas and liquid flow rates), controlled and known interfacial area, compact and less energy-consuming, and less droplet dragging (Luis et al., 2011). The membrane-chromatography techniques attach the active ligands to the membrane's inner surface, thus reducing the transport limitations. It has been applied in the downstream processing of proteins (Charcosset, 1998; Thömmes and Kula, 1995).

The pressures-swing adsorption (PSA) techniques generally comprise two columns working in parallel, one for high-pressure adsorption and the other for low-pressure desorption (Peng et al., 2011). PSA has been applied in many separation systems, such as hydrogen purification (Khajuria and Pistikopoulos, 2013), methane purification (Olajossy et al., 2003), and

air separation (Hassan et al., 1986), etc. Instead of using pressure difference to perform the adsorption/desorption, the simulated moving bed (SMB) performs the adsorption/desorption via the differences in the mixtures/solvent affinities towards adsorption. A widely applied example in the process industry is the separation of xylene isomers (Minceva and Rodrigues, 2002).

2.3.2 Intensified Techniques

Process intensification is defined as the enhancement of a process at unit operational, functional and/or phenomena levels through the integration of unit operations, functions, and phenomena or targeted enhancement of the phenomena for a set of operations (Lutze et al., 2010). A successful application of the Eastman Kodak methyl acetate reactive distillation process, which combines the reactor with the distillation column, results in five times lower investment and energy usage than the traditional design (Malone and Doherty, 2000). Sharma and Mahajani (2002) presented an extensive review of the reaction systems implemented in the process industry or laboratory. More than 150 successful applications of reactive distillation in the process industry cover large ranges of reactions, such as hydrogenations, hydrodesulfurization, esterifications, and etherification (Harmsen, 2007). To address the feasibility analysis of reactive distillation, Shah et al. (2012) proposed a step-by-step evaluation algorithm to assess the technique's economic and thermodynamic feasibility.

The dividing wall column is designed to add a sidewall in the distillation column, which aims to separate multiple components simultaneously by controlling the downstream liquid and upstream gas flowrate. Comprehensive overviews of dividing wall columns, including theoretical description, application, and control issues, can refer to Dejanović et al. (2010 and Yildirim et al. (2011).

The reverse flow reactor periodically changes the feed flow direction, suppressing hot spot formation, thus improving catalyst stability and reducing the utility requirement for feed preheating and/or product cooling (Tian et al., 2018). It has been applied to many reactions, such as the oxidation of hydrocarbons and sulfur dioxide and the selective catalytic reduction of nitrogen oxides (Marín et al., 2019).

Other advanced intensified techniques include membrane reactors (Powell, 2017), reactive adsorption (Charpentier, 2007), oscillatory flow reactors (Bianchi et al., 2020), structured catalytic reactors (Kapteijn and Moulijn, 2022), microreactors (Kothare, 2006), and reactive distillation with a membrane (Buchaly et al., 2007).

Chapter 3 – **Hybrid Distillation Design and Analysis**

This chapter introduces the conceptual design and analysis of hybrid distillation systems, including distillation membrane/adsorption and extractive distillation. Two design approaches: simulation-based derivative-free optimization (DFO) and rigorous optimization, are presented and applied to solve the new design/retrofitting problems for both simple separating systems (methanol/water) and azeotrope mixtures separation (benzene/cyclohexane, methanol/methyl acetate). Section 3.1 presents a short-cut solvent evaluation and validation model for extractive distillation. Section 3.2 provides the DFO and mathematical optimization models for hybrid distillation design.

3.1 Solvent Selection of Extractive Distillation

Extractive distillation is a process class used for separating non-ideal mixtures, where a third component (solvent/entrainer) is employed to overcome the separation barrier and enhance the separation process. Figure 2 gives the acetone-methanol vapor-liquid equilibrium (VLE) plot with different solvents. The acetone-methanol binary mixture forms azeotropes with a composition of 78.8% acetone, but the azeotrope disappears after adding a third component, such as water and dimethyl sulfoxide (DMSO). Thus, the mixture can be separated through distillation, and a general process flowsheet for extractive distillation is given in Figure 3. The first distillation column is used for separating the lightest product, and the second column is employed for separating the solvent and heavy product. Since different solvents and solvent compositions significantly influence the VLE behavior (refer to Figure 2), the overall process capital/operating cost highly depends on solvent selection. Current widely applied solvent selection method is based on computer-aided molecular design (CAMD) and optimization, where CAMD identify the list of potentially feasible solvents that meet desired thermodynamic properties such as solubility and

relative volatility, and the process optimization is followed to select the optimal solvent for all the potential candidates (Medina-Herrera et al., 2014). For example, Cignitti et al. (2019) proposed an optimization model to design and identify suitable solvents by maximizing the separation driving force based on the group contribution method. The optimum solvent was then validated by rigorous process simulation/optimization. Other methods identify the optimal solvent based on solvent physical/process properties rather than rigorous optimization. For instance, Kossack et al. (2008) proposed a rectification body method that can calculate process properties such as minimum solvent flowrate and minimum energy demand for selecting the optimal solvent. But the method is computationally expensive. Shen et al. (2015) proposed a solvent screening method based on five solvent physical properties, such as boiling point and selectivity. After adding weighted attributes to these properties, the solvents were ranked based on their 'total score,' and the ranking results were validated by process simulation. However, these methods only use physical properties as their design/screening criteria without considering the effects of process properties. For example, a higher boiling point solvent is often preferred in solvent screening due to its ease of regeneration, but this may result in the use of a higher grade of utility, which has a higher utility cost.

This study presents a fast solvent evaluation and selection (FSES) model for screening a list of potentially feasible solvents. This model employs both physical properties and separation process properties, such as minimum energy consumption, the minimum number of stages, etc., for solvent selection. Given a list of potential solvents, the model can quickly evaluate the performance of the different solvents and provide recommendations on the best option. This study includes 1) solvent evaluation and 2) evaluation results validation. In the solvent evaluation, the model is applied to rank a list of solvents. The ranking results are validated by rigorous process simulation models where the operating/design variables are identified via DFO.

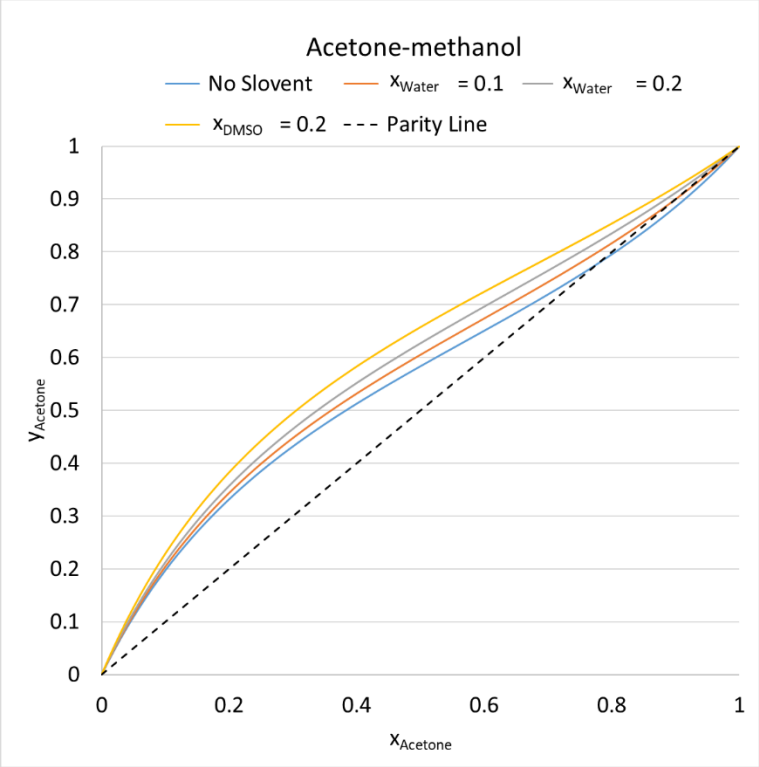

Figure 2. Vapor-liquid equilibrium plot of acetone-methanol mixture with different solvents.

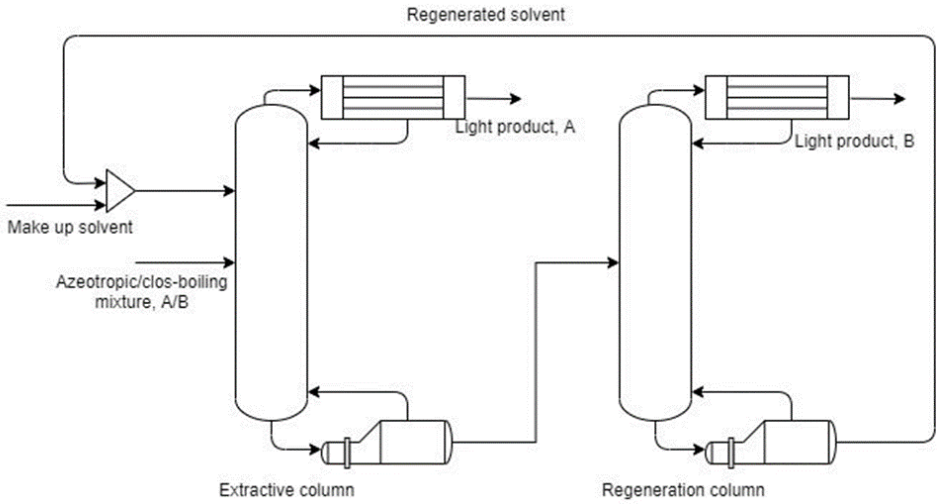

Figure 3. General process flowsheet for extractive distillation.

3.1.1 FSES Model

The solvent evaluation model aims to quickly and reliably assess different solvents based on various performance indicators. This model considers the process and physical properties in the

evaluation process. Firstly, a short-cut calculation model, which is based on Underwood and Fenske equations, is applied to calculate the process properties like minimum reflux ratio and the number of stages of a column. The Underwood and Fenske equations assume that the system has constant relative volatility. A typical extractive distillation system involves two columns, where the second column is simply solvent recovery distillation. Therefore, for the second column, the Underwood and Fenske equations can be applied to calculate the minimum number of stages (N_{min}) and reflux ratio (R_{min}). However, these two equations cannot be directly applied to the extractive distillation column. Figure 4 shows the vapor-liquid equilibrium curve and liquid composition profile across the extractive distillation column. The extractive distillation column is divided into three sections: rectification, extraction, and stripping, and the relative volatility is different for each section (i), which means this change in relative volatility ($\alpha_{lh,i}$) across the sections has to be accounted for. Here, we assume that each section's relative volatility is constant, so the Fenske equation can be used separately to calculate the minimum number of stages ($N_{min,i}$). The minimum reflux ratio is calculated when the operating line intersects with the VLE curve. In this way, the column minimum reboiler duty can be calculated using the stage enthalpy balance. The extractive distillation column is described by Equation 3.1 – 3.6, where Equation 3.1 is only applied for estimating the minimum solvent flowrate (F_E) of ternary systems that do not have a separation boundary (Gerbaud et al., 2019). For ternary systems with a separation boundary, such as the acetone/chloroform/ethylene glycol system, one can assume the distillate/bottom composition (x_D, x_W) and calculate the minimum solvent flowrate through mass balance.

$$\left(\frac{F_E}{F_{AB}}\right)_{min} = \frac{(RR+1)D}{F_{AB}} \times \frac{(x_{PA}-y_{PA}^*)}{(x_E-x_{PA})} + \frac{D(x_D-x_{PA})}{F_{AB}(x_E-x_{PA})} \quad 3.1$$

$$N_{min,i} = \frac{lg\left[\left(x_{i,l}/x_{i,h}\right)/\left(x_{i+1,l}/x_{i+1,h}\right)\right]}{\lg(\alpha_{lh,i})}, i = 0,1,2 \quad 3.2$$

$$N_{min} = \sum_{i=0}^{2} N_{min,i} \quad 3.3$$

$$R_{min,j} = \frac{F_E x_{j,l} + D(x_D - y_{j,l})}{D(y_{j,l} - x_{j,l})}, j = 1,2 \quad 3.4$$

$$R_{min} = max\{R_{min,1}, R_{min,2}\} \quad 3.5$$

$$Q_{reboiler,min} = (R_{min} + 1)DH_{D,V} + WH_W - H_E F_E - H_{AB} F_{AB} - R_{min} DH_{D,L} \quad 3.6$$

In the model, F_E is the solvent flowrate. F_{AB} is the raw material flowrate, AA is the predefined reflux ratio for solvent flowrate calculation. D and W are the distillate and bottom flowrates. x_D and x_W are the distillate and bottom compositions. x_E is the inlet solvent composition. x_{PA} is the minimum solvent composition that breaks the azeotropes after adding the solvent, and component A is the lightest component in the system. y_{PA}^* is the vapor composition in equilibrium with x_{PA}. $N_{min,i}$ is the minimum number of stages in the i^{th} section. $x_{i,l}$ and $x_{i,h}$ are the light and heavy component compositions in the i^{th} section. $\alpha_{lh,i}$ is the geometric relative volatility of the i^{th} section. $x_{j,l}$ and $y_{j,l}$ are the light compound liquid and vapor compositions at the first ($j = 1$) and last ($j = 2$) stage of the extractive section. R_{min} is the minimum reflux ratio. $H_{D,V}$ are $H_{D,L}$ are the vapor and liquid enthalpies of the distillate product. H_E and H_{AB} are the enthalpies of solvent and binary raw materials. The inlet is assumed to be at boiling point ($q = 1$). After analyzing different extractive distillations systems, $x_{1,E}$ is usually between 60 % to 80%, $x_{2,E}$ is close to $x_{2,E}$, and the difference is in the range of 5%.

We calculate the minimum reboiler duty, number of stages, and reflux ratio for each solvent by applying the proposed calculation method. Eight properties, including six process properties, e.g., the minimum number of stages, reboiler duty, and reflux ratio, and two physical properties, e.g., solvent flowrate and boiling point, are considered in the evaluation model. These properties are selected because they directly influence the process capital and/or utility cost. Given N number

of potential solvents, for each property, a value from one to M is assigned (where one is given to the best solvent with that property). Finally, the solvents are ranked based on summation scores, and the best solvent has the overall lowest score (Table 1).

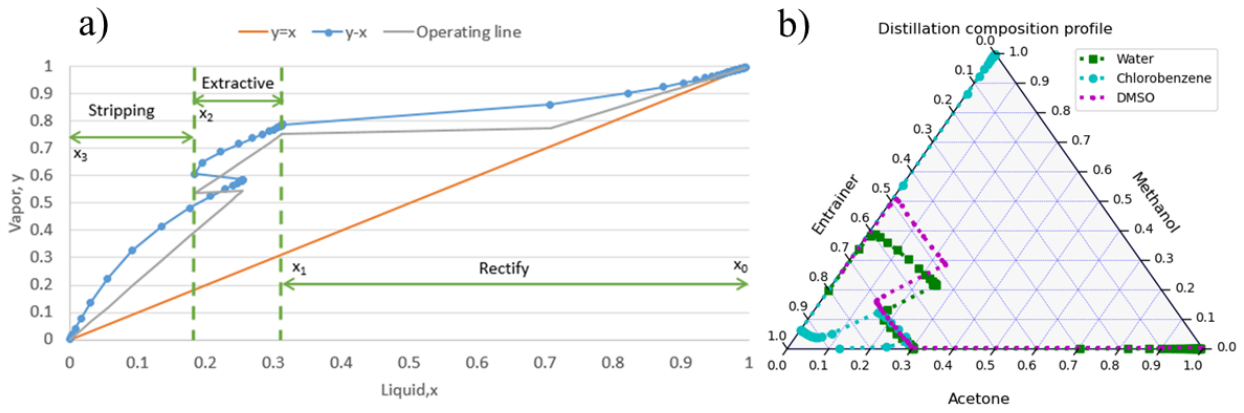

Figure 4. a) VLE plot of acetone/methanol/water extractive distillation. (x_0, x_1, x_2, x_3 – boundary composition in each section). b) Liquid composition profile in acetone/methanol/solvent separation system.

Table 1. Solvent ranking algorithm for extractive distillation. (S_i denotes solvent i; $V_{i,j}$ denotes the value of property j for solvent i; $Score_{i,j}$ represent the assigned score of property j for solvent i; $Score_i$ denotes the total ranking score for solvent i)

Solvent i	Properties, j						Total score of solvent i
	Reflux ratio		Stages		Heat duty		
S_1	$V_{1,1}$	$Score_{1,1}$	$V_{1,2}$	$Score_{1,2}$	$V_{1,3}$	$Score_{1,3}$	
			…				
S_i	$V_{i,1,min}$	1	$V_{i,2,max}$	M	$V_{i,3}$	$Score_{i,3}$	$Score_i = \sum_j Score_{i,j}$
			…				
S_M	$V_{M,1}$	$Score_{M,1}$	$V_{N,2}$	$Score_{M,2}$	$V_{M,3}$	$Score_{M,3}$	

3.1.2 Validation Model

To validate the rankings given by the solvent evaluation method, DFO was employed to optimally design the extractive distillation setups. The total annualized cost (TAC), which

considers both capital (IC) and utility costs (AUC), is the objective function. The number of stages (N_k), inlet stage ($N_{k,feed}, N_{1,S}$), and solvent flowrate (F_S) are the decision variables. A generalized form of the optimization problem solved by the simulation-based optimization algorithms is given in Equations 3.7 - 3.15.

$$min: TAC = \frac{i(i+1)^n}{(i+1)^n - 1} \times IC + AUC \quad 3.7$$

$$st. IC = \sum_j Cost_j(q_{s,j}) \quad 3.8$$

$$AUC = \sum_j Utility_j(q_{o,j}) \quad 3.9$$

$$q = \Theta\left(F_S, N_k, N_{k,feed}, N_{1,S}\right), k = 1, 2 \quad 3.10$$

$$x_m \geq purity \quad 3.11$$

$$F_{s,L} \leq F_S \leq F_{S,U} \quad 3.12$$

$$N_{k,feed,L} \leq N_{k,feed} \leq N_{k,feed,U} \quad 3.13$$

$$N_{k,L} \leq N_k \leq N_{k,U} \quad 3.14$$

$$N_{1,S,L} \leq N_{1,S} \leq N_{1,S,U} \quad 3.15$$

Where, TAC is the total annualized cost, IC is the investment cost, AUC is the annualized utility cost, i is interest, n is plant life ($n = 5$ is used in this model), $Cost_j$ is the investment cost of equipment j, $Utility_j$ is the utility cost of equipment$j$, $q_{s,j}$ is the sizing variable for equipment j, $q_{o,j}$ is the operating variable for equipment j, x_m is the product purity of component m, $\Theta(F_S, N_{k,feed}, N_{1,S})$ is the process simulation model, F_S is the solvent flowrate rate, N_k is the number of stages of column k, $N_{k,feed}$ is the materials feed stages of column k, $N_{1,S}$ is the solvent feed stage of the first column, and L and U represent the lower and upper bounds. The detailed capital/operating cost estimation model are provided in Appendix 1.

The optimization procedure is demonstrated in Figure 5. Given the decision variables' initial upper and lower bounds, the inner loop runs the process simulation. The simulation results are used to calculate the objective function, which is used by an open-source DFO solver RBFOpt

(Costa and Nannicini, 2018; Nannicini, 2021), to determine the decision variables for the next iteration. The optimal solutions ($X_{opt,i}$) and the associated best design parameters ($N_{opt,i}$) are identified after reaching the maximum number of iterations (M). The overall optimization procedure terminates after reaching a stable objective value. Here, to generate stable results that are not influenced by the initial lower and upper bounds, an outer loop that revises the initial upper (N^U) and lower bound (N^L) values based on the identified best design parameters is applied. The updated upper and lower bounds are sent back to the inner loop.

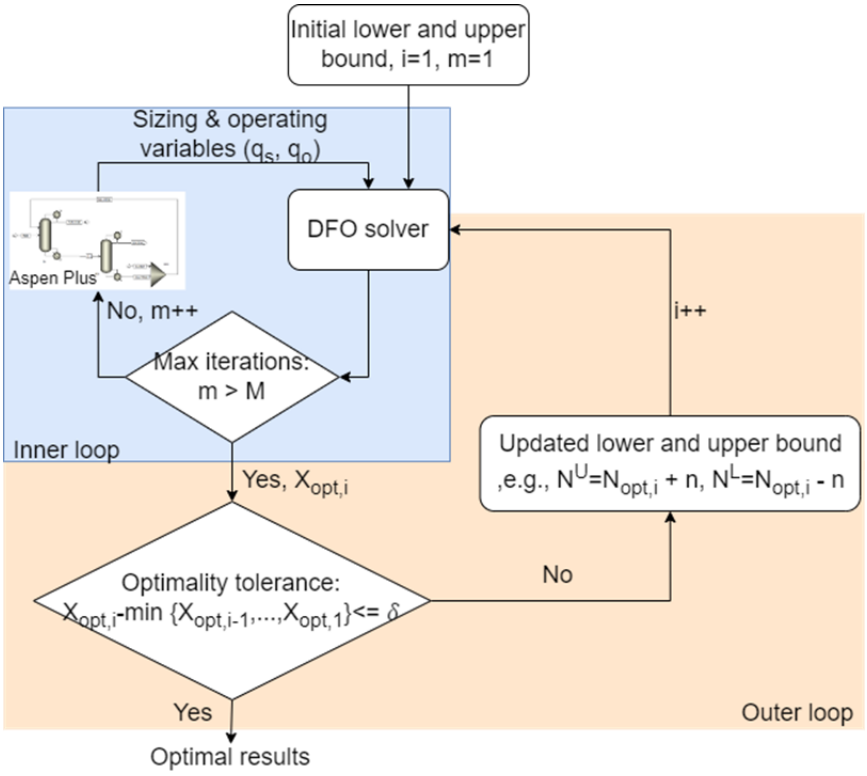

Figure 5. The optimization procedure for simulation-based optimization which integrates the process simulation with a DFO algorithm for designing hybrid separation systems. (δ denotes the optimality tolerance (0.5% in the case study), n denotes the change of lower and upper bounds based on the newest identified optimal solution (10 for column stages, 0.5 for the solvent ratio)).

3.1.3 Results and Discussion

Four separation systems, acetone/chloroform, acetone/methanol, benzene/cyclohexane, and methanol/methyl acetate, with their potential solvents, were selected from the review paper by Gerbaud et al. (2019). With equimolar composition in the inlet stream, Table 2 gives an example of properties calculation and ranking results for acetone/chloroform mixture. Five solvents DMSO (Dimethyl sulfoxide), EG (ethylene glycol), chlorobenzene, o-xylene, and benzene, are considered for separating the acetone/chloroform mixture. The FSES model ranks the five solvents in the following order: DMSO (Dimethyl sulfoxide) > EG (ethylene glycol) > chlorobenzene > o-xylene > benzene. The optimization results also confirmed that DMSO is the best solvent for acetone/chloroform separation. However, the FSES model predicts that o-xylene is better than chlorobenzene, and the optimization results yield contradictory findings. This is because the system has a separation boundary, and we have to approximate this boundary using calculated residue curves from process simulation software. The solvent flowrate of o-xylene is 1.22 times larger than chlorobenzene but 1.61 times larger from the DFO results, which means that the o-xylene system has higher reboiler duty than the predictions.

Table 2. Properties calculation and ranking results for acetone/methanol separation.

	EG	DMSO	o-xylene	Benzene	Chlorobenzene
Solvent flowrate, kmol/h	228.22	162.85	612.44	304.25	503.14
Stages D1	8.96	10.55	14.9	17.08	25.1
Reflux ratio D1	1.92	1.5	7.3	10.96	6.76
Reboiler duty D1, kW	465.4	655.72	2,852.98	4,911.97	3,068.34
Stages D2	2.82	2.88	5.21	20.15	6.33
Reflux ratio D2	0.06	0.05	1.26	8.04	1.71
Reboiler duty D2, kW	1,181.82	817.98	1,464.14	3,654.45	1,219.64
Boiling point, °C	197.3	189	144.4	80	131
Total score	16	14	28	33	29
TAC, 10^6 \$/y	0.77	0.66	1.05	1.29	0.94

The FSES model and DFO results for the other three binary systems are listed in Table 3, and the optimal design parameters of the identified best solvent are listed in Table 4. For the acetone/methanol binary mixture, the FSES model and DFO results give the same order: DMSO > water > EG > ethanol > 2-proponal for acetone/methanol separation. For the benzene/cyclohexane case, the short-cut model predicts the following order: sulfolane > furfural > dimethyl phthalate > N-Methyl-2-pyrrolidone (NMP) > aniline, but the DFO results show that the NMP has better performance than dimethyl phthalate. Although the evaluation model correctly represents that the dimethyl phthalate system has a lower number of stages, its high boiling point results in higher column temperatures, which requires a furnace. Due to this, the capital cost of dimethyl phthalate system is higher than the NMP system. For the methanol/methyl acetate case study, only three solvents were selected because of the lack of experimental phase equilibrium data. Among these three solvents, the short-cut evaluation method predicts that DMSO has the best performance, but the DFO results show that 2-methoxyethanol has a better performance. The evaluation model shows that the 2-methoxyethanol has a smaller number of stages for the extractive column and a higher number of stages for the second column, which results in similar capital costs. However, the predicted minimum reboiler duty does not correctly represent the utility cost. Two reasons may cause this deviation: 1) Boiling point, DMSO has a higher boiling point than 2-methoxyethanol, so different types of utilities have to be used. However, in this model, we rank the properties only based on their relative heat duty, and the different types of utilities are not considered. 2) Boundary composition (x_1, x_2). The boundary composition influences the sections' relative volatility and thus influences the calculated reboiler duty. The same $x_{1,E}$ value is used in all cases, but DFO proves that DMSO $x_{1,E}$ is equal to 60%, while 2-methoxyethanol, EG has similar $x_{1,E}$ values around 70%.

Table 3. FSES model ranking and DFO results for acetone/methanol, benzene/cyclohexane and methanol/methyl acetate systems.

Solvents	Score	TAC, 10^6\$	Solvents	Score	TAC, 10^6\$
Acetone/Methanol			Benzene/Cyclohexane		
Water	20	3.32	Dimethyl phthalate	22	0.95
2-Proponal	35	7.6	NMP	24	0.76
Ethanol	27	6.64	Aniline	34	0.97
DMSO	14	2.87	Sulfolane	19	0.69
EG	24	4.63	Furfural	21	0.72
Methanol/Methyl Acetate					
DMSO	13	1.05			
EG	18	1.11			
2-Methoxyethanol	17	0.98			

Table 4. Design parameters of the identified best solvent for the four separation systems.

		Acetone/ chloroform	Acetone/ methanol	Benzene/ cyclohexane	Methanol/ methyl acetate
Best identified solvent		DMSO	DMSO	Sulfolane	2-methoxyethanol
F_{AB} (equimolar), kmol/h		100	540	100	100
T1	N_1	36	41	25	49
	$N_{1,f}$	13	27	13	37
	$N_{1,s}$	3	3	2	6
T2	N_2	13	19	13	23
	$N_{2,f}$	4	14	4	8
F_s, kmol/h		111	399.6	88	263

3.1.4 Conclusions

This study presents a simple and reliable short-cut evaluation method to assist in solvent selection for solvent-based distillation. The proposed method was applied to four different extractive distillation systems. By incorporating process properties into the solvent ranking algorithm, the solvent exhibiting the best process performance in terms of lower capital and utility costs was identified. The evaluation results were validated by a rigorous design approach where the key operating parameters are optimally designed. Both the solvent evaluation and the

optimized process results demonstrated that DMSO, DMSO, sulfolane, are the best solvent for separating acetone/chloroform, acetone/methanol, and benzene/cyclohexane azeotrope systems, respectively. Although the FSES model gives imperfect ranking order for these azeotrope systems, this model could provide efficient preliminary evaluation for solvent selection before performing rigorous simulation and optimization. Especially this model could apply in process synthesis for selecting the 'best' solvent for separating azeotrope mixtures.

3.2 Hybrid Distillation Design

Figure 6 shows the relationship between normalized separation driving force and distillation reboiler duty as a function of feed concentration for different binary systems. In Figure 6, the driving force is defined as the concentration difference between the two phases, thus representing the ease of separation. The distillation reboiler duty linearly increases with the product purity but exponentially increases after a certain point. In most cases, around 40% of energy is used to purify the product from 90% to 99.8%. This indicates that the distillation may be efficient in a certain composition region but may not be efficient enough for high-purity product separation. As the distillation/membrane maximum driving forces are located at different positions in the product composition space, the separation can ideally be divided into two regions where Region I is more efficient for distillation and Region II is more efficient for membrane separation. Tula et al. (2017) integrated distillation with membrane and adsorption for C4/C5 isomers and methanol/water separation. They determined the boundary (switching composition) of Region I and II by maintaining a reasonable separation driving force through the whole column. O'Connell et al. (2019) further applied this idea for ethylbenzene/styrene hybrid separation. The switching composition was determined by analyzing the trade-off between maximum membrane price and payback time. However, the membrane permeability is a function of inlet conditions, such as

pressure, temperature, and composition (Figure 7), which influence the additional membrane investment. Therefore, the relationship of these parameters with membrane selectivity and permeability must be considered when determining the switching composition and the corresponding operating/design parameters for hybrid distillation design. Additionally, combining a membrane with an existing distillation column, initially designed for directly separating the mixture without membrane assistance, may result in underperforming "overdesign", as the existing column is not designed and optimized for separating the mixture at new conditions. This may provide opportunities to improve the process throughput. Hence, it is also crucial to analyze the impact of applying hybrid distillation for column retrofitting. In summary, determining the optimal operating region is essential for designing an efficient new hybrid distillation process. To combine low energy-intensive separation techniques with an existing column with fixed column stages, one has to further analyze the distillation operability at new conditions.

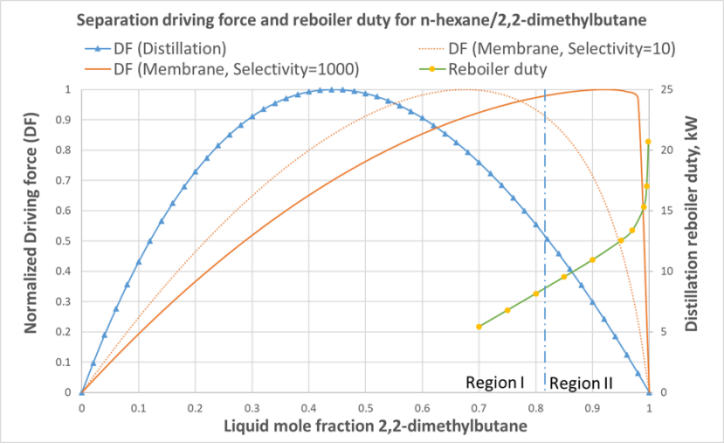

Figure 6. Separation driving force and distillation reboiler duty versus product purity.

As mentioned before, hybrid separation can be divided into two energy-efficient regions, where distillation can be used until a certain purity. Other energy-efficient separation techniques, like membrane, adsorption, etc., can be applied for final purification. Figure 8 gives the commonly

used hybrid configuration for the process industry, which is simple for construction and has lower investment costs than the other reported intensified configurations. In this work, we solve the hybrid distillation design problem with an integrated model combining distillation and membrane. Here, the distillation model is either based on a process simulator or a short-cut column model that uses Underwood, Fenske, Gilliland, and Kirkbride equations to estimate the distillation design/operating conditions. In this way, the optimal design parameters, such as membrane stages, switching composition, etc., represented as decision variables, can be identified by minimizing the system's annualized cost or maximizing the process profit.

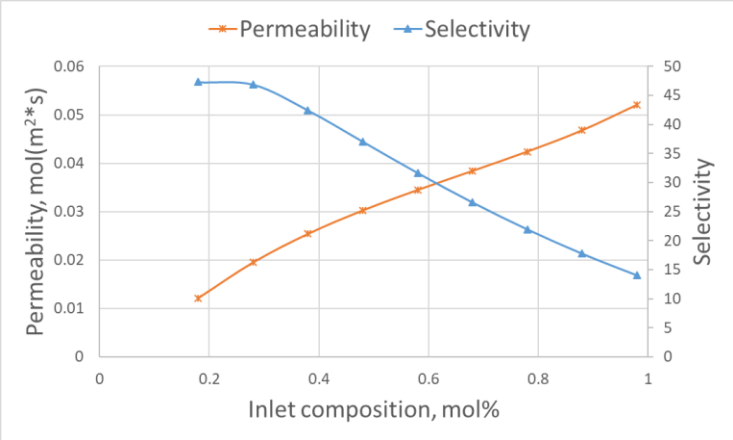

Figure 7. Relationship between membrane permeability and selectivity with inlet composition.

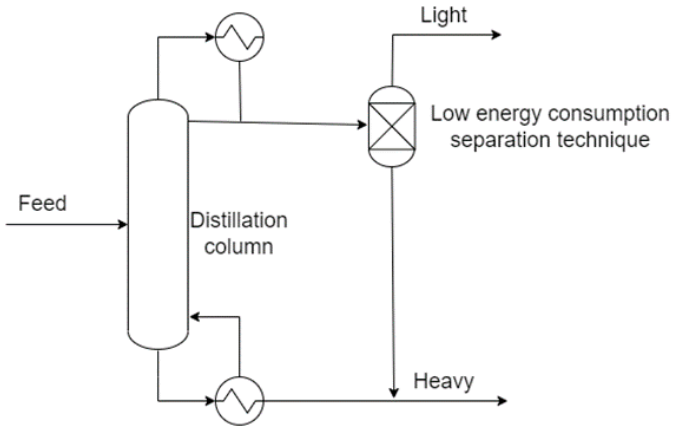

Figure 8. Hybrid distillation process scheme.

3.2.1 Problem Solution Strategies

Two solution approaches: simulation-based optimization (DFO) and mathematical optimization, are presented to solve the distillation hybrid design problem. The DFO approach intends to determine the efficient operating region for hybrid distillation by optimizing the process design/operating parameters, such as membrane inlet composition, membrane operating pressure, column stages, etc. The mathematical optimization aims to design and optimize the hybrid process and analyze the distillation "overdeign" effects at new operating conditions. Overall, based on these two approaches, the hybrid distillation performance, like energy consumption, capital cost, and column capacity, can be optimized. The two proposed approaches are explained next.

3.2.1.1 Simulation-based Optimization

The simulation-based optimization integrates the process simulator and a DFO algorithm to select operating/design variables. It is similar to the validation model explained in Section 3.1.2, except for different decision variables considered in hybrid distillation design.

3.2.1.2 Mathematical optimization

The formulation is based on a short-cut distillation model (Gadalla et al., 2003), involving mass/energy balance calculations at different operating/design conditions. As mentioned in Section 3.2, combining low energy-intensive separation techniques with an existing distillation column with a fixed number of stages may cause underperforming distillation. Therefore, in this model, two objectives: 1) total annualized cost that represents the additional investment cost because of adding low energy-intensive separation techniques and 2) process profit that relates to process capacity are considered. A generalized bi-objective nonlinear programming model (NLP) is formulated in Equations 3.16 – 3.21. The ε-Constraint method (Deb, 2011) is used to solve the bi-objective optimization problem, where a series of optimization problems are constructed by

transforming one objective (total annualized cost in this study) into a constraint. And these constrained optimization problems are solved using a global optimization solver, which was BARON v. 2020.4.14 for this study.

$$\min_{x,y} F_1 = f_1(x,q) \quad 3.16$$

$$\max_{x,y} F_2 = f_2(x,q) \quad 3.17$$

$$st.\, h(x,q) = 0 \quad 3.18$$

$$g(x,q) \leq 0 \quad 3.19$$

$$q = q(x) \quad 3.20$$

$$x \in R^+ \quad 3.21$$

Here, F_1 is the total annualized cost, F_2 is the profit, $g(x,q)$ denotes the hydraulic and purity constraints, q represents the variables such as column size and heat duty, that are estimated based on decision variables x, and $h(x,q)$ denotes the thermodynamic model and distillation model.

The short-cut distillation model considers near-ideal mixtures; therefore, constant relative volatility is used to calculate the vapor-liquid phase equilibrium. As mentioned, the problem incorporates the "overdesign" effect of the original distillation column. The hydraulic analysis is performed at the new operating conditions. Equations 3.22 – 3.33 are used to calculate the column mass balance, and the energy balance is further calculated based on the column/stage enthalpy equations.

$$R_{min} = \frac{x_{d,lk} - x_{f,lk}}{y_{f,lk} - x_{f,lk}} \quad 3.22$$

$$\frac{N_R}{N_S} = \left[\left(\frac{B}{D}\right)\left(\frac{x_{f,hk}}{x_{f,lk}}\right)\left(\frac{x_{b,lk}}{x_{d,hk}}\right)^2\right]^{0.206} \quad 3.23$$

$$Bx_{b,hk} = F_f R_{HK} x_{f,hk} \quad 3.24$$

$$F_f = B + D \quad 3.25$$

$$Dx_{d,lk} = F_f R_{LK} x_{f,lk} \quad 3.26$$

$$N = N_R + N_S \quad 3.27$$

$$x_{f,lk} = Dx_{d,lk} + B(1 - x_{b,hk}) \quad 3.28$$

$$\phi_{Fenske} = (\frac{R_{LK}}{1-R_{LK}})(\frac{R_{HK}}{1-R_{HK}}) \quad 3.29$$

$$\phi_{Fenske} = (\frac{\alpha_{LK}}{\alpha_{HK}})^{N_{min}} \quad 3.30$$

$$N_{min} = N\eta(1-\psi_{Gill}) - \psi_{Gill} \quad 3.31$$

$$\xi = \frac{R-R_{min}}{R+1} \quad 3.32$$

$$\psi_{Gill} = 1 - e^{\left[(\frac{1+54.4\xi}{11+117.2\xi})(\frac{\xi-1}{\xi^{0.5}})\right]} \quad 3.33$$

F_f is the feed flowrate (kmol/h), B is the bottom flowrate (kmol/h), D is the distillate flowrate (kmol/h), x and y are liquid and vapor composition (lk: light key, hk: heavy key, f: feed, d: distillate, b: bottom), N is the column stages, N_R and N_S are the numbers of stages in rectifying and stripping section, α is the relative volatility, R_{min} is the minimum reflux ratio, R R denotes the reflux ratio, R_{lk} and R_{hk} are the recovery rate of light/heavy key components, N_{min} is the minimum number of stages, η is the column efficiency. $\phi_{Fenske}, \psi_{Gill}$ and ξ denote the intermediate variables for Fenske and Gilliland equations.

Equations 3.34 – 3.41 are used to perform the column hydraulic analysis to ensure normal operation of the distillation column. Equations 3.34 – 3.37 assume that the liquid and vapor volume flowrates are constant in rectifying and stripping sections. Equations 3.38 – 3.41 are used to calculate the required column diameter at different conditions with the liquid and vapor volume flowrates in each section.

$$L_R = RD \quad 3.34$$

$$V_R = (R+1)D \quad 3.35$$

$$L_S = L_R + qF_{f,v} \quad 3.36$$

$$V_S = V_R - (1-q)F_{f,v} \quad 3.37$$

$$C_{sb} = a - b \times e^{\left(-\frac{c}{F_{LV}}\right)} \quad 3.38$$

$$F_{LV} = \frac{L}{V}\sqrt{\frac{\rho_V}{\rho_L}} \quad 3.39$$

$$U_{max} = C_{sb}\sqrt{\frac{\rho_L - \rho_V}{\rho_V}} \quad 3.40$$

$$D_T = \sqrt{\frac{4V}{\pi U_{des}(1 - D_C)}} \quad 3.41$$

In Equations 3.34 – 3.41, $a, b,$ and c are the constant coefficients ($a = 0.365, b = 0.359, c = 0.364$) for calculating the capacity factor C_{sb}, L_R, V_R, L_S and V_S are liquid and vapor volumetric flowrates (m^3/s) for the rectifying and stripping sections, respectively, ρ_L and ρ_V are the liquid and vapor densities (kg/m^3), q represents the feed conditions ($q = 0$ (saturated vapor), $q = 1$ (saturated liquid)), F_{LV} is the flow parameter, D_c is the ratio of downcomer area to the cross-sectional area of stage (≈12%), U_{max} is the flooding velocity (m/s), $U_{des}$is the lower bound of design velocity, which is 70 - 80% of U_{max}, and D_T is the required tray diameter.

3.2.3 Results and Discussion of Case Studies

The presented approaches were applied and illustrated through three case studies involving methanol/methyl acetate, benzene/cyclohexane, and methanol/water separation.

3.2.3.1 Methanol/methyl acetate separation

The binary azeotrope mixture, methanol (33 kmol/h) and methyl acetate (67 kmol/h) at 1 atm, 20°C, is separated, where the required product purities are 99.5 mol% of methyl acetate and 98.5 mol% of methanol. Based on the literature, this separation is primarily achieved by extractive distillation, where different solvents are discussed by Gerbaud et al. (2019). Other separation techniques, such as zeolite-based membrane (Dong et al., 2020), may be economically feasible for small inlet flowrates. Here, the hybrid extractive distillation membrane system is considered, where the extractive distillation is applied to separate the azeotrope mixture to a certain purity (Region I), and the membrane is applied for the final purification step (Region II). The detailed process flow scheme is shown in Figure 9. The binary mixture and the best solvent 2-methoxyethanol (refer Section 3.1.3) are first fed into an extractive distillation column (T1) for

separation. The bottom stream, which includes methanol and solvent, is sent to the second distillation column (T2) to recover the solvent and get the methanol product. The distillate stream is sent to a pump unit before entering the membrane for separation because the membrane inlet pressure affects its permeability and selectivity. After membrane separation, the retentate stream has 99.5 mol% of methyl acetate. The methanol-rich stream (permeate) either mixes with the final product methanol or passes through the second membrane system before mixing. As the membrane separation driving force is the vapor pressure difference of the permeate compound between the permeate and feed side, we specify the total pressure at the permeate side as near vacuum (2 kPa). The permeate stream, which is near vacuum, passes through a compressor and heat exchanger to maintain the same inlet pressure/temperature as the first membrane before entering the second stage membrane. Also, the permeate stream is heated/compressed before mixing with the methanol product to keep the same outlet conditions as the distillation column. The membrane model (Equation 3.42 – 3.48 and Table. 5) presented by Dong et al. (2020) is used to estimates the membrane permeability and selectivity.

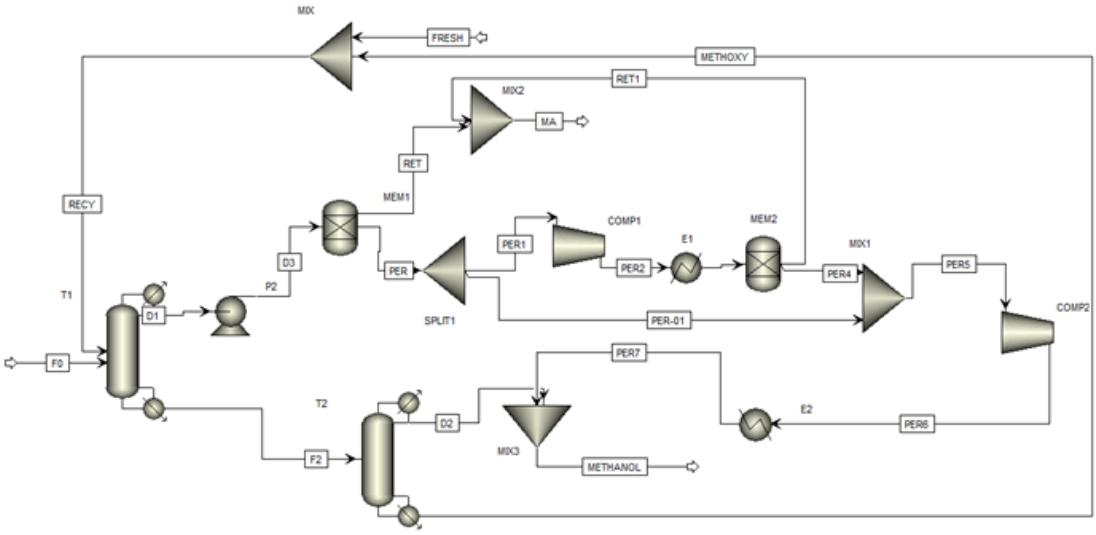

Figure 9. Process scheme of the methanol/methyl acetate hybrid separation process.

$$J_i = L_i\left(r_{1,i}^s x_{1,i}^s - \frac{p_2 x_{2,i}^s}{p_{v,i}}\exp\left[\frac{v_i(p_{v,i}-p_1)}{RT}\right]\right) \quad 3.42$$

$$J_j = L_j\left(r_{1,j}^s x_{1,j}^s - \frac{p_2 x_{2,j}^s}{p_{v,j}}\exp\left[\frac{v_j(p_{v,j}-p_1)}{RT}\right]\right) \quad 3.43$$

$$\log_{10}(p_v) = A - \frac{B}{T+C} \quad 3.44$$

$$\ln r_i = -\ln(x_i + \Lambda_{ij}x_j) + x_j\left[\frac{\Lambda_{ij}}{x_i+\Lambda_{ij}x_j} - \frac{\Lambda_{ji}}{x_j+\Lambda_{ji}x_i}\right] \quad 3.45$$

$$\ln r_j = -\ln(x_j + \Lambda_{ji}x_i) + x_i\left[\frac{\Lambda_{ji}}{x_j+\Lambda_{ji}x_i} - \frac{\Lambda_{ij}}{x_i+\Lambda_{ij}x_j}\right] \quad 3.46$$

$$\beta_{i/j} = \frac{J_i/J_j}{x_{1,i}/x_{1,j}} \quad 3.47$$

$$x_{2,i}^s = \frac{J_i}{J_i+J_j} \quad 3.48$$

x, molar fraction; r, activity coefficient; μ, chemical potential; p, pressure (Pa); s, solution phase; 1 and 2, parameters on the feed and permeate sides; J, permeation flux (mol m^{-2} s^{-1}); v, molar volume (m^3 mol^{-1}) of the component; R and T, gas constant (8.314 J mol^{-1} K^{-1}) and temperature (K); P_v, saturation vapor pressure of the component (kPa); β, separation factor;

Table 5. Parameters for methanol (i)/methyl acetate (j) membrane permeation model.

L_i	L_j	A_i	B_i	C_i	A_j	B_j	C_j	Λ_{ij}	Λ_{ji}
0.063	0.0014	7.720	1574.99	-34.29	7.065	1157.63	-53.42	0.6977	0.4733

In this problem, distillation column stages, stream inlet stage, membrane inlet pressure, membrane stages, distillation switching composition, and solvent flowrate are the decision/input variables for the process simulation. The initial lower and upper bounds of these decision variables are listed in Table 6. The simulation results, including heat duty, column stages, column diameter, membrane inlet flowrate, inlet/outlet temperature of the heat exchanger, and inlet/outlet pressure of pump/compressor, are used to calculate the process annualized cost, which is the objective function. This way, the decision variables are optimized by minimizing annualized cost.

Table 6. Initial lower/upper bound of the decision variables for methanol/methyl acetate hybrid extractive distillation.

	Lower bound	Upper bound
Stages, T1	25	50
Feed inlet stage, T1	15	41
Solvent inlet stage, T1	2	25
Solvent flowrate (kmol/h)	50	350
Membrane inlet pressure (kpa)	302	1,000
Membrane stage	1	2
Stages, T2	10	35
Feed inlet stage, T2	2	25
Distillate composition (mol%), T1	85	99.1
Distillate composition (mol%), T2	95	99

Table 7 gives the distillation and its DFO hybrid configuration design results. The extractive distillation system produces 99.5 mol% of methyl acetate by adding 263.27 kmol/h of solvent into the distillation column, which has 49 stages. It requires 23 stages for the second column to produce 98.5 mol% of methanol. However, for the hybrid system, the extractive distillation column, which has 37 stages, is applied to separate the binary mixture into 90.29 mol%, and the following two stages of membrane with inlet pressure at 809.73 kPa are applied to get 99.5 mol% of methyl acetate. This hybrid system requires 157.75 kmol/h of solvent, 40% lower than extractive distillation. Additionally, the hybrid separation could get the same product with the same annualized cost (3% difference) but consumes 25% less energy.

3.2.3.2 Benzene/cyclohexane separation

The binary mixture of benzene (50 kmol/h) and cyclohexane (50 kmol/h) at 1 atm and 78°C is separated, where the cyclohexane and benzene products are required to be at 99.5 mol% purity. Because these two components form an azeotrope with a composition of 55 mol% benzene at atmospheric pressure, extractive distillation is the most common technique to perform the separation. The potential organic solvents such as aniline, sulfolane, furfural, etc., are presented by Gerbaud et al. (2019). Other separation methods, such as PVA-based pervaporation membrane

(Lu et al., 2006), are also economically feasible for small inlet flowrates. Therefore, the hybrid extractive distillation system, which is similar to the methanol/methyl acetate case, is considered in this case study. The detailed process flow scheme of the hybrid extractive distillation system is shown in Figure 10. The process is similar to the methanol/methyl acetate case study, except for the best solvent sulfolane (refer to Section 3.1.3) used for extractive distillation. Because the membrane model (Equations 3.49 – 3.50) is based on the regression of experimental data tested at a fixed temperature, the distillate stream is heated/cooled to 50 °C before entering the membrane for separation.

Table 7. Design/operation parameters for methanol/methyl acetate extractive distillation and hybrid distillation.

	Extractive distillation	Extractive distillation membrane
Stages, T1	49	37
Feed inlet stage, T1	37	25
Solvent inlet stage, T1	6	9
Distillate composition (mol%), T1	99.5	90.29
Reboiler duty (GJ/h), T1	8.69	6.97
Solvent flowrate (kmol/h)	263.27	157.75
Membrane inlet pressure (kpa)	-	809.73
Membrane stage	-	2
Stages, T2	23	27
Feed inlet stage, T2	8	14
Distillate composition (mol%), T2	98.5	98.54
Reboiler duty, T2	3.76	2.60
Total annualized cost (10^6 \$/y)	0.98	1.1

In this problem, distillation column stages, stream inlet stages, membrane stages, distillation switching composition, and solvent flowrate are the decision/input variables for optimization/process simulation. The initial lower and upper bounds of these decision variables are listed in Table 8. The optimization model is the same as the model presented in the methanol/ methyl acetate case study.

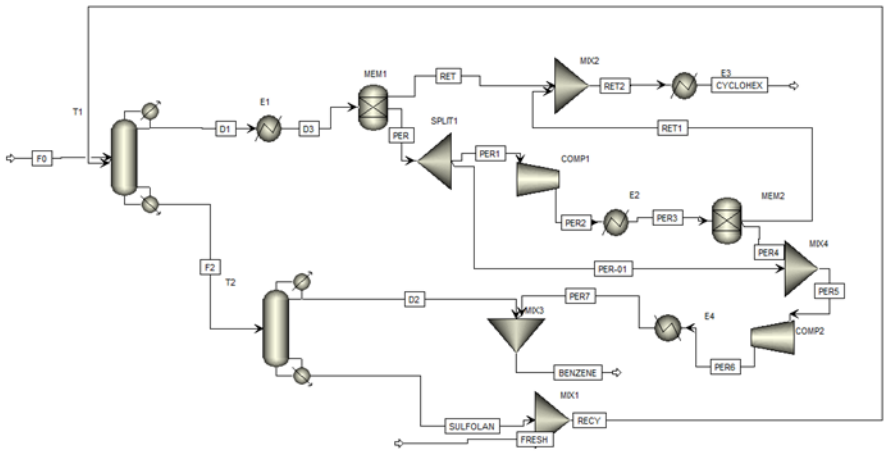

Figure 10. Process scheme of the benzene/cyclohexane hybrid separation process.

$$J_t = 0.58x_b + 22.8, R^2 = 0.99 \quad (3.49)$$

$$\beta_{b/c} = -650{,}136\ln(x_b) + 304.573, R^2 = 0.99 \quad (3.50)$$

x, mass fraction; J_t, total permeation flux (g m^{-2} h^{-1}); β, separation factor; b, benzene; c, cyclohexane;

Table 8. Initial lower/upper bound of the decision variables for benzene/cyclohexane hybrid extractive distillation.

	Lower bound	Upper bound
Stages, T1	25	45
Feed inlet stage, T1	15	40
Solvent inlet stage, T1	2	22
Solvent flowrate (kmol/h)	50	250
Membrane stage	1	2
Stages, T2	15	35
Feed inlet stage, T2	5	25
Distillate composition (mol%), T1	75	99.1
Distillate composition (mol%), T2	99.4	99.7

Table 9 gives the distillation and its DFO hybrid configuration design results. The extractive distillation system produces 99.5 mol% of cyclohexane by adding 94.85 kmol/h of solvent into the distillation column, which has 23 stages. It requires 19 stages for the second column to produce 99.5 mol% of benzene. For the hybrid system, the extractive distillation column, which has 25 stages, is applied to separate the binary mixture into 99.1 mol%, and the

following two stages of membrane are applied to get 99.5 mol% of cyclohexane. This hybrid system requires 90.08 kmol/h of solvent, which is only 5% lower than extractive distillation. Also, compared to extractive distillation, the hybrid separation has a 59% higher annualized cost but little energy cost savings. This is because the membrane has low permeability, and the membrane inlet composition has to be high enough to achieve the separation target, which leads to little energy savings and higher investment costs.

Table 9. Design/operation parameters for benzene/cyclohexane extractive distillation and hybrid distillation.

	Extractive distillation	Extractive distillation membrane
Stages, T1	23	25
Feed inlet stage, T1	12	15
Solvent inlet stage, T1	2	7
Distillate composition (mol%), T1	99.5	99.1
Reboiler duty (GJ/h), T1	3.11	3.24
Solvent flowrate (kmol/h)	94.85	90.08
Membrane stage	-	2
Stages, T2	19	15
Feed inlet stage, T2	7	13
Distillate composition (mol%), T2	99.5	99.51
Reboiler duty, T2	5.64	5.59
Total annualized cost (10^6 \$/y)	0.64	1.02

3.2.3.3 Methanol/water separation

In this case study, the binary mixture of methanol (315.37 kmol/h) and water (1026.63 kmol/h) at 2.5 atm and 107°C is separated, and the methanol and water product purity requirements are 99.9 mol%. A base case existing distillation column design (Turton et al., 2008), which has 32 stages (feed stage at 12) with 60% of stage efficiency and 36.9 GJ/h of reboiler duty, has been used to perform this separation task. Here, the hybrid distillation system, which adds an energy-efficient separation technique such as membrane and adsorption to the base case distillation column, is considered. This hybrid system uses distillation to separate the binary mixture into certain purity (Region I) so that the following membrane/adsorption is applied to perform the final purification

(Region II). The simulation-based optimization is used to determine the optimal operating/design parameters for this retrofitting hybrid distillation design problem, and mathematical optimization is further used to analyze the "overdesign" effects of the distillation at new operating conditions and investigate the potential of capacity enhancement.

3.2.3.3.1 Simulation-based optimization applied to retrofitting methanol-water distillation column

A zeolite-based vapor permeation membrane (Okamoto et al., 2001; Sommer and Melin, 2005) (Equations 3.51 – 3.52 and Table 10) and a zeolite molecular sieve adsorbent (Gabruś et al., 2015) (Equations 3.53 – 3.56 and Table 11) are used in this hybrid distillation system. Their process schemes are shown in Figures 11 and 12, which have similar configurations. The binary mixture (S1) is first fed into the distillation column (B1) for separation. The distillate stream S2, containing water and methanol component, is sent to the membrane/adsorption system to obtain the methanol product. The water-rich stream (permeate/adsorbed) either mixes with the water product S11 from the bottom of the distillation column or passes through the second membrane/adsorption system before mixing. The water product stream S21 requires 99.9 mol% purity. For the distillation-membrane process, the permeate stream is near vacuum, and it has to pass through a compressor/pump (B13, B3) and heat exchanger (B16, B6) to maintain the same inlet pressure/temperature as the first membrane (B4) before the second stage membrane (B7) separation. For the distillation-adsorption process, to ensure the vapor phase adsorption, a heat exchanger (B2, B13), which heats the adsorption inlet mixture to 101 °C, is included in the adsorption system (B4, B7). For both processes, to maintain the same outlet conditions of the products as the original base case distillation column, the outlet mixture from the membrane/adsorption system has to be heated/compressed.

In this problem, distillation switching composition and the number of membrane stages are the decision/input variables for the process simulation. The initial lower and upper bounds of these decision variables are listed in Table 12. The simulation results provide key parameters such as heat exchanger heat duty, membrane/adsorption inlet flowrate, heat exchanger inlet/outlet temperatures, and pump/compressor inlet/outlet pressures. These parameters are utilized to calculate the process annualized cost, which serves as the objective function. The details of the optimization model are similar to the model presented in the methanol/ methyl acetate case study.

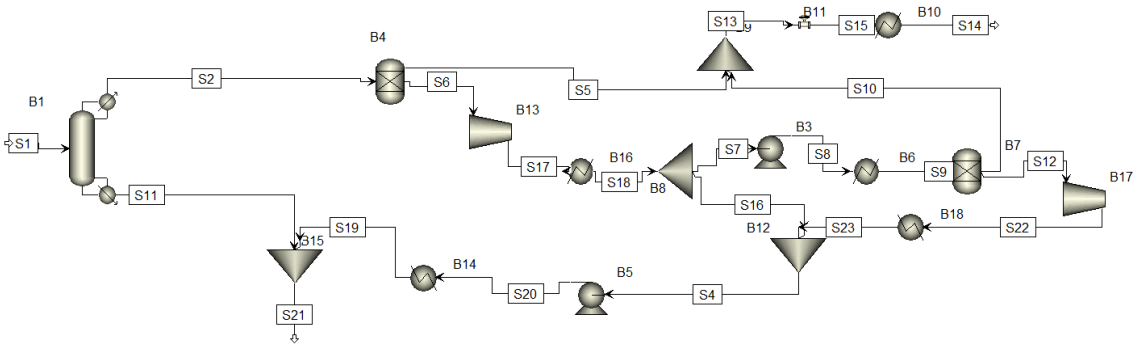

Figure 11. Process scheme of the hybrid distillation-membrane/adsorption separation process.

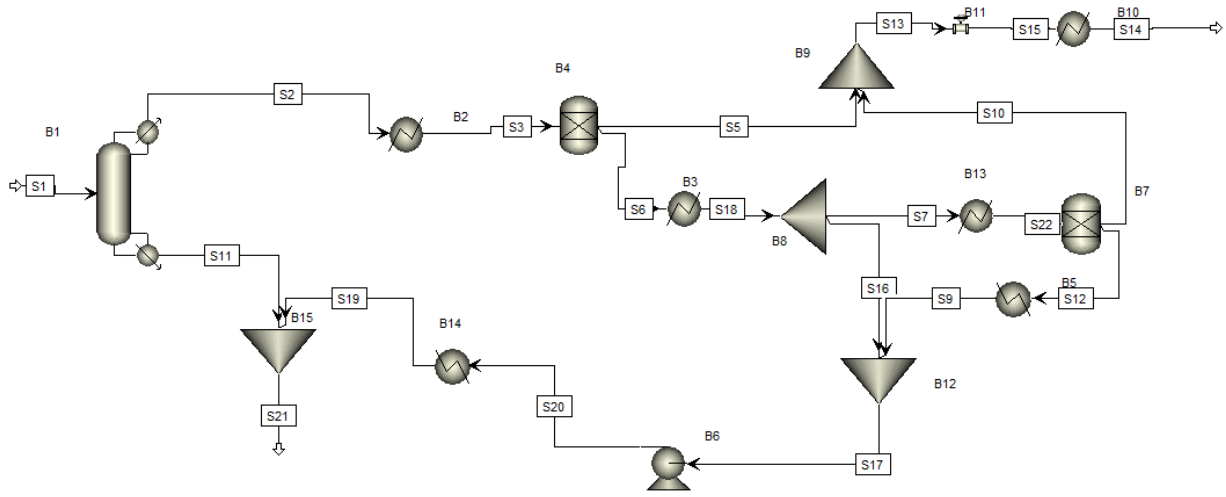

Figure 12. Process scheme of the hybrid distillation-adsorption separation process.

$$J_w = Q_{w,ref}\exp\left[\frac{E_w}{R}\left(\frac{1}{T_{ref}}-\frac{1}{T_F}\right)\right]\left(x_{w,F}P_F - y_{w,P}P_P\right) \quad 3.51$$

$$J_m = Q_{M,ref}\exp\left[\frac{E_M}{R}\left(\frac{1}{T_{ref}}-\frac{1}{T_F}\right)\right]\left(x_{M,F}P_F - y_{M,P}P_P\right) \quad 3.52$$

P_P, total pressure at permeate side (bar); y_P, mole concentration at permeate side; x_F, mole concentration at feed side; J, permeability (kg/m^2*h); T_F, feed temperature (K); P_F, feed pressure (Kpa); T_{ref}, reference temperature (353.15K); R, gas constant (8.314 kJ kmol^{-1} K^{-1}); m, methanol; w, water;

Table 10. Parameters for methanol/water vapor permeation model.

Component	Permeance, Q_ref (kg/m2*h*bar)	Activation energy, E (kJ/kmol)
Water (w)	10.39	12.6
Methanol (m)	0.003	8.3

$$q = q_s\frac{b*p^n}{1+b*p^n} \quad 3.53$$

$$q_s = a_0 + \frac{a_1}{T+273}+\frac{a_2}{(T+273)^2} \quad 3.54$$

$$b = e^{\left(b_0+\frac{b_1}{T+273}+\frac{b_2}{(T+273)^2}\right.} \quad 3.55$$

$$n = n_0+\frac{a_1}{T+273} \quad 3.56$$

T, operating temperature (°C); P, partial vapor pressure (Pa); q, adsorption capacity (mol/Kg); q_s, saturated adsorption capacity (mol/Kg);

Table 11. Parameters for methanol/water adsorption model.

$\mathbf{a_0}$ (mol/kg)	$\mathbf{a_1}$ (1/k)	$\mathbf{a_2}$ (1/k)	$\mathbf{b_0}$ (1/Pa)	$\mathbf{b_1}$ (1/k)	$\mathbf{b_2}$ (1/k)	$\mathbf{n_0}$	$\mathbf{n_1}$ (1/k)
0.24486	-29.161	743.36	-10.659	1969.4	933.58	-0.09294	340.56

Table 12. Initial lower/upper bound of the decision variables.

	Lower bound	Upper bound
Membrane stage	1	2
Top switching (methanol), mol%	75	99.5
Bottom switching (water), mol%	90	99.95

Table 13 gives the identified optimal design/operating parameters for methanol/water hybrid distillation. The optimal top switching composition for membrane and adsorption hybrid is 88 mol% and 97 mol% of methanol, respectively. Only one membrane stage is required for membrane hybrid separation, but two for adsorption when the adsorbent has lower selectivity. Because the membrane price is higher than the adsorbent, the membrane hybrid system has 24% higher annualized cost than the adsorption hybrid system. Compared with the base case distillation, the hybrid distillation yields at least 30% of energy savings.

Table 13. Design/operation parameters for methanol/water hybrid distillation separation.

	Vapor permeation hybrid	Adsorption hybrid	
		Selectivity = 500	Selectivity = 1000
Top switching (methanol), mol%	88.4%	97.58%	96.68%
Bottom switching (water), mol%	99.90%	99.91%	99.95%
Membrane stage	1	2	1
Reboiler duty (GJ/h)	22.66	23.66	23.51
Annualized cost (10^6 $/y)	1.95	1.54	1.49

3.2.3.3.2 Mathematical optimization applied to retrofitting methanol-water distillation column

According to the results obtained by the simulation-based optimization approach, the distillation membrane hybrid could significantly save distillation energy cost. Furthermore, it may allow increasing the capacity of the original distillation column as it is designed to purify the mixture into 99.9 mol% but is used only for 88.4 mol% at hybrid conditions. Mathematical

optimization is applied here to investigate this potential capacity increase effect of the methanol/water hybrid distillation membrane system. A schematic depiction of the distillation-membrane process is shown in Figure 13. The binary mixture is first fed into an existing distillation column for separation. Then, a membrane system is used to purify the distillate. In the process, a compressor is used to keep the product in the same conditions as the original distillation column. The optimal decision variables, distillation top/bottom composition and process flowrate, are determined by transforming the second objective function: total annualized cost into a constraint and maximizing the process profit. The detailed model is included in Appendix 1.

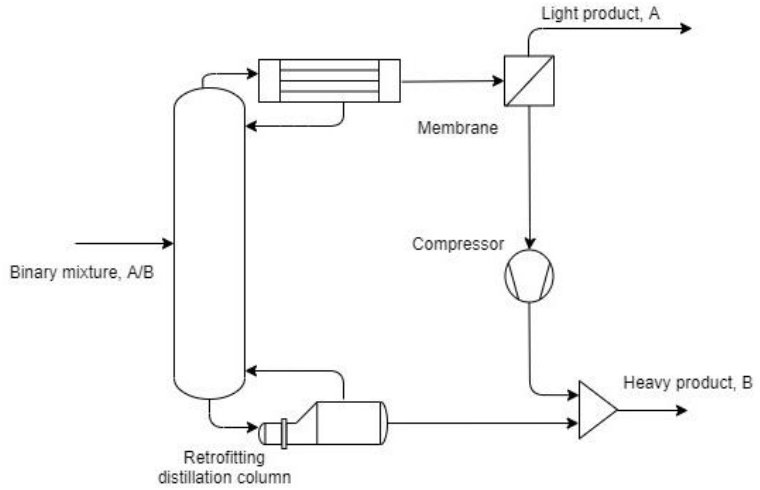

Figure 13. Distillation-membrane process scheme for mathematical optimization.

Table 14 lists example solutions of the optimization problem, and the resulting Pareto front is shown in Figure 14. As can be seen in Table 14, the annualized cost and profit vary as switching composition and process flowrate change. When the annualized cost is lower than $3.2 million/year, the optimization results indicate that the annualized cost and profit increase along with the increase of capacity with the same switching compositions. This is because separating the binary mixture into 92% purity, rather than 99.9%, leads to a lower column reflux ratio, which reduces column internal liquid/vapor flowrate. This provides the opportunity to increase the

process throughput by up to 20%. However, when the annualized cost is higher than $3.2 million/year, both objective values increase with increasing capacity and decreasing switching composition. This is because the process has to further reduce switching composition to improve the column capacity. As can be seen from Figure 14, profit increases faster when annualized cost is lower than $3.2 million/year. This indicates that with the same cost increment, one can achieve a higher profit increase in this region. Therefore, a switching composition of 92.4 mol% is suggested for this hybrid operation, which can achieve up to 20% capacity improvement.

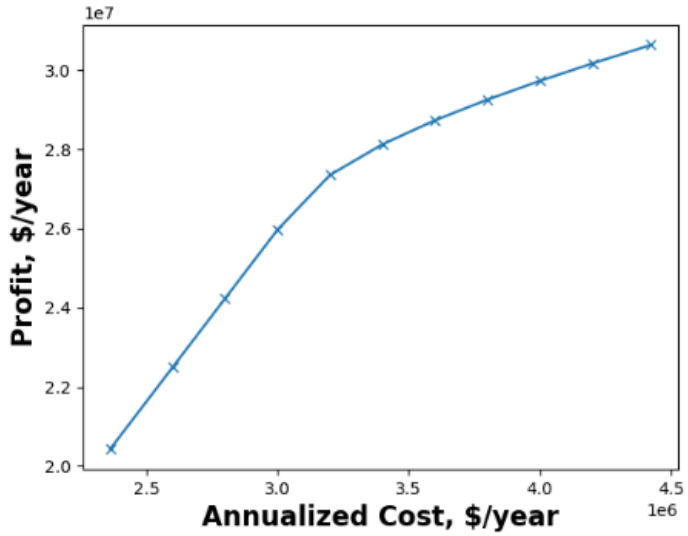

Figure 14. Pareto front of the bi-objective optimization results.

Table 14. Example bi-objective optimal solutions for methanol/water retrofitting hybrid distillation at different cases.

	Case 1	Case 2	Case 3	Case 4	Case 5	Case 6
Profit, $10^7 \$/year$	3.1	2.9	2.7	2.6	2.4	2.2
Annualized cost, $10^6 \$/year$	4.4	3.8	3.2	3	2.8	2.6
Top switching composition	0.75	0.81	0.9	0.92	0.92	0.92
Capacity improvement	35%	31%	25.4%	21.3%	15.7%	9.2%

3.2.4 Conclusions

Distillation is energy-intensive for separating both simple and azeotrope mixtures, especially for separation tasks that require high-purity products. However, within a certain

composition, distillation is thermally efficient. Thus, combining distillation with other energy-efficient separation techniques is a potential way to improve the distillation separation efficiency. To determine the optimum operating region of distillation and the other separation techniques, two design approaches, simulation-based optimization, and mathematical optimization, are presented. The simulation-based optimization strategy utilizes readily available process simulation tools to perform the process simulation and a derivative-free optimization (DFO) solver to decide the input design/operating variables. A solving algorithm that includes inner DFO optimization, and outer lower and upper bounds updating, is developed so that stable optimal decision variables in the hybrid distillation process, such as column stages, solvent flowrate, column feed stage, and column switching composition, etc., can be determined without the influence of initial boundaries. The mathematical optimization utilizes the short-cut distillation model to determine the optimal decision variables, primarily focusing on exploring the potential of capacity enhancement for applying hybrid distillation to an existing column.

These two design approaches are applied to design hybrid separation systems for separating methanol/methyl acetate, benzene/cyclohexane, and methanol/water mixtures. In the methanol/methyl acetate case study, the optimal operating conditions for hybrid extractive distillation is to purify methyl acetate into 90 mol% through distillation. And then, pure methyl acetate is generated after passing through two stages of membrane. Compared with extractive distillation, the hybrid system has 40% and 25% of solvent and energy usage savings. In the benzene/cyclohexane case study, the hybrid extractive distillation does not provide any energy savings because of low membrane permeability, which indicates that this hybrid extractive distillation may not be economical when the membrane permeability is too low. In the methanol/water retrofitting separation case study, the simulation-optimization approach is first

applied to identify the efficient operating region, which revealed that the switching composition is 88.4 mol% for the distillation membrane hybrid system and around 97 mol% for the distillation adsorption hybrid system. Also, it verified that the adsorption selectivity may influence the decision of the switching composition and adsorption stages. Hybrid distillation systems yield at least 30% energy savings compared to the base case distillation. The mathematical optimization is further applied to investigate the capability of capacity improvement when using hybrid separation for an existing column that has fixed number of stages, and the results prove that applying hybrid distillation could efficiently improve 20% of column throughput.

This study offers valuable insights into hybrid process design, highlighting its potential for energy savings and its impact on distillation column performance. The hybrid distillation approach demonstrates significant benefits in separating both azeotropes and simple mixtures, such as reduced energy consumption, decreased solvent usage, and enhanced capacity. However, it is essential to acknowledge that the application of hybrid distillation is constrained by factors such as membrane/adsorption selectivity/permeability.

Chapter 4 – **An Integrated Framework for Sustainable Process Design**

This chapter presents a three stages systematic process synthesis framework, integrating different reaction pathways and innovative separation techniques. The three stage integrated process synthesis framework is shown in Figure 15. In stage one, the input is the target compound (raw materials or products) so that the forward synthesis or retrosynthesis model can be used to generate multiple novel reaction pathways. The reaction synthesis stage aims to identify novel reaction pathways with lower environmental impact and capital/operating cost. In stage two, the downstream separation synthesis is applied to find its corresponding optimal process flowsheets. In stage three, different reaction pathways with their optimal process flowsheets will be designed and verified. In this way, by only giving raw materials or target products, one can find an optimal reaction pathway and its process flowsheet.

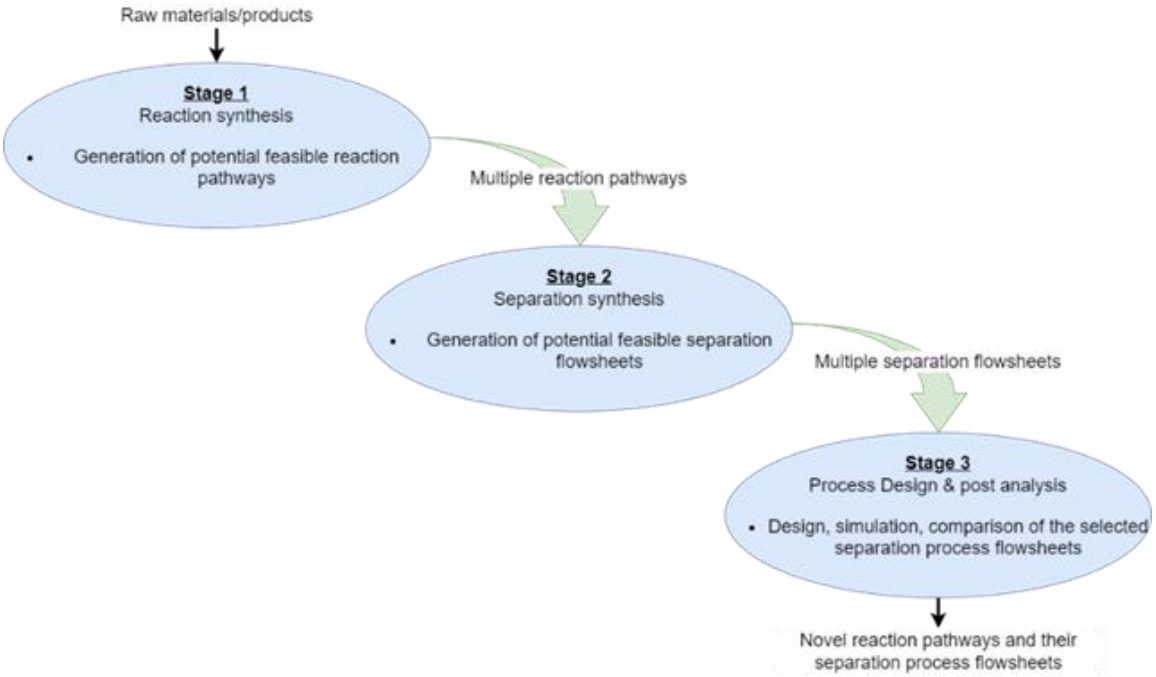

Figure 15. Integrated framework for process synthesis problem.

Section 4.1 presents a feasible reaction pathway generation and screening algorithm. Section 4.2 discusses the detailed separation synthesis model based on the extension of the synthesis algorithm presented by Tula et al. (2015), which can be applied to both new process design and retrofitting problems. Section 4.3 gives four case studies using the proposed three stage synthesis framework.

4.1 Reaction Synthesis

The reaction synthesis was initially developed to assist the research of organic chemistry and the pharmaceutical industry. Here, one can also apply the developed reaction synthesis programs to process synthesis problems. The general framework is shown in Figure 16. Firstly, a specific target product or material is given to the reaction synthesis model. In step RS1, a constructed retrosynthesis or forward synthesis model is applied to generate multiple feasible reaction pathways. In this paper, a machine learning based reaction synthesis tool is used to generate all the potential reaction pathways for a given component as it has demonstrated better prediction performance than other models (Segler and Waller, 2017b). Generally, the input chemical molecules are converted into molecular descriptors, which contain the atomic information, number of neighboring atoms and types of chemical bonds, etc. Therefore, the developed machine learning classification method (deep neural network) can read the input information and identify the associated reaction rules. In this way, all potential reaction pathways can be generated based on these reaction rules. The predicted pathways and the added external literature pathways are passed to step RS2. In step RS2, a rule-based screening method is used to select the optimal reaction pathways. The screening method includes the following rules/conditions:

1) Viable reactants that have a good production pipeline.

2) Reaction pathways that have lower absolute reaction enthalpy values.

3) Toxicity for reaction *i*: $LC50_i = min\{LC50_{i,j}\}$, *j* represents component *j*. Reaction pathways that have lower toxicity.

4) Separation driving force of reaction components *i*: $DF_i = min\{DF_{ij}\} \times \prod_{j,k} DF_{jk}$ $(i: reactant; j,k(j \neq k): product)$ .Reactions that have a higher DF value are selected as they may be easier for separation.

5) Economic viability.

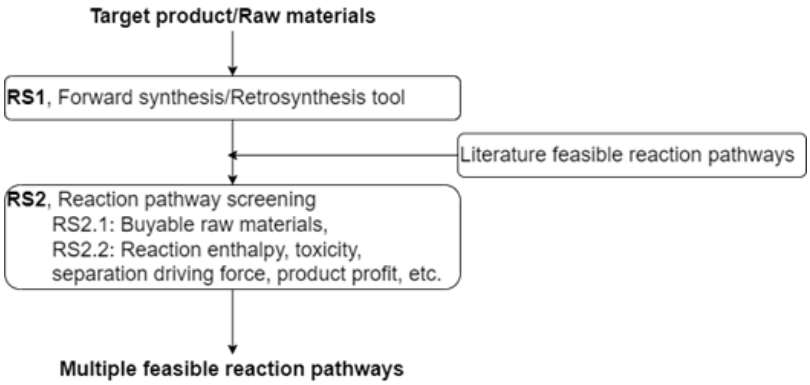

Figure 16. A general framework for reaction synthesis.

4.2 Separation Synthesis

In this section, the developed separation synthesis methodology for both new process design and retrofitting will be explained in detail with the help of work and data flow. Two major challenges need to be solved for the separation synthesis problem: separation techniques feasibility analysis, fast and efficient evaluation of generated process designs. Here, the thermodynamically based insights are employed to generate all the feasible separation techniques (search space). A generalized feasibility evaluation rule for hybrid/intensified techniques is developed and listed in Table 15, and the rules for conventional separation techniques are reported by Jaksland et al. (1995). A utility evaluation model based on enthalpy balance and the first principle model is

proposed to evaluate and screen the generated process designs. Top alternatives from the screening step are further analyzed based on sustainable and economic factors using rigorous models. Case studies of DMC, acrylic acid, cumene, and styrene production are used to illustrate the methodology. Sections 4.2.1 and 4.2.2 give a detailed description of the new process and retrofitting design framework.

Table 15. List of typical intensified/hybrid equipment and its feasibility evaluation rules.

Intensified & hybrid equipment	Feasibility evaluation
Dividing wall column	Near-ideal multi-component mixture (Asprion and Kaibel, 2010), distillate stream flowrate
Membrane-assisted distillation	Membrane selection, economically unviable if large permeate streams or sharp splits (Skiborowski et al., 2013)
Membrane crystallization	Membrane selection, melting point
Pressure-swing distillation	Vapor pressure is pressure sensitive (Babi and Gani, 2014)
Distillation crystallization	Relative volatility, melting point
Distillation adsorption	Adsorbent selection
Solvent-based (extractive, azeotropic) distillation	Solvent/entrainer properties, e.g. boiling point, formation of azeotrope, miscibility of the mixture, etc. (García-Herreros et al., 2011; Ivonne et al., 2001; Rodríguez-Donis et al., 2001)
Reactive distillation	Number of product, reaction temperature, relative volatility, etc. (Shah et al., 2012)
Reactive adsorption	Multifunctional catalyst selection (Charpentier, 2007)
Membrane reactor	Membrane selection (Powell, 2017)

4.2.1. New Process Design

The framework is based on the concept reported by Tula et al. (2015). This framework extends the original search space by adding hybrid/intensified separation techniques. Additionally, instead of inputting a selected reaction pathway to the system, this framework will use the generated results from the reaction synthesis step as input. In this way, the framework can generate different process alternatives for different reaction pathways. The detailed framework is shown in Figure 17.

4.2.1.1 Step N.1: Synthesis problem definition

In this step, the definition of the raw materials (inputs) and desired products (outputs) are considered based on the identified reaction pathways coming from the reaction synthesis step. Here, the multiple feasible reaction pathways, including raw materials, products, solvents, catalysts, and reaction conditions, are the input of this step. It is important to know that these inputs are varied along with the selection of catalyst/reactor and reaction conditions. For example, different types of catalysts and operating conditions can lead to different reaction conversion rates and selectivity, which will finally influence our outlet mixture compositions. In this framework, we aim to identify the best downstream separation with respect to different potential reaction pathways without prior knowledge of reaction conditions. In this case, it is essential to study the influence of different types of components when determining the best process to produce/utilize the target product/raw material. Based on this concept, component toxicity and binary mixture separation driving force are considered in our pathway screening criteria before separation synthesis. Also, to ensure consistency in comparison, all pathways use the same conditions. However, in case that reaction conditions are given, the outlet mixture composition corresponding to the best operating conditions should be considered for separation synthesis.

4.2.1.2 Step N.2: Mixture analysis

In this step, binary pairs of all the chemical compounds are generated and further studied. For example, if there are four components in the system, six binary pairs are generated. For each identified binary pair, azeotropic and eutectic points are generated using ICAS SLE toolbox and Aspen Plus. Binary ratio matrix is generated based on 15 pure component properties, such as boiling point, vapor pressure, melting point, molecule diameters, etc. The pure component properties are extracted from ICAS database, and the missing properties are searched from the

literature. The generated binary ratio matrix and the azeotropic/eutectic information are sent to step N.3. An example of a binary ration matrix for a binary pair A and B is shown in Table 16.

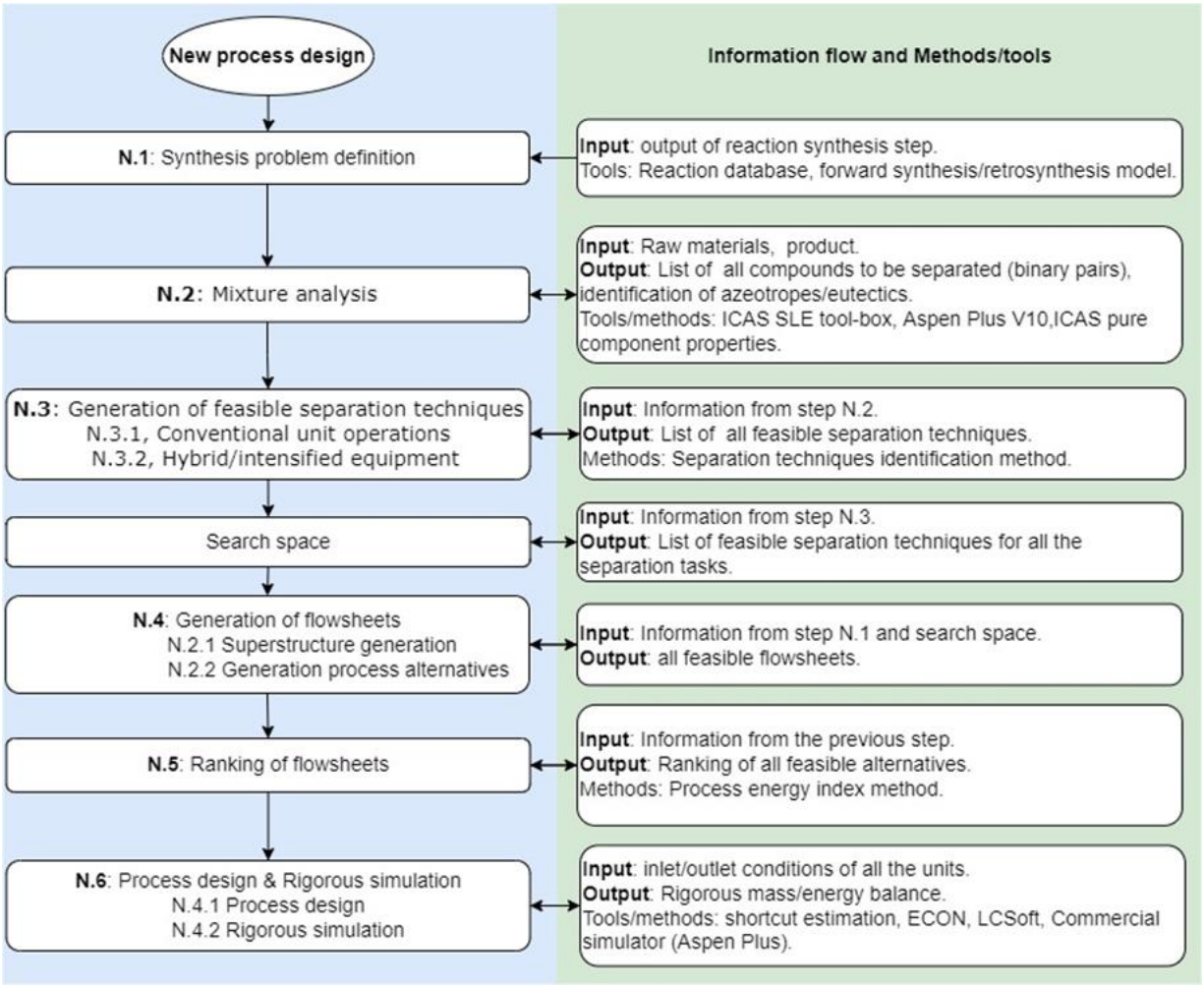

Figure 17. A framework for new process design problem.

Table 16. Example of binary ratio matrix for a binary pair A/B.

Component	Boiling point (k)	Melting point (k)	Vapor pressure (kPa, 30°C)	Solubility parameter	Radius of gyration (Å)	Molar volume (m^3/kmol)
A	383	178	4.87	18.32	3.47	0.11
B	353	278	15.89	18.73	3	0.089
Binary ratio	1.09	1.56	3.27	1.02	1.15	1.24

4.2.1.3 Step N.3: Generation of feasible separation techniques

In this step, the conventional separation techniques' selection criteria presented by Jaksland et al. (1995) are applied here to perform feasibility analysis based on the data generated in the previous step. For example, distillation is feasible only when the boiling point ratio is greater than 1.01, the vapor pressure ratio is greater than 1.05, and no azeotropic point exists. For the binary mixture A and B in Table 16, distillation is a feasible technique, and it is added to the search space under the separation task of A/B.

For the extended innovative separation techniques, the detailed selection criteria are explained in Section 4.3. These criteria are applied to identify the feasibility of intensified/hybrid separation techniques and are added to the alternative search space. In this way, the search space includes all the feasible separation techniques (both conventional and hybrid/intensified) for each of the binary pairs (separation tasks). For example, the distillation-liquid membrane is feasible if the boiling point is greater than 1.01, vapor pressure greater than 1.05, solubility parameter greater than 1.01, the radius of gyration greater than 1.02, and molar volume greater than 1.2. For the binary mixture A and B in Table 16, the distillation-liquid membrane technique is feasible for separating components A and B. So, this separation technique is also added to the search space under the separation task of A/B.

4.2.1.4 Step N.4: Generation of flowsheets

In this step, all the possible separation process alternatives are generated based on the superstructure of identified separation techniques. Here, combinatorial algorithms are applied to generate the separation superstructure, which guarantees the correct inlet and outlet connection of different separation tasks. For instance, with mixture A, B, and C, separation superstructure (iABC)(A/BC)(B/C) and (iABC)(AB/C)(A/B) is generated. For each separation task in the

superstructure, multiple feasible separation techniques are available. In this way, different process flowsheets are generated and sent to step N.5 for further evaluation.

4.2.1.5 Step N.5: Ranking of flowsheets

Once all the feasible process alternatives are generated from the previous step, ranking the feasible alternatives is performed to select the most promising alternative. The ranking of the alternatives is based on the process energy index, which is the summation of the estimated energy consumption of each unit operation present in the process flowsheet. For example, the energy consumption for distillation and hybrid distillation is estimated based on first principle-based models (Lange, 2017), as shown in Equation 4.1 and 4.2. Energy consumption for the other unit operations is based on enthalpy balances (Equation 4.3). After the evaluation step, the top alternatives with lower process energy index are selected. Finally, these top alternatives are further evaluated using rigorous models. In this way, the method identifies the best process alternatives and their optimized design/operating conditions.

$$Q_d = 57 \times \sum_i \frac{w_i}{\Delta T_i} \quad (4.1)$$

$$Q_{dhs} = \eta \times Q_d \quad (4.2)$$

$$Q_{hs} = H_{out}N_{out} - H_{in}N_{in} \quad (4.3)$$

Where Q_d is the reboiler duty (GJ per ton of inlet); w_i is the inlet mass fraction of component i; ΔT_i is the atmosphere boiling point different between component i and $i+1$ (ranked based on boiling point); Q_{dhs} is the reboiler duty for distillation hybrid separation techniques; η is a constant coefficient, and it is 0.6 in the calculation, as in the distillation column around 40% of energy is used for purifying the product from 90% to 99.8%; Q_{hs} is the heat duty for hybrids separation except for distillation hybrid, and it is calculated based on mass and enthalpy balance; H_{out} and H_{in} are the enthalpy at outlet and inlet conditions; N_{out} and N_{in} are the outlet

and inlet flowrate. For example, if we have a separation task in Table 17, then the calculated example of heat duty is shown below. Noted here, five hybrid/intensified unit operations (distillation-membrane, distillation-adsorption, distillation-crystallization, membrane-crystallization, and dividing wall column) are considered in this paper. The energy index for the first three distillation-based hybrid separation techniques is calculated by Equation 4.1 and 4.2. The energy index for the membrane-crystallization is calculated based on enthalpy balance (Equation 4.3). The dividing wall column is treated as two single distillations, so its energy index is calculated based on Equation 4.1. Table 17 gives a process energy index calculation example.

Table 17. Example of process energy index calculation.

Component	Mass flowrate (kg)	Boiling point	Mass fraction	Distillation energy index (A/BC)	Distillation-membrane energy index (B/C)	Process energy index
A	100	60	0.5	57	0.6×57	0.143
B		80	0.3	$\times \left(\frac{0.5}{80-60}\right)$	$\times \left(\frac{0.3/(0.3+0.2)}{100-80}\right.$	$+ 0.051$
C		100	0.2	$\times 0.1$	$\times 0.05$	$= 0.194\ GJ$
				$= 0.143\ GJ$	$= 0.051\ GJ$	

4.2.1.6 Step N.6: Process design & rigorous simulation

The top process alternatives that are selected in the previous step are further evaluated and analyzed using rigorous models. First, the process operating and design parameters, such as temperature, pressure, column stages, etc., will be determined based on shortcut methods. Then, the preliminary process design parameters will be applied to perform the rigorous process simulation. Here, the process design parameters will be further optimized based on the sensitivity analysis. Based on the simulation results, environmental and sustainability indices are estimated.

4.2.2 Retrofit Design

The target of the retrofitting problem is to redesign the existing facilities to either improve the processing capacity or process efficiency. The proposed framework is based on an analysis and improvement approach, where the existing process is first analyzed and the process hot spots are identified. Further, these identified hot spots are eliminated by substituting feasible alternative unit operations. The detailed framework is shown in Figure 18.

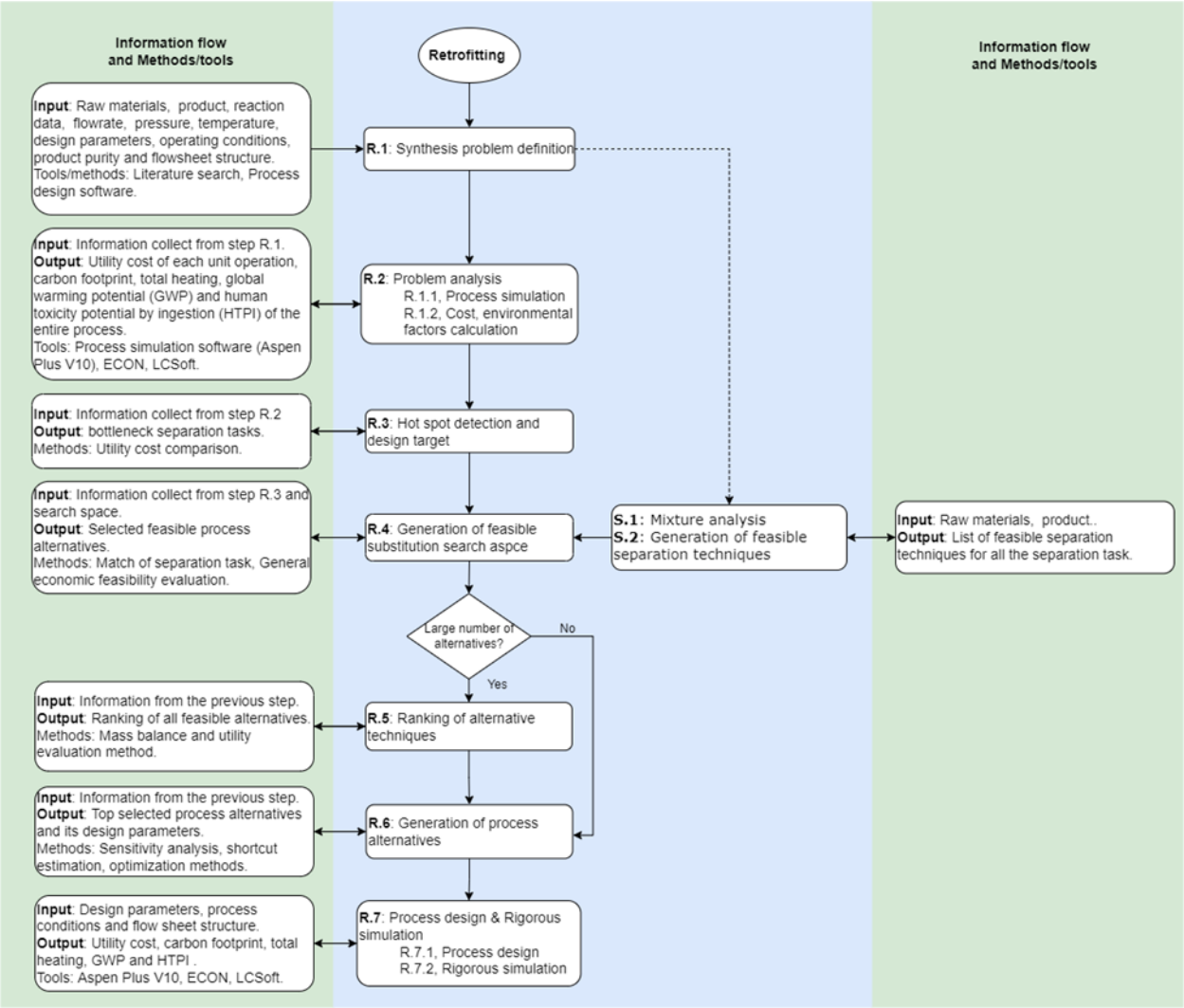

Figure 18. A framework of retrofitting problems.

4.2.2.1 Step R.1: Synthesis problem definition

The main task of this step is to determine the base case in which the operating conditions, raw materials, products, design parameters, product purity, and flowrate are given. With known process structure and operating data, the remaining task is to evaluate each unit operation, such as energy cost and carbon emissions, and find the process hot spots.

4.2.2.2 Step R.2: Problem analysis

In this step, the mass and energy balance results of the base case are used to calculate economic and environmental factors. The economic factor, such as utility cost, is calculated from an economic analysis tool ECON (Kalakul et al., 2014). The environmental factors, including global warming potential (GWP), carbon footprint, and human toxicity potential by ingestion (HTPI), are calculated from a life cycle analysis tool LCSoft (Chavewanmas et al., 2017). Then this process evaluation data is sent to the next step to identify the process hot spot.

4.2.2.3 Step R.3: Hot spot detection and design target

Based on the techno-economic analysis performed in the previous step, the process hot spots are identified, which are translated into process targets. The process design targets can vary from reducing energy consumption, increasing the process's throughput, reducing overall environmental impact, etc. In this work, we focus on identifying a process with lower energy consumption and less environmental impact. The separation tasks that are identified as process hot spots are sent to the next step.

4.2.2.4 Step R.4: Generation of feasible substitution search space

In this step, based on the identified hot spot separation tasks, feasible alternative techniques are identified. In order to achieve this, two inputs are required: hot spot separation tasks and feasible separation search space. Here, the feasible separation search space is generated based on the same

procedure mentioned in Section 4.2.1.3. For example, a distillation column that separates component A from a mixture of A, B, and C is identified as the hot spot separation task. Then, the separation task (A/BC) is sent, wherefrom the search of feasible separation techniques like distillation membrane, adsorption, and dividing wall column is selected once those criteria are satisfied. However, from the list of feasible separation techniques, only the economically feasible alternatives are considered through predefined selection rules that are explained in Section 4.3. In this way, the selected alternative techniques are both thermodynamic and economically feasible. Additionally, if many alternatives are available, it is necessary to reduce the alternative research space and only consider the top alternatives. So, a ranking algorithm is applied in the next step if the alternative space is too large.

4.2.2.5 Step R.5: Ranking of alternative techniques

In this step, all the generated alternatives are evaluated using energy-based index. The calculation method for the same is described in Section 4.2.1.5. From this step, only the top ranked alternatives are passed to the next step R.6.

4.2.2.6 Step R.6: Generation of alternative processes

In this step, different process alternatives are generated depending on the number of selected alternative techniques from the previous step. Replacing the hot spot unit with all the available alternatives given from the previous step, multiple process alternatives are generated and sent to the next step for further evaluation.

4.2.2.7 Step R.7: Process design & rigorous simulation

In this step, a process simulation tool is used here to perform the rigorous simulation. Firstly, the process design parameters for all these alternatives are determined through sensitivity analysis or optimization methods. For example, if the distillation-membrane hybrid separation system is one

feasible alternative, one needs to decide the membrane feed composition. By comparing the performance under different operating conditions, we can select the most promote case. Or, we can establish an optimization model to search for the optimum design parameters by minimizing/maximizing the predefined objective functions. Once the design parameters are decided, the process simulation tool is applied to calculate the process's energy & mass balance. This information is further used to calculate the utility cost and process sustainability. Based on this, we can compare the performance of different process alternatives with the base case process, and the best process alternative that matches the design target is selected.

4.3 Hybrid & Intensified Equipment and Corresponding Selection Criteria

Five innovative separation techniques, including distillation-membrane, distillation-adsorption, distillation-crystallization, membrane-crystallization, and dividing wall column, are considered in this paper, and the corresponding selection criteria are listed in Table 18. As long as the binary ratio properties in Table 18 are satisfied, the hybrid/intensified separation technique is feasible. The generalized selection rules of each separation technique are explained in the following sections.

4.3.1 Distillation Membrane

In the distillation membrane system, distillation is used to purify the distillate until a certain composition (switching composition), and the following membrane system is used to further purify the distillate into the final product. Depending on the category of the membrane, distillation membrane can be divided into three hybrid separation techniques: distillation liquid membrane (dllmA/B), distillation gas membrane (dlgmA/B), and distillation pervaporation (dlpvA/B). As long as the binary ratio properties in Table 18 are satisfied, the distillation-membrane separation

is feasible. For example, the distillation pervaporation is feasible if the following properties are satisfied:

1) The binary ratio of boiling point for the key pair should be > 1.01
2) The binary ratio of vapor pressure for the key pair should be > 1.05
3) The binary ratio of solubility parameter for the key pair should be > 1.01
4) The binary ratio of molar volume for the key pair should be > 1.08
5) The distillation membrane is economically practical if the following general rules are satisfied:

The distillation membrane is applied for binary system separation, which does not have a complicated downstream process.

1) The membrane locates at the top where the distillate is the feed stream, and the heavy component should be the permeate compound.
2) The required product purity is higher than 99%.

Table 18. Recommended feasibility criteria for five new separation techniques.

Separation techniques	SFLIES notation	P_1	P_2	P_3	P_4	P_5	P_6	P_7	P_8	P_9	P_10
Distillation-membrane	(dllmA/B)	1.01	1.05	1.01	1.02	1.2	-	-	-	-	-
	(dlgmA/B)	1.01	1.05	-	-	-	1.07	1.1	-	-	-
	(dlpvA/B)	1.01	1.05	1.01	-	1.08	-	-	-	-	-
Distillation-adsorption	(dladA/B)	1.01	1.05	-	-	-	-	-	-	1.05	-
		1.01	1.05	-	-	-	-	-	-	-	1.08
Distillation-crystallization	(dlczA/B)	1.01	1.05	-	-	-	-	-	1.2	-	-
Membrane-crystallization	(czmA/B)	-	-	1.01	1.02	1.2	-	-	1.2	-	-
		-	-	1.01	-	1.08	-	-	1.2	-	-
Dividing wall column	(dwcA/B/C)	1.01	1.05	-	-		-	-		-	-

A and B: two different components; P_1: boiling point; P_2: vapor pressure; P_3: solubility parameter; P_4: radius of gyration; P_5: molar volume; P_6: Van der Waals volume; P_7: critical temperature; P_8: melting point; P_9: dipole moment; P_10: polarizability

To simulate and determine the distillation-membrane operating/design parameters, one can directly use the membrane selectivity and operating data when a suitable membrane permeation model is lacking so that the membrane acts like a splitter and is attached after the distillation column. In this way, the two units can be simulated as hybrid distillation membrane. When a membrane permeation model that gives an explicit equation to represent the relationship between membrane permeability and operating conditions like inlet composition, temperature, and pressure is available, one can imbed this model into the distillation simulation, e.g., build the permeation model in Python and connect it with Aspen Plus, so that the design/operating parameters can be determined by performing sensitivity analysis or derivative-free optimization (DFO).

4.3.2 Distillation Crystallization

Distillation crystallization (dlczA/B) is treated as a separation technique that can be applied to any binary system that satisfies the following criteria:

1) The binary ratio of boiling point for the key pair should be > 1.01
2) The binary ratio of vapor pressure for the key pair should be > 1.05
3) The binary ratio of melting point for the key pair should be > 1.2

The distillation crystallization is economically practical if the following general rule is satisfied:

1) The crystallization separation is performed at a temperature greater than 10 °C because of the practical problems associated with low-temperature refrigerants.
2) The recovery of the key component should satisfy the product specification.

For distillation-crystallization simulation, the thermodynamic solid-liquid equilibrium (SLE) of the input mixture should be considered and connected with distillation. The

crystallization unit acts like a splitter and is attached after the distillation column when only limited equilibrium data points are available. When the SLE diagram is available, one can correlate this phase diagram and build explicit equations in Python, so that the design/operating parameters can be determined by connecting this crystallization model with the distillation model in Aspen Plus.

4.3.3 Distillation Adsorption

The distillation adsorption is similar to the distillation membrane, where the adsorption unit is also used for the final product purification. The distillation adsorption can be applied to any binary system as long as the following criteria are satisfied:

1) The binary ratio of boiling point for the key pair should be > 1.01
2) The binary ratio of vapor pressure for the key pair should be > 1.05
3) The binary ratio of dipole moment for the key pair should be > 1.05, or the binary ratio of polarizability for the key pair should be > 1.08

The distillation adsorption is economically practical if the following general rules are satisfied:

1) The distillation adsorption is applied for binary system separation, which does not have a complicated downstream process.
2) The adsorption unit locates at the top where distillate is the feed stream, and the heavy component should be the adsorbed compound.
3) The required product purity is higher than 99%.

The simulation of distillation-adsorption is similar to distillation-membrane, the adsorption unit also acts as a splitter, and the adsorbent selectivity and loading capacity are considered when the adsorption kinetic model is not available. When the adsorption kinetic that represents the

relationship between adsorption and operating temperature/pressure is available, one can construct this model and connect it with the distillation column in Aspen Plus for more rigorous simulation.

4.3.4 Membrane Crystallization

The membrane crystallization system facilitates crystal growth by creating a supersaturated solution through membrane separation. As a new separation technology, which could reduce the utility cost of crystallization, membrane crystallization (czmA/B) can be applied to any binary system once the following criteria are satisfied.

1) The binary ratio of solubility parameter for the key pair should be > 1.01
2) The binary ratio of melting point for the key pair should be > 1.08 (pervaporation), 1.2 (liquid membrane)
3) The binary ratio of molar volume for the key pair should be > 1.2
4) The binary ratio of radius of gyration for the key pair should be > 1.02 (liquid membrane)

The membrane crystallization is economically practical if the following general rule is satisfied:

1) The crystallization separation is performed at a temperature greater than 10 °C.
2) The selective recovery of the key component should satisfy the product specification.

The mixtures in the membrane-crystallization system perform membrane permeation and crystallization simultaneously. Currently, there is no reported mechanistic model to support the process design and simulation. Thus, this unit is simulated as a splitter, and the simulation results are solely dependent on available experimental data.

4.3.5 Dividing Wall Column

The dividing wall column (dwcA/B/C) can be applied for any ternary system once each binary satisfies the following criteria:

1) No binary azeotrope.
2) The binary ratio of boiling point for the key pair should be > 1.01
3) The binary ratio of vapor pressure for the key pair should be > 1.05

The dividing wall column is economically practical if the following general rules are satisfied:

1) The product purity is less than 99.5%.
2) The distillate stream flowrate is higher enough to give a reasonable downstream liquid flowrate.

For dividing-wall column simulation, one has to determine the main/side column stages, reflux ratio and vapor/liquid split ratio, etc., inside the column. Generally, to determine these parameters in process simulation, one should first simulate the two distillation columns that separate the ternary mixture. The results provide an initial estimation of the number of main/side column stages (Dejanović et al., 2010). Based on this initial estimation, one can determine the column design/operating parameters by using the distillation design specification tools. For rigorous simulation, one has to construct an optimization model to determine the optimal operating/design variables by minimizing the distillation cost.

4.4 Case Studies

Each step of the framework is highlighted through case studies involving acrylic acid, DMC, cumene, and styrene production. The acrylic acid case study aims to identify the optimal

separation route for acrylic acid production, considering solvent evaluation, extractive distillation, and extraction as part of this new process synthesis problem. The DMC case study aims to find the best reaction pathway and separation route for DMC production, which is a new process synthesis problem. The cumene and styrene production case studies aim to identify alternative separation techniques to substitute the hot spot unit, which is retrofitting design problems.

4.4.1 New Process Design: Acrylic Acid Production

This case study aims to find an optimal flowsheet for acrylic acid production (96.81 kmol/h production rate) by converting propylene into acrylic acid. The objective is to test the solvent evaluation method (refer to Section 3.1.1) and find the sustainable separation process flowsheet that includes solvent-based separation techniques to separate the azeotrope mixtures (acrylic/water, acetic acid/water).

4.4.1.1 Reaction synthesis

The following reactions (R-1) and (R-2) that produce acrylic via catalytic partial oxidation of propylene are considered in the reaction synthesis. As the purpose of this case study is to test the proposed FSES model, only one reaction is considered and sent to the next step for separation synthesis.

$$C_3H_6(Propylene) + 1.5O_2 \rightarrow C_3H_4O_2(Acrylic\ acid) + H_2O \quad \text{(R-1)}$$

$$C_3H_6 + 1.5O_2 \rightarrow C_2H_4O_2(Acetic\ acid) + CO_2 \quad \text{(R-2)}$$

4.4.1.2 Separation synthesis

Step N.1: The reaction outlet mixture, including flowrate and product specification, for propylene oxidation is extracted from literature (Turton et al., 2008). The liquid mixture has three components, water (1156.7 kmol/h), acetic acid (6.08 kmol/h), and acrylic acid (86.81 kmol//h) at

2.4 bar and 40 °C. The product requires 95 mol% purity of acetic acid and 99.9 mol% of acrylic acid.

Step N.2: For this mixture, acrylic acid/water and acetic acid/water are identified as binary azeotropes. The FSES model is employed here to identify the related solvents that can overcome the azeotrope point. Table 19 lists the solvent evaluation results after applying the FSES model based on the potential solvents presented by Gerbaud et al. (2019). Sulfolane and adiponitrile are identified as the top two solvents for extractive distillation, while diisopropyl ether and ethyl acetate emerged as the top choices for extraction in organic/water separation. It should be noted that the solvent ethyl acetate is not included in the separation synthesis due to its relatively high solubility with water, which would pose challenges for downstream separation processes.

Table 19. Solvent evaluation results for organic (acrylic acid, acetic acid)/water separations.

Extractive distillation		Extraction	
Solvents	Ranking score	Solvents	Ranking score
Sulfolane	28	Ethyl acetate	21
Tributylamine	32	Diisopropyl ether	19
Pelargonic acid	34	Isopropyl acetate	24
Adiponitrile	24	methyl propyl ketone	28
2-Hydroxyethyl formate	47	Methyl t-Butyl Ether (MTBE)	28

Step N.3: A total of 12 binary pairs are generated for all the components present in the liquid mixtures. Table 20 shows all the considered properties of all the compounds. Table 21 gives an example of the binary ratio matrix of pure component properties for all the binary pairs.

Table 20. Pure component properties for the acrylic acid production synthesis problem.

Property	Water (A)	Acetic acid (B)	Acrylic acid (C)	Adiponitrile (S1)	Sulfolane (S2)	Diisopropyl ether (S3)
Boiling point (K)	373.15	391.05	414.15	568.15	560.45	341.65
Radius of gyration (Å)	0.62	2.61	2.98	3.98	3.31	3.91
Melting point (K)	273.15	289.81	286.15	275.55	300.55	187.65
Molar volume (m^3/Kmol)	0.02	0.06	0.07	0.11	0.10	0.14
Solubility parameter $(Mpa)^{0.5}$	47.81	19.01	18.43	24.57	26.11	14.45
Van der Walls volume (m^3/kmol)	0.01	0.03	0.04	0.07	0.06	0.07
Vapor pressure (KPa), 30 °C	4.24	2.78	0.76	0.00	0.00	24.59
Critical temperature (K)	647.13	591.95	615.00	781.00	853.00	500.05
Triple point pressure (Pa)	0.01	0.01	0.00	0.00	0.00	0.00
Triple point temperature (K)	273.16	289.81	286.15	275.55	300.55	187.65
Kinetic diameter (Å)	2.65	4.40	-	-	-	-
Polarizability ($Å^3$)	1.50	5.15	6.38		10.73	12.65
Dipole moment (Debye)	1.85	1.74	1.46	3.75	4.68	1.13
Molecular weight (g/mol)	18.02	60.05	72.06	108.14	120.17	102.18

Step N.4: Figure 19 gives the separation superstructure for acrylic acid production. A total of 112 process alternatives are generated.

Step N.5: Using the process energy index method described in Section 4.2.1, all the generated alternatives are screened, and the top three alternatives (P1, P2, P3) are listed in Table 22. For the list of all alternatives and their corresponding energy indices, refer to Appendix 2. Because of no reported membrane or adsorbent for acetic acid/acrylic acid, solvent/acetic acid,

and solvent/acrylic acid, these separation techniques with their hybrid technologies are not selected. Noted, to compare the performance of extraction and extractive distillation, the extraction process P4 is also selected for further analysis despite its high process energy index.

Step N.6: For these selected four process alternatives, Figure 20 shows their simulation results, including utility/capital cost and process environmental factors like carbon footprint and global warming potential (GWP). From Figure 20, the process alternative 1, which is based on hybrid membrane distillation, has the lowest utility cost and environmental impact compared to the other alternatives, but has the highest capital cost because of low membrane permeability. Process alternative 3, which uses extractive distillation with solvent sulfolane, has better performance than extraction. The results suggest that for acrylic acid production, extractive distillation with solvent sulfolane is recommended for mixture separation, and the application of hybrid membrane distillation is constrained by membrane performance. Figure 21 shows recommended process flowsheets for producing acrylic acid via propylene oxidation.

Table 21. Binary ratio matrix of a select set of properties for the acrylic acid production synthesis problem.

Binary pair	Boiling point	Radius of gyration	Melting point	Molar volume	Solubility parameter	Van der Walls volume	Vapor pressure
A/B	1.05	4.24	1.06	3.19	2.52	2.69	1.53
A/C	1.11	4.84	1.05	3.81	2.59	3.25	5.60
B/C	1.06	1.14	1.01	1.20	1.03	1.21	3.67
A/S1	1.52	6.47	1.01	6.24	1.95	5.68	24,132.75
B/S1	1.45	1.52	1.05	1.95	1.29	2.11	15,823.78
C/S1	1.37	1.34	1.04	1.63	1.33	1.75	4,311.30
A/S2	1.50	5.38	1.10	5.27	1.83	4.95	4,208.13
B/S2	1.43	1.27	1.04	1.65	1.37	1.84	2,759.26
C/S2	1.35	1.11	1.05	1.38	1.42	1.52	751.78
A/S3	1.09	6.35	1.46	7.85	3.31	5.82	5.80
B/S3	1.14	1.50	1.54	2.46	1.32	2.16	8.84
C/S3	1.21	1.31	1.52	2.06	1.28	1.79	32.45

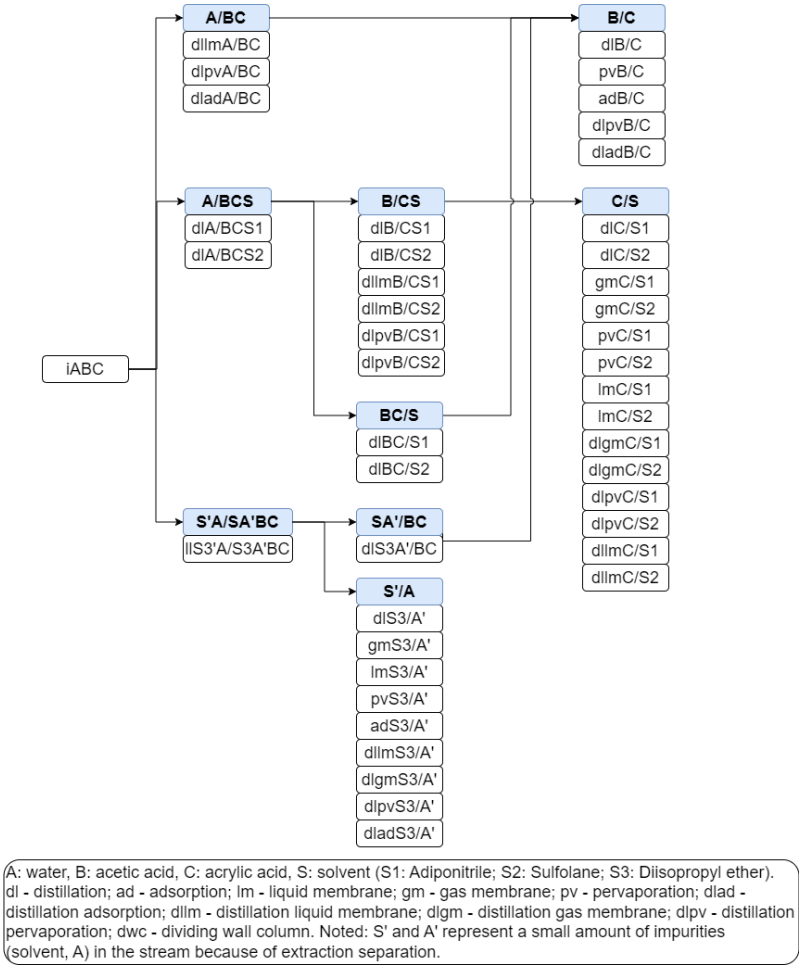

Figure 19. Separation superstructure for acrylic acid production.

Table 22. Selected four process alternatives for acrylic acid production.

Process alternatives		Process energy index, GJ	Components
P1	(dlpvA/BC)(dlB/C)	44.88	A: water
P2	(dlA/BCS1)<1(dlB/CS1))(dlC/S1)1	76.69	B: acetic acid
P3	(dlA/BCS2)<1(dlB/CS2)(dlC/S2)1	76.82	C: acrylic acid
P4	(dlS3'A/S3A'BC)<1<2(dlS3'/A)1(dlS3A'/BC)2(dlB/C)	204.25	S1: adiponitrile S2: sulfolane S3: diisopropyl ether

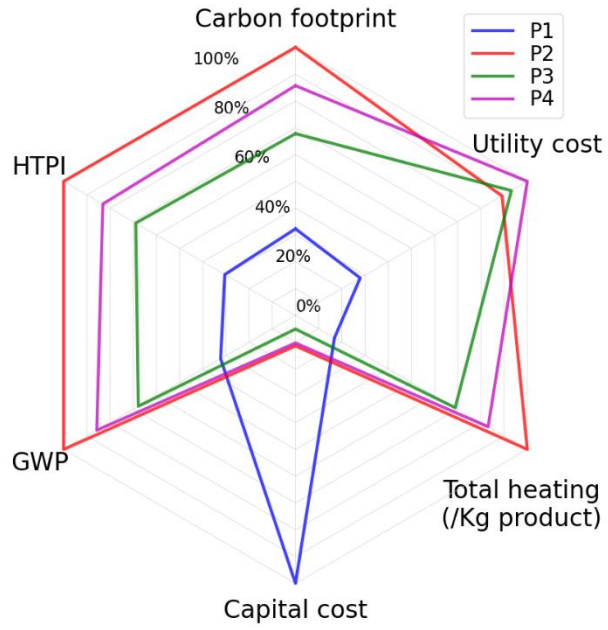

Figure 20. Comparison of selected four process alternatives for acrylic acid production.

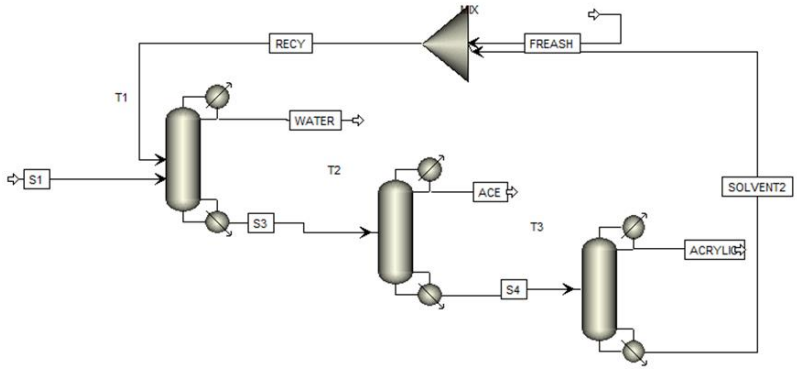

Figure 21. Recommend process flowsheet for acrylic acid production via propylene oxidation.

4.4.2 New Process Design: DMC Production

This case study aims to find an optimal process route for DMC production (56.4 kmol/h production rate), considering various sources of raw materials. Here, the objective is to find the process flowsheet, including reaction pathways and associated separation process, which has low capital & operational cost and, at the same time, is sustainable.

4.4.2.1 Reaction synthesis

Since the product is fixed with respect to reaction synthesis, this case study is a retrosynthesis problem where one has to find the best raw material and its corresponding reaction pathways for DMC production. The Retrosynthesis tool ASKCOS is used to generate different feasible reaction pathways (github.com/ASKCOS). Eleven reaction pathways are considered, including eight from ASKCOS and three from literature (Kongpanna et al., 2015). Using the screening method described in Section 4.1, all the potential feasible reaction pathways with their screening results are given in Table 23. The top three reaction pathways 1-3 are sent to the next step for further analysis.

Table 23. Potential feasible reaction pathways and the screening results for DMC production.

No.	Source	Reactants		Products		ΔH	LC50	DF	Remarks
1	Literature	CH_3OH	$C_3H_6O_3$	$C_3H_6O_3$	$C_3H_8O_2$	26.67	129.51	0	Selected
2	Literature	CH_3OH	$C_3H_4O_3$	$C_3H_6O_3$	$C_2H_6O_2$	-22.05	129.51	0	Selected
3	ASKCOS	CH_3OH	CO_2	$C_3H_6O_3$	H_2O	-22.9	129.51	0	Selected
4	ASKCOS	CH_3OH	CCl_2O	$C_3H_6O_3$	HCl	-70.75	128.14	0	-
5	ASKCOS	CH_3OH	$C_2H_3ClO_2$	$C_3H_6O_3$	HCl	0.88	47.46	0	Violation of rule 3)
6	ASKCOS	CH_3OH	CH_4N_2O	$C_3H_6O_3$	NH_3	109.99	129.51	0	Violation of rule 2)
7	ASKCOS	CH_3OH	CO, O_2	$C_3H_6O_3$	H_2O	-305.7	129.51	0	Violation of rule 2)
8	Literature	CO	CH_3ONO	$C_3H_6O_3$	NO	-189.6	63.67	1	Violation of rule 2)
9	ASKCOS	CH_3OH	CH_2O-	$C_3H_6O_3$	-	-	-	-	Violation of rule 1)
10	ASKCOS	CH_3OH	$C_2H_6O_4S$	$C_3H_6O_3$	-	-	-	-	Violation of rule 1)
11	ASKCOS	CH_3OH	$C_2H_4O_3$	$C_3H_6O_3$	-	-	-	-	Violation of rule 1)

4.4.2.2 Separation synthesis

Step N.1: Table 24 lists the raw materials, inlet conditions, and product specifications for all the considered reaction pathways to produce 56.4 kmol/h amount of DMC. Here, the mixture

flowrate for pathway 1 is extracted from literature (Kongpanna et al., 2015). To keep consistency in comparison, the component flowrates of pathways 2 and 3 are the same as pathway 1.

Table 24. Inlet conditions for DMC separation synthesis.

		Reaction pathway 1	Reaction pathway 2	Reaction pathway 3
CH_3OH	kmol/h	56.4	56.4	56.4
$C_3H_6O_3$	kmol/h	56.4	56.4	46.8
H_2O	kmol/h	-	-	46.8
$C_3H_4O_3$	kmol/h	-	18.2	-
$C_2H_6O_2$	kmol/h	-	46.8	-
$C_3H_6O_3$	kmol/h	18.2	-	-
$C_3H_8O_2$	kmol/h	46.8	-	-
Pressure	bar		10	
Purity specification	mol%		CH_3OH, $C_3H_6O_3$: 99.5 mol%	

Step N.2: For these reaction pathways, DMC/methanol and DMC/water are identified as binary azeotropes. The FSES model is employed here to identify the related solvents that can overcome the azeotrope point. Solvent aniline is identified as the best solvent for DMC/methanol separation after screening the solvents considered from the review literature (Gerbaud et al., 2019).

Step N.3: A total of 21 binary pairs are generated for all the components present in the three reaction pathways (Reaction pathway 1: 9 binary pairs, Reaction pathway 2: 9 binary pairs, Reaction pathway 3: 3 binary pairs). The properties of all the components in reaction pathways 1, 2, and 3 are given in Appendix 2.

Step N.4: Figure 22 gives the separation superstructure for reaction pathway 1. The separation superstructure of reaction pathways 2 and 3 are given in Appendix 2. Based on the separation structure, a total of 127, 146, and 16 process alternatives are generated for reaction pathways 1, 2, and 3, respectively.

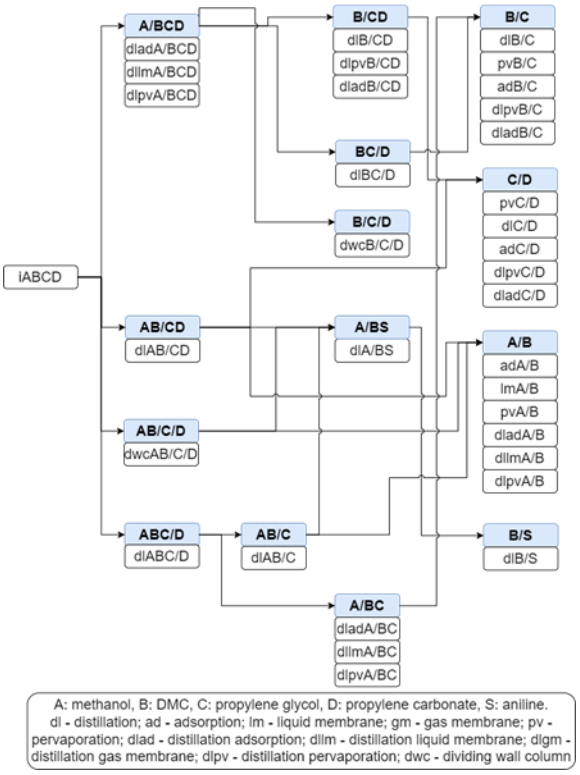

Figure 22. Separation superstructure for DMC production via reaction pathway 1.

Step N.5: Similar to the acrylic acid production case study, all the generated alternatives are screened, and the top six alternatives (two for each reaction pathway) are selected and listed in Table 25. For the list of all alternatives and their corresponding energy indices, refer to Appendix 2. Because of no reported membrane or adsorbent for DMC/ethylene glycol, DMC/propylene glycol, ethylene glycol/ethylene carbonate, and propylene glycol/propylene carbonate separation, these separation techniques with their hybrid technologies are not selected.

Table 25. Top six alternatives for the selected three DMC production pathways.

Process alternatives		Process energy index, GJ	Components
R1_P1	(dlpvA/BCD)(dlB/CD)(dlC/D)	9.52	A:methanol B: DMC C:propylene glycol
R1_P2	(dlpvA/BCD)(dwcB/C/D)	9.52	

			D:propylene carbonate
R2_P1	(dlpvA/BCD)(dlB/CD)(dlC/D)	9.63	A:methanol
R2_P2	(dlpvA/BCD)(dwcB/C/D)	9.63	B: DMC C:ethylene glycol D:ethylene carbonate
R3_P1	(dlpvA/BC)(deB'C/BC')<1<2(pvBC/B')1(azBC/C')2	3.77	A:methanol
R3_P2	(dlpvA/BC)(deB'C/BC')<1<2(azBC/B')1(azBC/C')2	29.83	B: DMC C:water

Step N.6: Figure 23 plots the simulation results for these top six process alternatives. From Figure 23, the process alternative from reaction pathway 1 has the lowest utility, capital cost, and environmental impact compared to the top alternatives from other pathways. Reaction pathway 3 has two azeotropes, leading to higher separation costs and carbon emissions. Figure 24 shows the best two process flowsheets for producing DMC with respect to the given design constraints and objective function.

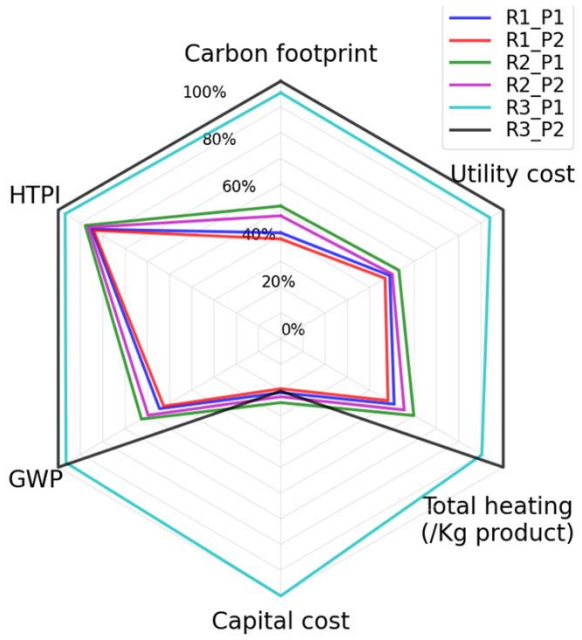

Figure 23. Comparison of six process alternatives for DMC production.

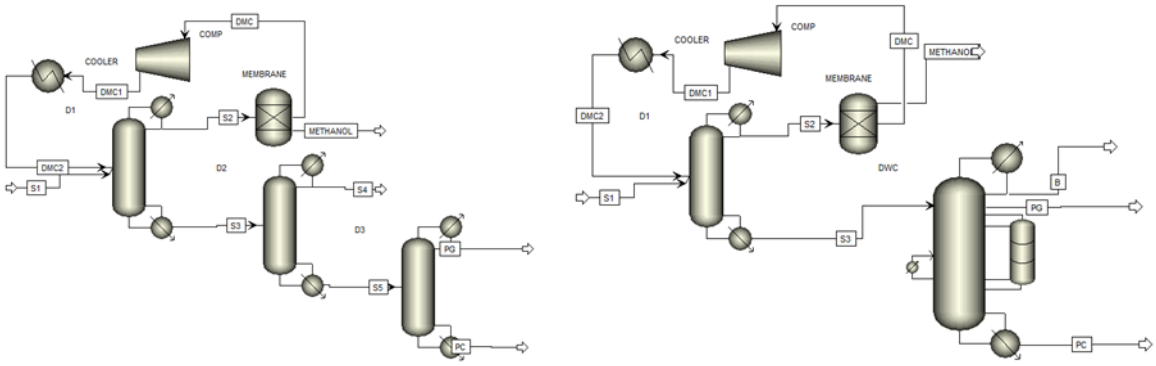

Figure 24. Best two separation configurations (from left to right R1_P1, R1_P2) for DMC production.

4.4.3 New Process Design: Isobutylene Utilization

This case study aims to find an optimal flowsheet for isobutylene utilization considering various target products. Here, the objective is to find the process route that yields the highest profit and ensures sustainability.

4.4.3.1 Reaction synthesis

Since the raw material isobutylene is fixed with respect to reaction synthesis, this case study is a forward synthesis problem where one has to predict the potential product by reacting isobutylene with the other reactants. Reactions with the top 37 high volume chemicals (Chenier, 2012) were tested in ASKCOS to generate different feasible chemical products, 35 of which are screened out because of economics or undesirable isomers. A total of nine reaction pathways are considered and listed in Table 26. The top three reaction pathways 1-3 are sent to the next step for further analysis.

4.4.3.2 Separation synthesis

Step N.1: Table 27 lists the raw materials, inlet conditions, and product specifications for all three selected reaction pathways. To keep consistency in comparison, the component flowrate of all the pathways are the same.

Table 26. Potential feasible reaction pathways and the screening results for isobutylene utilization.

No.	Source	Reactants	Products	ΔH, kJ	LC50, mg/L	DF	Remarks
1	Literature	Water, CO	Pivalic acid	-148.6	67.08	0.52	Selected
2		Formaldehyde	Prenol	-113.7		0.85	Selected
3		Ammonia	tert-Butylamine	-86		0.44	Selected
4		Water	tert-Butanol	-57.4	134.52	Separation Barrier	Violation of rule 4)
5		Methanol	Methyl methacrylate	-1,465			
6		Formaldehyde	Isoprene	-82.9	76.01	0.35	-
7		Ammonia	Methacrylonitrile	-1,459	7.66	0.08	Violation of rule 3)
8		Methane	Neopentane	-64.5		Separation Barrier	Violation of rule 4)
9	ASKCOS	Adipic acid	6-(tert-Butoxy)-6-oxohexanoic acid	-76.53	134.52	0.15	Violation of rule 4)

Table 27. Inlet conditions for isobutylene utilization separation synthesis.

		Reaction pathway 1	Reaction pathway 2	Reaction pathway 3
Water		50	-	-
Pivalic acid		50	-	-
Isobutylene		50	50	50
Formaldehyde	kmol/h	-	50	-
Prenol		-	50	-
Ammonia		-	-	50
tert-Butylamine		-	-	50
Pressure	bar	10		
Purity specification	mol%	Pivalic acid, Prenol, tert-Butylamine >= 99.5%		

Step N.2: For these reaction pathways, no binary azeotrope exists in the system.

Step N.3: A total of 9 binary pairs (three for each reaction pathway) are generated for all the components present in the three reactions. The properties of all the components in reaction pathways 1, 2, and 3 are given in Appendix 2.

Step N.4: Figure 25 gives the separation superstructure for reaction pathway 1. The separation superstructure of reaction pathways 2 and 3 are given in Appendix 2. Based on the

separation structure, a total of 38, 20, and 28 process alternatives are generated for reaction pathways 1, 2, and 3, respectively.

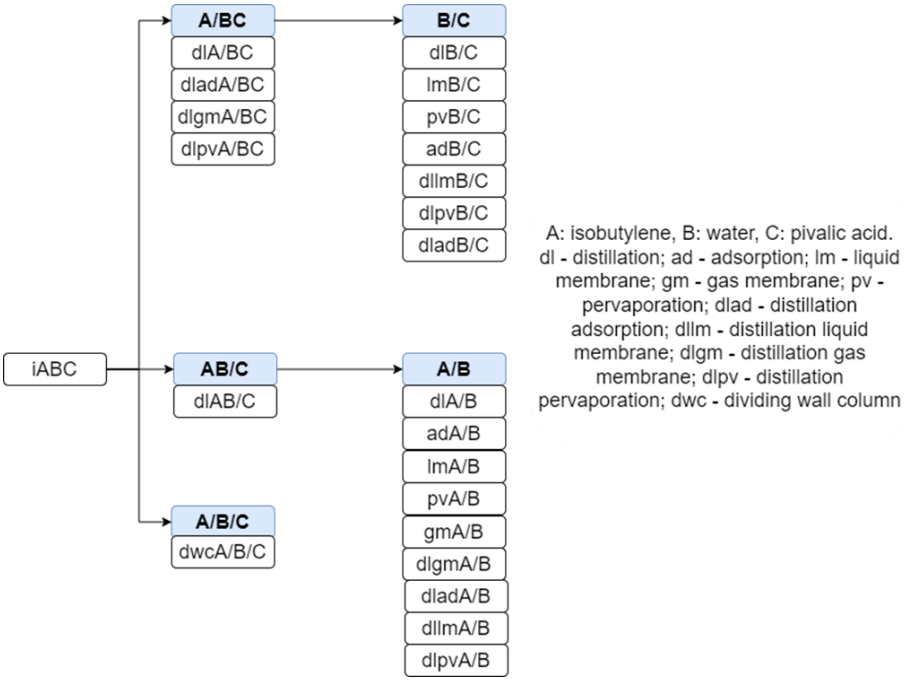

Figure 25. Separation superstructure for isobutylene utilization via reaction pathway 1.

Step N.5: All the generated alternatives are screened, and the top six alternatives (two for each reaction pathway) are selected and listed in Table 28. For the list of all alternatives and their corresponding energy indices, refer to Appendix 2. Because of no reported membrane/adsorbent for all the binary pairs in the system, the membrane/adsorption techniques and their hybrid technologies are not selected.

Step N.6: For these top six process alternatives, Figure 26 plots the simulation results. From Figure 26, process alternative R1_P1, which uses water, carbon monoxide, and isobutylene for pivalic acid production, has the lowest cost and environmental impact but the highest process profit. In this case, the results suggest that the process route utilizing isobutylene for pivalic acid

production offers the most profitable and sustainable process. The corresponding process flowsheets are depicted in Figure 27.

Table 28. Top six alternatives for the selected three isobutylene utilization pathways.

Process alternatives		Process energy index, GJ	Components
R1_P1	(dlA/BC)(dlB/C)	2.54	A: Isobutylene
R1_P2	(dwcA/BC)	2.54	B: Water
			C: Pivalic acid
R2_P1	(dlA/BC)(dlB/C)	8.93	A: Formaldehyde
R2_P2	(dwcA/BC)	8.92	B: Isobutylene
			C: Prenol
R3_P1	(dlA/BC)(dlB/C)	5.45	A: Ammonia
R3_P2	(dwcA/BC)	5.45	B: Isobutylene
			C: tert-Butylamine

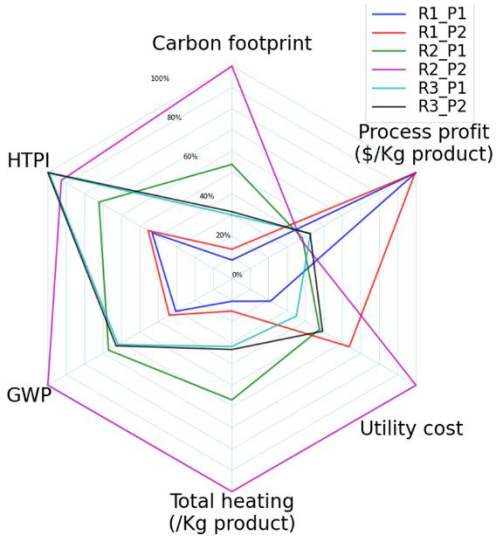

Figure 26. Comparison of six process alternatives for DMC production.

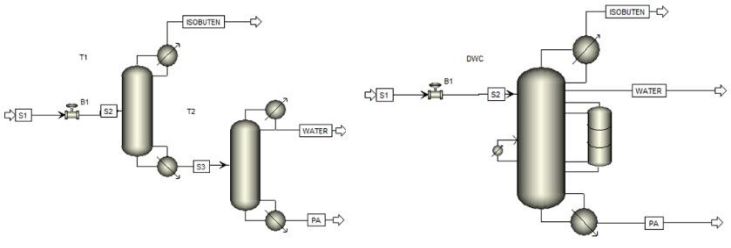

Figure 27. Best two separation configurations (from left to right R1_P1, R1_P2) using isobutylene for pivalic acid production.

4.4.4 Retrofitting Design: Cumene Production

4.4.4.1 Step R.1: Synthesis problem definition

In this case study, the existing literature process flowsheet (base case) for producing cumene (Turton et al., 2008) using benzene, propylene, and propane mixtures is considered. The inlet stream conditions are given in Table 29. The product specification requires a minimum purity of 99 wt% for cumene product.

Table 29. Inlet stream conditions for retrofitting of cumene production.

	Inlet 1	Inlet 2
(A) Propylene, kmol/h	0	105
(B) Propane, kmol/h	0	5.27
(C) Benzene, kmol/h	105	0
(D) Cumene, kmol/h	0	0
(E) P-diisopropyl benzene	0	0
Pressure, atm	0.99	11.51
Temperature, k	298.15	298.15

4.4.4.2 Step R.2: Problem analysis

Figure 28 shows the base case process (SFILES: (iC)[(iAB)](reABC/ABCD)<1(flEDC/AB)(dlED/C)1(dlE/D)), and the process utility cost is given in Table 30.

4.4.4.3 Step R.3: Hot spot detection and design target

From Table 30, columns T-801 and T-802 have the second and third highest energy costs, so the two benzene and cumene distillation columns are treated as the hot spot of the base case process, and the corresponding separation tasks C/DE and D/E are sent to the next step.

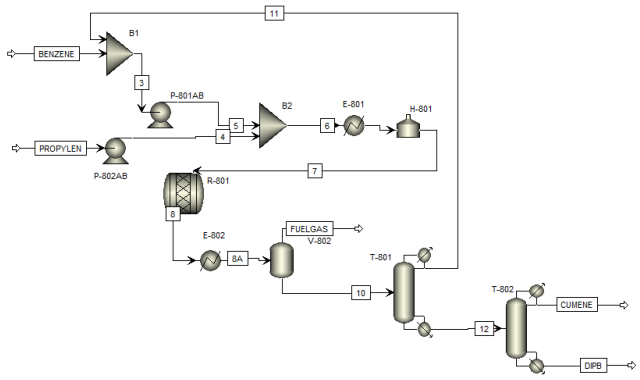

Figure 28. Base case process of cumene production.

Table 30. Rigorous simulation and cost estimation results for cumene production.

	Feed heater E-801	Feed fire heater H-801	Product cooler E-802	Benzene column T-801 (dlABC/DE)	Cumene column T-802 (dlD/E)
Stages	-	-	-	27	37
Product purity	-	-	-	-	D: >99 wt%
Heat duty (GJ/h)	12.94	6.67	16.64	Condenser: 5.44	Condenser: 5.76
				Reboiler: 7.08	Reboiler: 5.79
Utility cost ($/h)	127.23	40.02	5.89	71.53	58.94

4.4.4.4 Step R.4: Generation of feasible substitution search space

Step S.1 (mixture analysis): The five compounds in the system form 10 binary pairs (A/B, A/C… D/E). For each binary pair, no binary azeotropes are detected, and the binary pair A/B has a eutectic point at 76 k with a mixture of 50% A.

Step S.2 (Generation of feasible separation techniques): The feasible separation techniques of these 10 binary pairs are identified based on the pure component properties from Appendix 2. Table 31 gives the feasible separation techniques for the separation task of C/D, D/E, and C/D/E.

Table 31. Identified separation techniques of selected two binary pairs and one ternary pair for cumene production.

Binary pair	Separation techniques identified
C/D	distillation (dl), gas separation membrane (gm), liquid membrane (lm), pervaporation (pv), adsorption (ad), distillation-membrane (dlgm, dlgm, dlpv), distillation-adsorption(dlad)
D/E	distillation (dl), liquid membrane (lm), pervaporation (pv), distillation-membrane (dllm, dlpv)
C/D/E	dividing wall column distillation (dwc)

For separation tasks C/DE and D/E, a total of 15 separation techniques are identified based on results from Table 31. However, membrane/adsorption techniques are used as the final purification step, where the inlet has binary components, and the permeating/adsorbing compound has a relatively low flowrate. So, both membrane/adsorption and hybrid separation for separation task C/DE are excluded from the identified feasible solutions. Additionally, the distillation-membrane (dllm, dlpv) hybrid for separation task D/E is also excluded from the solutions because the product purity requirement is 99%, which violates the general rule that the distillation membrane hybrid is better suited for higher product purity. So, the generated set of feasible separation techniques only includes liquid membrane (lm), pervaporation (pv), and dividing wall column (dwc) for the separation task of D/E. Within these three solutions, researchers (Zhai et al., 2015) have investigated the application of dividing wall columns for industry cumene production, which also validates our proposed framework.

4.4.4.5 Step R.6: Generation of process alternatives

Table 32 lists the identified feasible alternative solutions. Since there is no reported information about membrane, we select a pseudo membrane and compare its performance with the dividing wall column. The corresponding process configurations are plotted in Figure 29.

Table 32. Identified feasible alternative solutions for cumene production.

Base case process	(iC)[(iAB)](reABC/ABCD)<1(flEDC/AB)(dlED/C)1(dlE/D)
Process alternative 1	(iC)[(iAB)](reABC/ABCD)<1(flEDC/AB)1(dwcE/D/C)
Process alternative 2	(iC)[(iAB)](reABC/ABCD)<1(flEDC/AB)(dlED/C)1(lmE/D)
Process alternative 3	(iC)[(iAB)](reABC/ABCD)<1(flEDC/AB)(dlED/C)1(pvE/D)

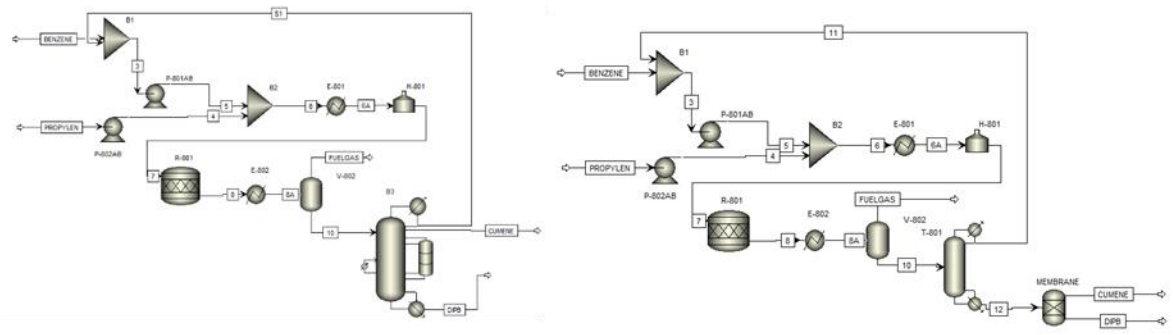

Figure 29. Flow diagram of alternative 1 (left) and 2 (right) for cumene production.

4.4.4.6 Step R.7: Process design & rigorous simulation

In this step, the design parameters are first determined. For process alternative 2, the membrane selectivity is considered as 250. For process alternative 1 (Figure 29), a shortcut model from (Dejanović et al., 2010) is used for the initial estimation of the number of main/side column stages. Based on these design parameters, the rigorous simulation results of process alternative 1 are listed in Table 33. Figure 30 plots the comparison results between the two selected process alternatives and the base case process. Alternative 2, which uses membrane separation, has the most significant improvement of both utility cost and environmental sustainability. However, one has to note that the capital cost would be high if the flux of the membrane is low. Alternative 1, which uses a dividing wall column, shows an average 20% saving for energy and environmental factors without changing the upstream operating conditions. So, in this case study, the process of alternative 2 is suggested for future cumene production.

Table 33. Rigorous simulation results of alternative 1 for cumene production.

	(dwcE/D/C)	
	Prefactionator (P)	Main column (MC)
stages	24	45
Product purity	D:>99 wt%	
Heat duty (GJ/h)	Condenser: 5.57 Reboiler: 10.44	
Utility cost ($/h)	104.6	

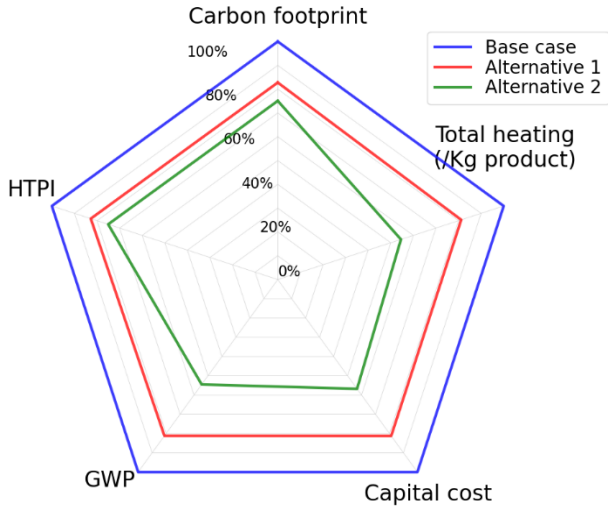

Figure 30. Comparison of three processes' downstream separation section for cumene production.

4.4.5 Retrofitting Design: Styrene Production

4.4.5.1 Step R.1: Synthesis problem definition

In this case study, the process flowsheet for producing styrene from ethylbenzene reported by Turton et al. (2008) is considered. The inlet stream conditions are given in Table 34, and the main reactions are listed in (R-3), (R-4), and (R-5). The product requires 99.95 mol% purity of styrene. In this process, because of the ethylbenzene equilibrium conversion (45%), a large amount of ethylbenzene is unreacted, which needs to be recycled back to the reactor.

$$C_6H_5C_2H_5 \leftrightarrow C_6H_5C_2H_3 + H_2 \quad \text{(R-3)}$$
$$C_6H_5C_2H_5 \rightarrow C_6H_6 + C_2H_4 \quad \text{(R-4)}$$

$$C_6H_5C_2H_5 + H_2 \leftrightarrow C_6H_5CH_3 + CH_4 \quad \text{(R-5)}$$

Table 34. Inlet conditions for the styrene production process.

	Inlet 1	Inlet 2
(A)Benzene, kmol/h	1.21	0
(B)Toluene, kmol/h	1.21	0
(C)Water, kmol/h	0	3,000
(D)Ethylbenzene, kmol/h	121	0
(E)Styrene, kmol/h	0	0
Pressure, atm	1.97	1.68
Temperature, k	409	995

4.4.5.2 Step R.2: Problem analysis

The base case process is shown in Figure 31 (SFILES: (iC)[(iABD)](reABCD/ABCDE)<1(flABDE/C)(dlDE/AB)1(dlE/D)). The simulation and utility cost results are listed in Table 35.

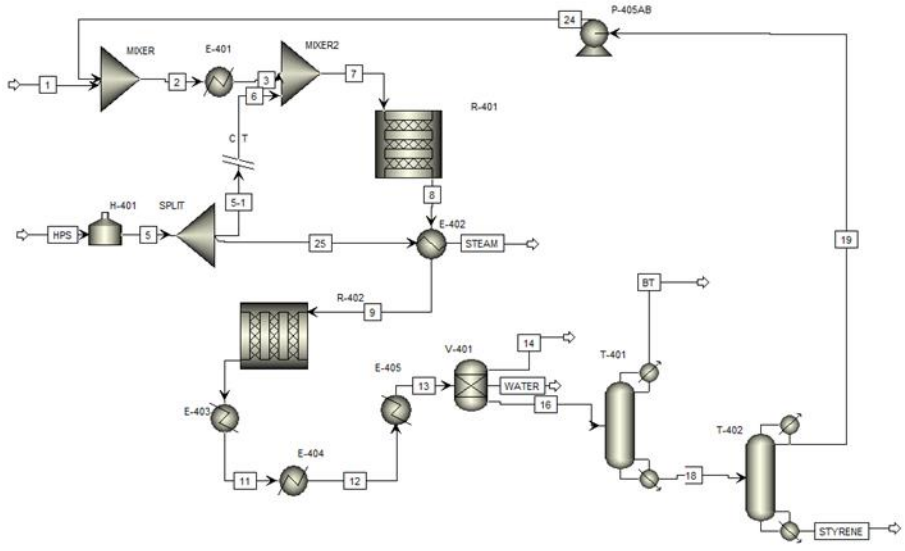

Figure 31. Base case process diagram of styrene production.

4.4.5.3 Step R.3: Hot spot detection and design target

From Table 35, the styrene column T-402, which has the second highest utility cost, is considered as the process hot spot. Thus, the separation task D/E is sent to the next step.

Table 35. Rigorous simulation and cost estimation results for styrene production.

	Feed heater E-401	Fire heater H-401	Product cooler E-403/4/5	Benzene column T-401 (dlAB/DE)	Styrene column T-402 (dlD/E)
Stages	-	-	-	61	93
Product purity	-	-	-	-	D:99.95 mol% E: 99.95 mol%
Heat duty (GJ/h)	14	212	steam generation	Condenser: 8.0 Reboiler: 11.0	Condenser: 47.3 Reboiler: 46.5
Utility cost ($/h)	136	1274	0	93	399

4.4.5.4 Step R.4: Generation of feasible substitution search space

Step S.1 (mixture analysis): As listed in reactions R-1, R-2, and R-3, there are eight components in the system. However, the three noncondensable gases and water are not considered for mixture analysis as they can be easily separated by flash and decantation, respectively. So, only four components, benzene, toluene, ethylbenzene, and styrene, are considered. It forms 6 binary pairs. No binary azeotropes are detected for these six binary pairs, and binary pairs A/E, and B/D have a eutectic point at 225 k, with a mixture of 35 % A and 158 k, with a mixture of 45% B, respectively.

Step S.2 (Generation of feasible separation techniques): The feasible separation techniques of these 6 binary pairs are generated based on the pure component properties listed in Appendix 2. Table 36 gives the feasible separation techniques for the separation task of toluene/ethylbenzene (B/D), ethylbenzene/styrene (D/E), and ternary mixture toluene/ethylbenzene/styrene (B/D/E).

For separation task D/E, from Table 36, three separation techniques: adsorption, distillation adsorption, and dividing wall column, are the potential alternatives for the styrene column. However, the dividing wall column is excluded because the product purity requirement is higher than 99.5%. So, in this step, the remaining two alternatives are considered as feasible separation

alternatives. As only two alternatives are available, we skip the ranking step and directly go to step R.6.

Table 36. Identified feasible separation techniques for separating B/D, D/E, and B/D/E of styrene production process.

Binary pair	Separation techniques identified
B/D	distillation (dl), liquid membrane (lm), adsorption (ad), pervaporation (pv), distillation-membrane (dllm,dlpv), distillation-adsorption(dlad)
D/E	Distillation (dl), adsorption (ad), distillation-adsorption (dlad)
B/D/E	dividing wall column distillation (dwc)

4.4.5.5 Step R.6: Generation of process alternatives

With two alternative separation techniques, two process alternatives are listed in Table 37. The flow scheme of these two process alternatives is shown in Figure 32.

Table 37. Identified feasible alternative solutions for styrene production.

Base case process	(iC)[(iABD)](reABCD/ABCDE)<1(flABDE/C)(dlDE/AB)1(dlE/D)
Process alternative 1	(iC)[(iABD)](reABCD/ABCDE)<1(flABDE/C)(dlDE/AB)1(adE/D)
Process alternative 2	(iC)[(iABD)](reABCD/ABCDE)<1(flABDE/C)(dlDE/AB)1(dladE/D)

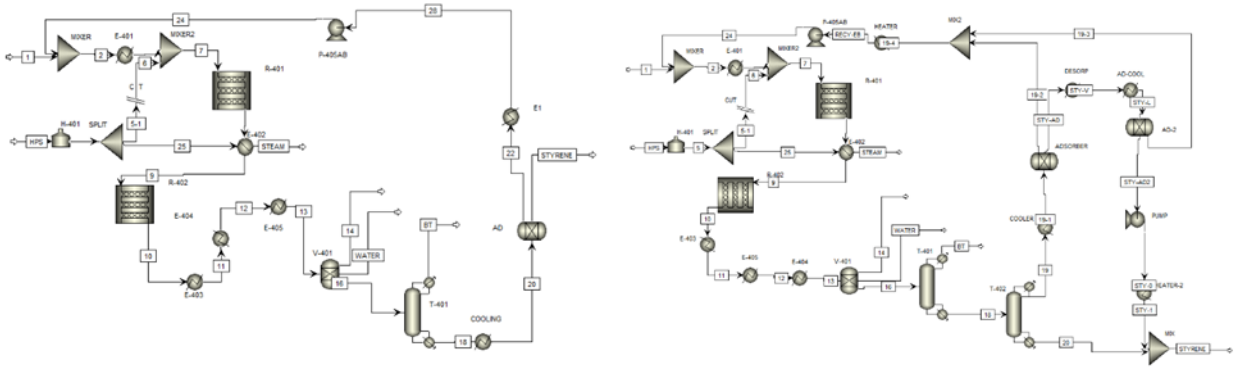

Figure 32. Process diagram of alternative 1 (left) and 2 (right) for styrene production.

4.4.5.6 Step R.7: Process design & rigorous simulation

Two process alternatives are selected from the previous step, and the design parameters, such as adsorbent loading capacity, selectivity, etc., are firstly decided. For adsorption (process alternative 1), literature (Zhou et al., 2019) reported a high selective (selectivity: 1,250; loading:

2.3 mol/Kg) molecular sieve adsorbent for styrene ethylbenzene separation. So, these data are considered for simulating the adsorption unit. For hybrid distillation adsorption (process alternative 2), the adsorption unit's inlet concentration (switching composition) needs to be determined. Usually, lower switching composition leads to lower distillation reboiler duty but higher adsorption capital cost because of a higher amount of adsorbed components. So the decision of switching composition should balance the additional capital cost and the distillation reboiler utility savings. Since there is no reported sorbent price data for the selected molecular sieve adsorbent, the maximum allowable sorbent price at different switching compositions and payback times is calculated in Table 38. Noted here, the payback time is defined as the ratio of additional capital expenditures and utility savings. An example of hybrid distillation simulation results at switching composition 90% is given in Table 39. Figure 33 plots their downstream separation section's utility cost and environmental factors for the selected two process alternatives. From Figure 33, alternative 1, which uses adsorption, significantly improves energy consumption and environmental impact. However, because of the large amount of adsorbed components, it may require a high investment cost. Alternative 2, which applies hybrid separation, can achieve 5% energy saving (switching composition at 90%) and around 3% improvement of environmental factors.

Table 38. Maximum adsorbent price for a double-adsorption system at different switching compositions.

	Switching composition of ethylbenzene, mol%			
	80%	85%	90%	95%
Total additional capital cost, $	127,200	125,100	123,500	122,000
Total utility savings, $/yr	695,560	520,347	367,532	231,540
Payback time, yr	Maximum adsorbent cost, $/Kg			
5	72.5	75.8	83.3	105.9
10	147.7	155.5	172.6	224.2
20	298.1	314.8	351.2	460.8

Table 39. Rigorous simulation results of alternative 2 for styrene production.

	Distillate cooler	Ethylbenzene heater	Styrene heater	Styrene column T-402 (dladD/E)
stages	-	-	-	93
Product purity	-	-	-	D:99.95 mol% E: 99.95 mol%
Heat duty (GJ/h)	1.58	1.34	0.69	Condenser: 41.97 Reboiler: 41.08
Utility cost ($/h)	0.56	10.88	5.67	352.53

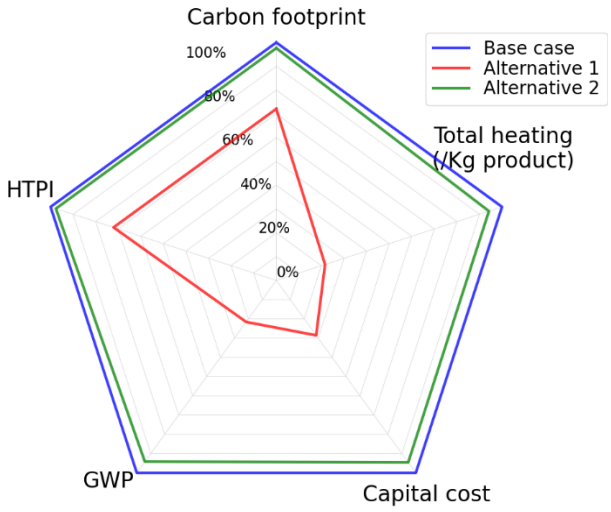

Figure 33. Comparison of three processes downstream separation section for styrene production.

4.5 Conclusions

This study presents an integrated process synthesis framework, including reaction synthesis and separation synthesis. Giving the product or raw materials, the reaction synthesis generates multiple feasible reaction pathways, while the separation synthesis identifies the best downstream separation flowsheet, including intensified/hybrid separation techniques. In the separation synthesis, solvent evaluation, agent-based distillation, and five hybrid/intensified separation techniques are considered, and the selection criteria of the five advanced separation technologies are presented. With the assistance of thermodynamically based insights, a fast and

reliable separation search space is now available to give suggestions on process design either for new or retrofitting purposes. The framework was applied to new process designs of acrylic acid production, DMC production, and isobutylene utilization case studies. 112 process alternatives were generated for acrylic acid production via the propylene oxidation pathway. The results reveal that for acrylic acid production, extractive distillation with solvent sulfolane is recommended for mixture separation, and the application of hybrid membrane distillation is constrained by membrane performance. For DMC production, three potential reaction pathways were selected, and 288 process alternatives were generated, including 7 conventional, 8 intensified, 261 hybrid, and 12 combined hybrid intensified solutions. Among these process alternatives, the identified best DMC production process is using propylene carbonate and methanol as reactants with distillation-membrane and dividing wall column for separation, resulting in 20% lower operating cost than the conventional extractive distillation process. For isobutylene utilization, 86 process alternatives were generated for the selected pathways, and the process that uses water, carbon monoxide, and isobutylene for pivalic acid production with distillation for separation yield the highest process profit.

This framework also applied to two retrofitting case studies, e.g., cumene and styrene production. It verifies that we could find feasible substitution separation techniques to replace the original energy-intensive separation unit through the available separation search space. In the cumene case study, three process alternatives were generated, including two conventional and one intensified alternative. Among these three alternatives, a dividing wall column is suggested for the separation of the cumene product, which can save 20% utility cost for the downstream separation section. In the styrene case study, one conventional and one hybrid process alternative was

generated. The selected hybrid distillation-adsorption process alternative can save up to 5% utility cost (switching composition at 90%) for styrene production.

In this study, we generate an integrated framework to assist the process design, focusing on identifying new reaction pathways and corresponding separation techniques to solve process design problems. Based on a given target product/raw material, this framework can be applied to identify its optimal raw material/products and their associated process configurations.

Chapter 5 – **Simultaneous Pathways and Downstream Separation Network Optimization**

This chapter presents an optimization framework, integrating reaction pathways selection and downstream separation network optimization. Figure 34 gives a typical chemical production process in the process industry. Different chemical products are generated after passing through various multistep reaction and separation processes by using different raw materials. From reaction to product separation, various feasible configurations can be generated based on different separation techniques and separation sequences, and the selected options significantly influence the overall process cost and sustainability. An expansion of the proposed generalized distillation network optimization model (Ryu and Maravelias, 2021) that considers the selection of heating utilities, different input mixtures, and process carbon emissions are developed in this study to identify the optimal sustainable process route for chemical production or raw material utilization. Section 5.1 provides an overview of the optimization framework, while Section 5.2 details the downstream network optimization model, including input parameters, decision variables, objectives, and constraints. Case studies are presented in Section 5.3, and finally, Section 5.4 concludes this study.

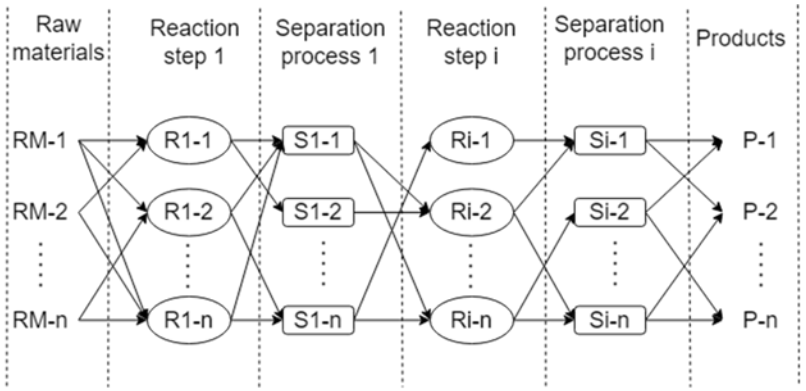

Figure 34. Process routes from the resources to products.

5.1 Optimization Framework

The primary objective is to construct an optimization framework that enables the identification of the best process route for producing a specific product or utilizing raw materials. This framework consists of two key components: 1) the selection of reaction routes to convert raw materials into products and 2) the identification of optimal separation configurations to transform the reaction outlet into the final product. Figure 35 illustrates the optimization framework for process route selection. The framework input requires a list of feasible pathways (N) that have S number of reaction steps. For pathway n, the separation network optimization, which determines the optimal separation process by minimizing/maximizing the process cost/profit, is applied to identify the optimal separation flowsheet for the reaction outlet mixture from reaction step s. By combining the optimal flowsheet for each step of the reaction, the optimal separation process for the entire pathway n can be determined. In this way, the optimal separation processes for all feasible pathways are generated, and the optimal process route can be decided by selecting the process flowsheet with the maximum/minimum overall objective values. Here, the input data of the network optimization are component flowrates and compositions, which are calculated based on reaction conversion rate and selectivity. The associated component thermodynamic properties, such as boiling point, relative volatility, and latent heat, are extracted from a thermodynamic database. For this study, the database within Aspen Plus was utilized.

In this framework, a generalized network optimization model is essential due to the varying number of components involved in different reaction pathways. An expansion of the downstream separation network optimization model (Ryu and Maravelias, 2021), considering the selection of different heating utilities, different inlet mixtures, and process carbon emissions, is employed to

perform the process route selection. A detailed description of the downstream network optimization model is provided in Section 5.2.

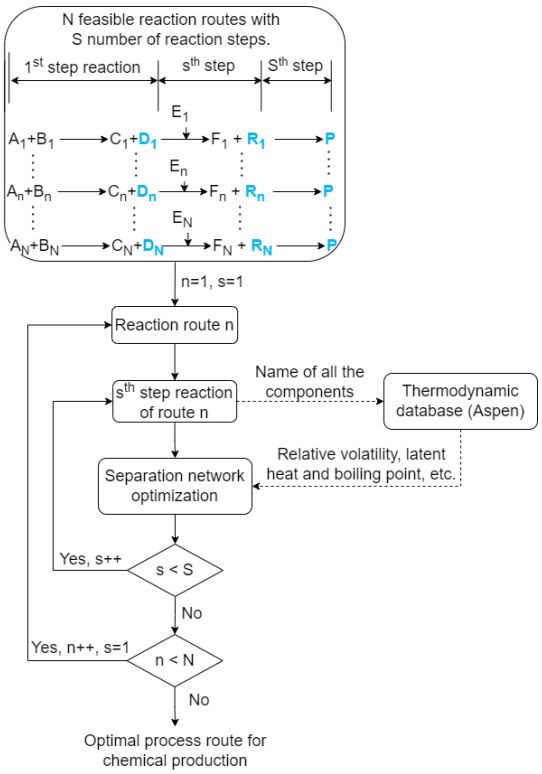

Figure 35. An optimization framework for process route selection.

5.2 Model Formulation

This section presents a detailed explanation of the developed mixed-integer nonlinear programming (MINLP) model. Our model expands Ryu and Maravelias (2021) model to identify a sustainable and profitable process route for raw material utilization. The constraints in Equations 5.1 – 5.7, 5.10 – 5.17, 5.19 – 5.44, and 5.47 – 5.76 were developed Ryu and Maravelias (2021) and are included here for completeness. To identify a sustainable and profitable process route for raw material utilization, we developed and incorporated constraints to include the selection of heat utilities, process carbon emissions, and process profit. Figure 36 illustrates the process routes optimization superstructure for one step of chemical production. In Figure 36, the target product

D is produced from different reaction pathways, resulting in different components in the outlet mixture. The outlet mixture, containing component A_i, B_i, C_i and D, is sent to the downstream separation section to produce a purified product. The downstream network is represented as nodes and arcs, where nodes denote mixtures and arcs denote streams, so that the connection of arcs and nodes represents the separation flowsheet. Depending on the different combinations of mixture nodes, various separation paths are generated, and the optimal process flowsheet is identified by minimizing the downstream separation cost or maximizing the process profit. In the downstream network optimization, the components of the inlet mixture, with decreasing order of volatilities, are defined in the ordered set $I = \{A, B, C, \dots\}(|I| = N)$ where i represents the element of set I. The separation network is defined by a matrix with N rows and N columns, where set J and K represent the rows and columns. Thus, the distillation and the interconnection streams can be denoted as matrix nodes and arcs.

The set of node (N^D), mixture node (N^M) and pure component node (N^P) in Fig. 3 are defined in Equations. 5.1 – 5.3.

$$N^D = \{(j,k)|j \le k, j \in J, k \in K\} \quad 5.1$$
$$N^M = \{(j,k)|j \le k, k < N-1, j \in J, k \in K\} \quad 5.2$$
$$N^P = \{(j,k)|j \le k, k = N-1, j \in J, k \in K\} \quad 5.3$$

The set of top/bottom arcs in Figure 36, representing the interconnection of upstream and downstream nodes, are defined Equations 5.4 – 5.5.

$$A^T = \{(j,k,j',k')|k' > k, j = j', (j,k) \in N^M, (j',k') \in N^D\} \quad 5.4$$
$$A^B = \{(j,k,j',k')|k' > k, k-j = k'-j', (j,k) \in N^M, (j',k') \in N^D\} \quad 5.5$$

For each node, the set of lightest and heaviest components are defined in Equations 5.6 – 5.7.

$$Lt = \{(j,k)|i = j, (j,k) \in N^D\} \quad 5.6$$

$$Ht = \{(j,k)|i = (N-1) - k + j, (j,k) \in N^D\} \quad 5.7$$

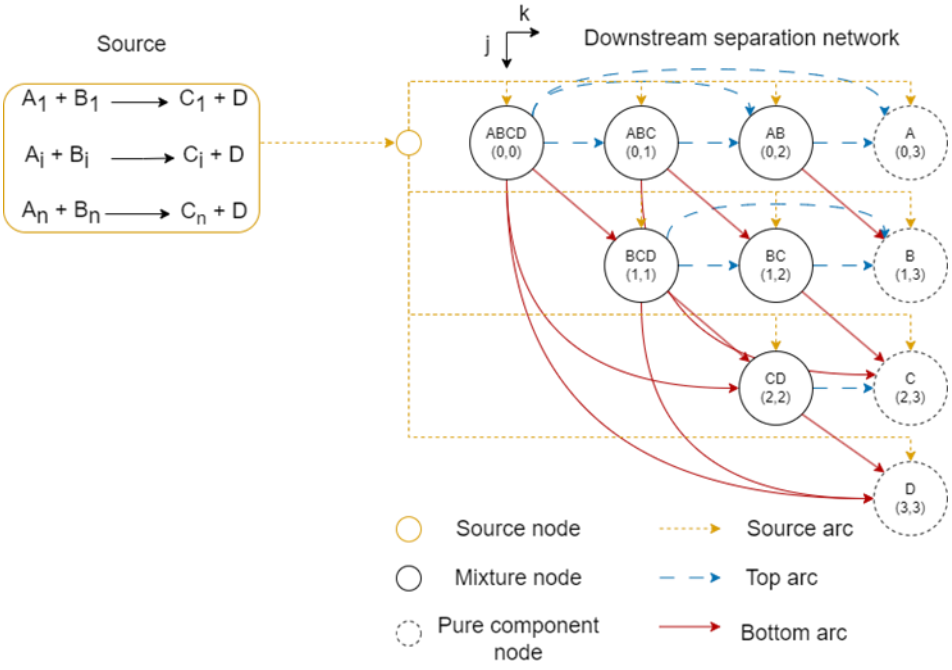

Figure 36. Superstructure representation of the distillation separation network.

5.2.1 Objective Function

The objective is to identify the optimal process route for chemical production or raw material utilization that ensures both process profit and sustainability. For the chemical production problem, the model determines the best production route by minimizing the operating cost (Equation 5.8). For raw material utilization, the model identifies the optimal utilization process route by maximizing the process profit per amount of carbon emissions (Equation 5.9).

$$\sum_j \sum_k U_{j,k} \quad 5.8$$

$$\frac{\sum_{i,i=j} P_i F_{i,j,N-1} - \sum_j \sum_k U_{j,k}}{\sum_j \sum_k C_{j,k}} \quad 5.9$$

Here, $U_{j,k}$ and $C_{j,k}$ denote the utility cost and carbon emissions of node jk. P_i denotes the selling price of component i, and $F_{i,j,N-1}$ denote the inlet flowrate of component i in the pure component node (refer to Figure 36).

5.2.2 Binary Variables

A binary variable yc_i is defined in Equation 5.10 to represent the existence of component i in the source. Binary variable $ys_{j,k}$ is given in Equation 5.11 to represent if the source stream is fed into column jk, and the binary variable $yn_{j,k}$ is introduced in Equation 5.12 to denote the activeness of this column. To represent the top and bottom stream connections between two columns ($jk, j'k'$), binary variables $yt_{j,k,j',k'}$ and $yb_{j,k,j',k'}$ are defined in Equation 5.13. Binary variable $yXR_{j,k,i}$ in Equation 5.14 denotes the difference of two active Underwood roots ($i, i+1$) in column jk. Additionally, binary variables $ylk_{j,k,i}, yhk_{j,k,i}$ and $ydc_{j,k,i}$ in Equation 5.15 – 5.17 are introduced to denote the light key, heavy key, and distributed component selection in column jk, respectively. And binary variable $yhu_{j,k,m}$ is defined in Equation 5.18 to represent if heating utility m ($m \in M$) is selected for column jk, where set M represents different types of heating utilities (low/medium/high pressure steam, natural gas).

$$yc_i = \begin{cases} 1, \ if\ component\ i\ present\ in\ the\ source \\ 0, \ otherwise \end{cases} \quad 5.10$$

$$ys_{j,k} = \begin{cases} 1, \ if\ source\ is\ assigned\ to\ column\ jk \\ 0, \ otherwise \end{cases} \quad 5.11$$

$$yn_{j,k} = \begin{cases} 1, \ if\ column\ jk\ \ is\ active \\ 0, \ otherwise \end{cases} \quad 5.12$$

$$yt_{j,k,j',k'},\ yb_{j,k,j',k'} = \begin{cases} 1, \ if\ top/bottom\ of\ column\ jk\ \ to\ column\ j'k'\ (jk\ \neq j'k') \\ 0, \ otherwise \end{cases} \quad 5.13$$

$$yXR_{j,k,i} = \begin{cases} 1, \ if\ active\ root\ i\ is\ different\ with\ i+1\ in\ column\ jk \\ 0, \ otherwise \end{cases} \quad 5.14$$

$$ylk_{j,k,i} = \begin{cases} 1, \ if\ component\ i\ is\ the\ light\ key\ in\ column\ jk \\ 0, \ otherwise \end{cases} \quad 5.15$$

$$yhk_{j,k,i} = \begin{cases} 1, \ if \ component \ i \ is \ the \ heavy \ key \ in \ column \ jk \\ 0, \ otherwise \end{cases} \quad 5.16$$

$$ydc_{j,k,i} = \begin{cases} 1, \ if \ component \ i \ is \ distributed \ in \ column \ jk \\ 0, \ otherwise \end{cases} \quad 5.17$$

$$yhu_{j,k,m} = \begin{cases} 1, \ if \ heating \ utility \ m \ is \ selected \ in \ column \ jk \\ 0, \ otherwise \end{cases} \quad 5.18$$

5.2.3 Parameters

The initial mole flowrate from the source is denoted as F_i^0. N denotes the total number of components in the source stream. The relative volatility, boiling point, selling price, and latent heat of each component in the source stream are denoted as Re_i, Tb_i, P_i and H_i, respectively. For different types of heating utility, their critical temperature and price are denoted as Tu_m and Pu_m. For cooling utility, the price of cooling water is denoted as P^w. Additionally, the component recovery and purity specifications are denoted as ps and rs. In this model, natural gas is set as the primary fuel for generating the utility. The standard natural gas carbon emissions factor (50.15 Kg CO_2/GJ) (Shi et al., 2022) is denoted as η.

5.2.4 Logic Rules and Connectivity

It is assumed that only one source arc is active (Equation 5.19), and the node is active if the associated source arc is active (Equation 5.20).

$$\sum_{(j,k)\in N^D} ys_{j,k} = 1 \quad 5.19$$

$$ys_{j,k} \le yn_{j,k}, (j',k') \in N^D \quad 5.20$$

Also, the node is deactivated if the lightest/heaviest key component does not exist in the source stream (Equations 5.21 – 5.24).

$$\Delta F yc_i \le F_i^0, i \in I \quad 5.21$$

$$F^M yc_i + \Delta F(1 - yc_i) \ge F_i^0, i \in I \quad 5.22$$

$$yn_{j,k} \le yc_i, (j,k,i) \in Lt \quad 5.23$$

$$yn_{j,k} \le yc_i, (j,k,i) \in Ht \quad 5.24$$

where ΔF and F^M represent relative small and large flowrate.

The associated upstream and downstream arcs should remain active if the mixture node is active, and the corresponding constraints are defined below (Equations 5.35 – 5.30).

$$yn_{j',k'} \leq \sum_{(j,k,j',k')\in A^T} yt_{j,\,k,\,j',\,k'} + \sum_{(j,k,j',k')\in A^B} yb_{j,\,k,\,j',\,k'} + ys_{j',k'}, (j',k') \in N^M \quad 5.25$$

$$yn_{j',k'} \geq \sum_{(j,k,j',k')\in A^T} yt_{j,\,k,\,j',\,k'} + \sum_{(j,k,j',k')\in A^B} yb_{j,\,k,\,j',\,k'}, (j',k') \in N^M \quad 5.26$$

$$yn_{j,k} \leq \sum_{(j,k,j',k')\in A^T} yt_{j,\,k,\,j',\,k'}, (j,k) \in N^M \quad 5.27$$

$$yn_{j,k} \leq \sum_{(j,k,j',k')\in A^B} yb_{j,\,k,\,j',\,k'}, (j,k) \in N^M \quad 5.28$$

$$\sum_{(j,k,j',k')\in A^T} yt_{j,\,k,\,j',\,k'} = \sum_{(j,k,j',k')\in A^B} yb_{j,\,k,\,j',\,k'}, (j,k) \in N^M \quad 5.29$$

$$2yn_{j,k} = \sum_{(j,k,j',k')\in A^T} yt_{j,\,k,\,j',\,k'} + \sum_{(j,k,j',k')\in A^B} yb_{j,\,k,\,j',\,k'}, (j,k) \in N^M \quad 5.30$$

5.2.5 Material and Energy Balance

5.2.5.1 Column inlet/outlet

Equations 5.31 – 5.40 list the column mass balance constraints. From Figure 36, node jk has three inlet streams from the source node and upstream column node, with two outlet streams directed towards the downstream node. Equations 5.31 – 5.32 represent the mass balance between the source node and the distillation column, assuming that the source stream can only feed into one column node. Equation 5.33 is the mass balance for the inlet and outlet of the distillation node, and Equations 5.34 – 5.40 show the component mass balance in node $j'k'$, where the node inlet flowrate equals the three inlet streams from the connected source node and upstream column node jk.

$$\sum_j \sum_k Fs_{i,j,k} = F_i^0,\ i \in I \quad 5.31$$

$$Fs_{i,j,k} \le F^M ys_{j,k}, i \in I, (j,k) \in N^D \quad 5.32$$

$$F_{i,j,\,k} = F^t_{i,j,k} + F^b_{i,j,k},\ i \in I, (j,k) \in N^M \quad 5.33$$

$$F_{i,j',\,k'} = Fs_{i,j',k'} + \sum_{(j,k,j',k') \in A^T} F^t_{i,j,k,j',k'} + \sum_{(j,k,j',k') \in A^B} F^b_{i,j,k,j',k'}, i \in I \quad 5.34$$

$$F^t_{i,j,k,j',k'} \le F^t_{i,j,k}, i \in I, (j,k,j',k') \in A^T \quad 5.35$$

$$F^t_{i,j,k,j',k'} \ge F^t_{i,j,k} - F^M\left(1 - yt_{j,k,j',k'}\right), i \in I, (j,k,j',k') \in A^T \quad 5.36$$

$$F^t_{i,j,k,j',k'} \le F^M yt_{j,k,j',k'}, i \in I, (j,k,j',k') \in A^T \quad 5.37$$

$$F^b_{i,j,k,j',k'} \le F^b_{i,j,k}, i \in I, (j,k,j',k') \in A^B \quad 5.38$$

$$F^b_{i,j,k,j',k'} \ge F^b_{i,j,k} - F^M\left(1 - yb_{j,k,j',k'}\right), i \in I, (j,k,j',k') \in A^B \quad 5.39$$

$$F^b_{i,j,k,j',k'} \le F^M yb_{j,k,j',k'}, i \in I, (j,k,j',k') \in A^B \quad 5.40$$

In Equations 5.31 – 5.40, $Fs_{i,j,k}$ denotes the inlet flowrate of component i from the source to node jk. $F_{i,j,\,k}$ denotes the inlet flowrate of component i to node jk. $F^t_{i,j,k}, F^b_{i,j,k}$ are the outlet distillate and bottom flowrates of component i from node jk. $F^t_{i,j,k,j',k'}, F^b_{i,j,k,j',k'}$ are the flowrates of component i in distillate and bottom streams sent from node jk to $j'k'$.

5.2.5.2 Distillation internal liquid/vapor balance

The distillation has rectifying and stripping sections, and the corresponding vapor/liquid mass balance constraints are given in Equations 5.41 – 5.42. Equations 5.43 – 5.44 assume the component is completely recovered in the distillate/bottom stream if it is lighter/heavier than the light/heavy key component in the distillation. Equations 5.45 – 5.46 constraint that the lighter/heavier component has higher recovery in the distillate/bottom stream.

$$\sum_i F^t_{i,j,k} = Fv^t_{j,k} - Fl^t_{j,k}, i \in I, (j,k) \in N^M \quad 5.41$$

$$\sum_i F^b_{i,j,k} = Fl^b_{j,k} - Fv^b_{j,k}, i \in I, (j,k) \in N^M \quad 5.42$$

$$F^t_{i,j,k} \le (1 - \sum_{i',i'<i} yhk_{j,k,i'})\, F^M, i \in I, (j,k) \in N^M \quad 5.43$$

$$F^b_{i,j,k} \le \sum_{i',i' \le i} ylk_{j,k,i'}\, F^M, i \in I, (j,k) \in N^M \quad 5.44$$

$$F^t_{i,j,k} F_{i+1,j,k} \ge F^t_{i+1,j,k} F_{i,j,k}, i \in I, (j,k) \in N^M, i < N-1 \quad 5.45$$

$$F^b_{i,j,k}F_{i-1,j,k} \geq F^b_{i-1,j,k}F_{i,j,k}, i \in I, (j,k) \in N^M, i \geq 1 \quad 5.46$$

where $Fv^t_{j,k}, Fl^t_{j,k}$ represent the vapor and liquid flowrates in the rectifying section of node jk. $Fv^b_{j,k}, Fl^b_{j,k}$ are the vapor and liquid flowrate in the stripping section of node jk.

To estimate the vapor/liquid flowrate in the distillation column, a generalized Underwood method (Ryu and Maravelias, 2020) was applied and given in Equations 5.47 – 5.52. The upper and lower bound constraints for each Underwood root are given in Equations 5.53 – 5.54. Additionally, the number of Underwood roots are determined by the number of components and the selection of key component in the mixture node. Equations 5.55 – 5.61 give the corresponding constraints.

$$Re_i F_{i,j,k} = (Re_i - ur_{j,k,i'})uf_{i,i',j,k}, i \in I, i' \in I, (j,k) \in N^M, (i',j,k) \in R^A \quad 5.47$$
$$Re_i F^t_{i,j,k} = (Re_i - ur_{j,k,i'})ut_{i,i',j,k}, i \in I, i' \in I, (j,k) \in N^M, (i',j,k) \in R^A \quad 5.48$$
$$Re_i F^b_{i,j,k} = (Re_i - ur_{j,k,i'})ub_{i,i',j,k}, i \in I, i' \in I, (j,k) \in N^M, (i',j,k) \in R^A \quad 5.49$$
$$\sum_i uf_{i,i',j,k} = 0, i \in I, i' \in I, (j,k) \in N^M, (i',j,k) \in R^A \quad 5.50$$
$$\sum_i ut_{i,i',j,k} \leq Fv^t_{j,k}, i \in I, i' \in I, (j,k) \in N^M, (i',j,k) \in R^A \quad 5.51$$
$$\sum_i ub_{i,i',j,k} \leq Fv^b_{j,k}, i \in I, i' \in I, (j,k) \in N^M, (i',j,k) \in R^A \quad 5.52$$
$$ur_{j,k,i'} \geq \sum_i (Re_i + \Delta U) yhk_{j,k,i}, i \in I, i' \in I, (j,k) \in N^M, (i',j,k) \in R^A \quad 5.53$$
$$ur_{j,k,i'} \leq \sum_i (Re_i - \Delta U) ylk_{j,k,i}, i \in I, i' \in I, (j,k) \in N^M, (i',j,k) \in R^A \quad 5.54$$
$$yXR_{j,k,i} = ydc_{j,k,i+1} yc_{i+1}, i \in I, (j,k) \in N^M, (i,j,k) \in R^{AD} \quad 5.55$$
$$yXR_{j,k,i} \leq yn_{j,k}, i \in I, (j,k) \in N^M, (i,j,k) \in R^{AD} \quad 5.56$$
$$ur_{j,k,i} \geq (Re_{i+1} + \Delta U) yXR_{j,k,i}, i \in I, (j,k) \in N^M, (i,j,k) \in R^{AD} \quad 5.57$$
$$ur_{j,k,i+1} \leq (Re_{i+1} - \Delta U) yXR_{j,k,i} + Re^M(1 - yXR_{j,k,i}), i \in I, (j,k) \in N^M, (i,j,k) \in R^{AD} \quad 5.58$$
$$ur_{j,k,i} - ur_{j,k,i+1} = urg_{j,k,i}, i \in I, (j,k) \in N^M, (i,j,k) \in R^{AD} \quad 5.59$$
$$urg_{j,k,i} \geq 0.001 yXR_{j,k,i}, i \in I, (j,k) \in N^M, (i,j,k) \in R^{AD} \quad 5.60$$
$$urg_{j,k,i} \leq Re^M yXR_{j,k,i}, i \in I, (j,k) \in N^M, (i',j,k) \in R^{AD} \quad 5.61$$

In Equations 5.47 – 5.61, set $R^A = \{(i,j,k)|i > j, i \leq N-2-k+j, j \in J, k \in K\}$ represents the number of feasible Underwood roots in the mixture node jk, and set $R^{AD} = \{(i,j,k)|i > j, i \leq N-3-k+j, j \in J, k \in K\}$ represents the corresponding number of intervals. Continuous variable $ur_{j,k,i}$ and $ur_{j,k,i'}$ denote the Underwood root of element i and i' in the mixture node jk. The variables $uf_{i,i',j,k}$, $ut_{i,i',j,k}$ and $ub_{i,i',j,k}$ are three intermediate Underwood variables. The parameters Re^M and ΔU denote a relatively large and small number determined based on the component relative volatility, and $urg_{j,k,i}$ denotes the difference between two Underwood roots in the mixture node jk.

5.2.6 Key Component Selection

The selection of light/heavy key components is carried out according to the downstream node ($j'k'$ and $j''k''$) that connect to the same upstream node (jk). The set of feasible light and heavy key components are defined in Equations 5.62 – 5.63.

$$I^{LK} = \begin{cases} \{(j',k',j'',k'',i)|i \geq j', i \leq j''-1, j'' \leq N-1-k'+j'\} \\ \{(j',k',j'',k'')|i = N-1-k'+j', j'' > N-1-k'+j''\} \end{cases}, i \in I, (j,k) \in N^D, (j'',k'') \in N^D \quad 5.62$$

$$I^{HK} = \begin{cases} \{(j',k',j'',k'',i)|i \geq N-k'+j', i \leq N-1-k''+j'', j'' \leq N-1-k'+j'\} \\ \{(j',k',j'',k'')|i = j'', j'' > N-1-k'+j''\} \end{cases}, i \in I, (j,k) \in N^D, (j'',k'') \in N^D \quad 5.63$$

The light/heavy key component must exist when the mixture node is active, and the key component cannot be selected if the component does not exist in the source stream. The associated constraints are defined in Equations 5.64 – 5.67.

$$\sum_i ylk_{j,k,i} = yn_{j,k}, (j,k) \in N^M \quad 5.64$$

$$\sum_i yhk_{j,k,i} = yn_{j,k}, (j,k) \in N^M \quad 5.65$$

$$ylk_{j,k,i} \le yc_i, i \in I, (j,k) \in N^M \quad 5.66$$

$$yhk_{j,k,i} \le yc_i, i \in I, (j,k) \in N^M \quad 5.67$$

The component whose relative volatility is located between the light and heavy key components is distributed throughout the distillation column, and this constraint is defined in Equation 5.68.

$$ydc_{j,k,i} \le \sum_{i',i' \le i-1} ylk_{j,k,i'} - \sum_{i',i' \le i} yhk_{j,k,i'}, i \in I, (j,k) \in N^M \quad 5.68$$

Equations 5.69 – 5.70 ensure the existence of a key component if the mixture node is active and connected with downstream mixture nodes. Equations 5.71 – 5.72 assumes that the light/heavy key component is selected if it is the heaviest/lightest component in the set of feasible key components.

$$\sum_i ylk_{j,k,i} \ge yb_{j,k,j'',k''} + yt_{j,k,j',k'} - yn_{j,k}, (j,k) \in N^M, (j,k,j',k') \in A^T, (j,k,j'',k') \in A^B, (j',k',j'',k'',i) \in I^{LK} \quad 5.69$$

$$\sum_i yhk_{j,k,i} \ge yb_{j,k,j'',k''} + yt_{j,k,j',k'} - yn_{j,k}, (j,k) \in N^M, (j,k,j',k') \in A^T, (j,k,j'',k') \in A^B, (j',k',j'',k'',i) \in I^{LK} \quad 5.70$$

$$ylk_{j,k,i} \le 1 - yc_{i'} + (2yn_{j,k} - yb_{j,k,j'',k''} - yt_{j,k,j',k'}), (j,k) \in N^M, (j,k,j',k') \in A^T, i \in I, i' \in I, (j,k,j'',k'') \in A^B, (j',k',j'',k'',i) \in I^{LK}, (j',k',j'',k'',i') \in I^{LK}, i' > i \quad 5.71$$

$$yhk_{j,k,i} \le 1 - yc_{i'} + (2yn_{j,k} - yb_{j,k,j'',k''} - yt_{j,k,j',k'}), (j,k) \in N^M, (j,k,j',k') \in A^T, i \in I, i' \in I, (j,k,j'',k'') \in A^B, (j',k',j'',k'',i) \in I^{HK}, (j',k',j'',k'',i') \in I^{HK}, i' < i \quad 5.72$$

5.2.7 Heating and Cooling Cost Estimation

The heating/cooling cost is based on the column heat duty, which is determined by the enthalpy balance for the rectifying and stripping section. Equations 5.73 – 5.74 list the condenser and reboiler enthalpy balance constraints. In general, the mixture latent heat, averaging based on the pure component latent heats and mixture compositions, is employed to determine the vapor

condensation (Equation 5.73) and liquid vaporization (Equation 5.74) heat duties. Equations 5.75 – 5.76 assume that the distillation heat duty is equal to 0 if the associated column node is not selected.

$$cq_{j,k}\sum_{i}F_{i,j,k}^{t}=\sum_{i}H_{i}F_{i,j,k}^{t}Fv_{j,k}^{t},(j,k)\in N^{M} \quad 5.73$$

$$rq_{j,k}\sum_{i}F_{i,j,k}^{b}=\sum_{i}H_{i}F_{i,j,k}^{b}Fv_{j,k}^{b},(j,k)\in N^{M} \quad 5.74$$

$$0\leq cq_{j,k}\leq Q^{M}yn_{j,k},(j,k)\in N^{M} \quad 5.75$$

$$0\leq rq_{j,k}\leq Q^{M}yn_{j,k},(j,k)\in N^{M} \quad 5.76$$

where $cq_{j,k}$ and $rq_{j,k}$ represent the condenser and reboiler duty for mixture node jk, and Q^{M} denotes a relatively big value for heat duty.

It is assumed that cooling water is used as cooling utility for the column condenser, and the utility cost estimation constraint is given in Equation 5.77.

$$U_{j,k}^{t}\geq cq_{j,k}P^{w},(j,k)\in N^{M} \quad 5.77$$

where $U_{j,k}^{t}$ denotes the condenser utility cost.

The reboiler heating cost is based on the selection of heating utilities, which have different prices and operating ranges. Equations 5.78 – 5.79 gives the constraints for reboiler temperature calculation. Equations 5.80 – 5.87 list the constraints for heating cost estimation based on the calculated reboiler temperature. The distillation carbon emission rate is calculated in Equation 5.88.

$$T_{j,k}\sum_{i}F_{i,j,k}^{b}=\sum_{i}Tb_{i}F_{i,j,k}^{b},(j,k)\in N^{M} \quad 5.78$$

$$T_{j,k}\leq T^{M}yn_{j,k},(j,k)\in N^{M} \quad 5.79$$

$$U_{j,k}^{b}\geq\sum_{m}Pu_{m}rq_{j,k,m}^{\prime} \quad 5.80$$

$$\sum_{m} yhu_{j,k,m} = yn_{j,k}, (j,k) \in N^M \quad 5.81$$

$$T_{j,k} \leq \sum_{m} Tu_m yhu_{j,k,m}, (j,k) \in N^M \quad 5.82$$

$$T_{j,k} \geq \sum_{m,m>0} Tu_{m-1} yhu_m, (j,k) \in N^M \quad 5.83$$

$$rq'_{j,k,m} \leq rq_{j,k,m}, m \in M, (j,k) \in N^M \quad 5.84$$

$$rq'_{j,k,m} \leq Q^M yhu_{j,k,m}, m \in M, (j,k) \in N^M \quad 5.85$$

$$rq'_{j,k,m} \geq rq_{j,k,m} + Q^M (yhu_{j,k,m} - 1), m \in M, (j,k) \in N^M \quad 5.86$$

$$rq'_{j,k,m} \geq 0, m \in M, (j,k) \in N^M \quad 5.87$$

$$C_{j,k} = \eta rq_{j,k}, (j,k) \in N^M \quad 5.88$$

where $T_{j,k}$ denotes the reboiler temperature for mixture node jk. T^M is a relatively big number compared to boiling point. $U^b_{j,k}$ denotes the reboiler utility cost. $rq'_{j,k,m}$ is an intermediate variable for reboiler duty calculation.

The constraint for the distillation operating cost, including both condenser and reboiler, is shown in Equation 5.89.

$$U_{j,k} = U^t_{j,k} + U^b_{j,k}, (j,k) \in N^M \quad 5.89$$

5.2.8 Purity and Recovery Specification

The product purity and recovery rate must satisfy the required product specifications (purity: ps, recovery: rs), and the associated constraints are presented in Equations 5.90 – 5.91.

$$F_{i,j,k} \geq ps \sum_{i'} F_{i',j,k}, i = j, (j,k) \in N^P \quad 5.90$$

$$F_{i,j,k} \geq rsF^0_i, i = j, (j,k) \in N^P \quad 5.91$$

5.3 Application Examples

The developed optimization model was applied to three case studies to find the best process route for utilizing isobutylene/methanol and producing 1,4-Butanediol (BDO). The model was solved using BARON (20.4.14) through Pyomo (5.6.8) on a workstation with Intel Xeon E3-

1230V5 processor 3.40 GHz and 32 GB memory. Note that the separation pressure is adjusted for all the case studies to guarantee that cooling water is used for condensation. Parameters such as utility temperature and price used in the case studies are shown in Appendix 1.

5.3.1 Isobutylene Utilization

This case study considers three alternative isobutylene utilization reaction pathways that produce pivalic acid (PA) (R1), prenol (R2), and tert-butylamine (R3). The parameters such as reaction conversion rate, component relative volatility, price data (SunSirs, China Commodity Data Group), and latent heat are inputs for the optimization model. The component thermodynamic properties are extracted from the Aspen Plus database, and the remaining parameters are given in Table 40. We assume the isobutylene inlet flowrate is 150 kmol/h, and the co-reactant inlet flowrate is calculated based on reaction stoichiometry. The product purity is assumed to be 99.5 mol% with at least 90% recovery rate.

Table 40. Optimization input parameters for the isobutylene utilization case study.

Reaction pathways	Conversion rate	Price, $/kmol
$\text{Isobutylene} + \text{CO} + \text{Water} \rightarrow \text{PA}$	0.8	isotutylene: 51.8
$\text{Isobutylene} + \text{Formaldehyde} \rightarrow \text{Prenol}$	0.8	PA: 510.7
$\text{Isobutylene} + \text{Ammonia} \rightarrow \text{tert} - \text{Butylamine}$	0.52 (Bokade et al., 2014)	formaldehyde: 5.8 prenol: 301.5 ammonia: 13.4 tert-butylamine: 234.1

Because this case study aims to identify the optimal sustainable process route for isobutylene utilization, the objective is to maximize the profit per kg of carbon dioxide emission (refer to Equation 5.9). The optimal solution, including the reaction pathway and process configuration, is shown in Figure 37. The results reveal that using isobutylene for PA production has the highest process profit per kg of CO_2 emissions (291.6 $/(h, kg CO_2)), and the optimal separation configuration for PA production pathway is based on the sequence of component

boiling point. From Table 40, PA product has higher chemical price than prenol and amine products. Additionally, the identified optimal process configuration for pathway R1 has the lowest process carbon emissions compared to R2 and R3 (refer to Table 41), which implies that using isobutylene for PA production ensures both process profit and sustainability. Considering the current conditions that high isobutylene demand comes from alkylate production, an important gasoline additive, the market demand for isobutylene may drop with the development of the electric car. This case study suggests that using isobutylene for PA production may be profitable for future isobutylene utilization.

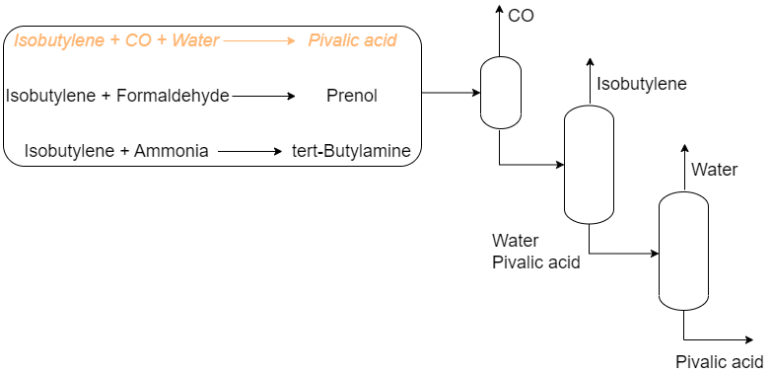

Figure 37. Optimal process route for isobutylene utilization.

Table 41. Process utility cost and carbon emissions for all the pathways' optimal process configurations of isobutylene utilization.

Reaction pathways	Process utility cost, $/h	Process carbon emissions, kg CO_2/h
R1	65.06	188.58
R2	42.29	210.55
R3	62.3	365.42

5.3.2 Methanol Utilization

In this case study, four reaction pathways are considered (Table 42). R1 uses methanol for dimethyl ether (DME) production. R2 converts methanol into gasoline with liquefied petroleum (LPG) gas as a by-product. R3 directly converts methanol into acetic acid (AA), and R4 utilizes

methanol and propylene carbonate (PC) to produce dimethyl carbonate (DMC) with by-product propylene glycol (PG). The reaction pathways, conversion rate, and component price are listed in Table 42. The methanol inlet flowrate is 150 kmol/h, and the co-reactant inlet flowrate is calculated based on reaction stoichiometry. The product purity is assumed to be 99.5 mol% with at least 90% recovery rate.

Table 42. Optimization input parameters for the methanol utilization case study.

Reaction pathways	Conversion rate	Price, $/kmol
$\text{Methanol} \rightarrow \text{DME} + \text{Water}$	0.82 (Luyben 2017)	DME:81.3; Methanol: 11.7
$\text{Methanol} \rightarrow \text{Gasoline} + \text{LPG}$	0.98	LPG:39.1; Gasoline:139
$\text{Methanol} \rightarrow \text{AA}$	0.95 (Kalck et al. 2020)	AA:26.4; DMC: 81.5
$\text{PC} + \text{Methanol} \rightarrow \text{DMC} + \text{PG}$	0.78 (Deng et al. 2019)	PG:103.9; PC: 15.8

Similar to the isobutylene utilization case study, the objective is to identify the optimal process route with the highest profit per kg of carbon dioxide emission. The solution for this case study is shown in Figure 38. The results show that using methanol for gasoline production is the best route for methanol utilization (78.2 $/(h, kg CO_2)). The process configuration, which separates gasoline first, has the best performance. From Table 42, chemical products, gasoline, PG, and DMC, have the top three highest chemical price, suggesting that the methanol utilization pathway R2 and R4 may lead to higher process profit. Table 43 lists all the pathways' process utility cost and carbon emissions based on their optimal process configurations. Pathway R3 has the lowest utility cost and process carbon emissions, but its product, AA, has lower price than gasoline. To ensure process profit and sustainability, pathway R2, whose optimal process has the second lowest utility cost and carbon emissions, is identified as the optimal pathway for methanol utilization. Additionally, pathway R4 has the highest process carbon emissions, resulting in lower objective values, although its products, PG and DMC, have high selling price. However, without considering the process carbon emission, pathway R4 leads to the highest overall process profit.

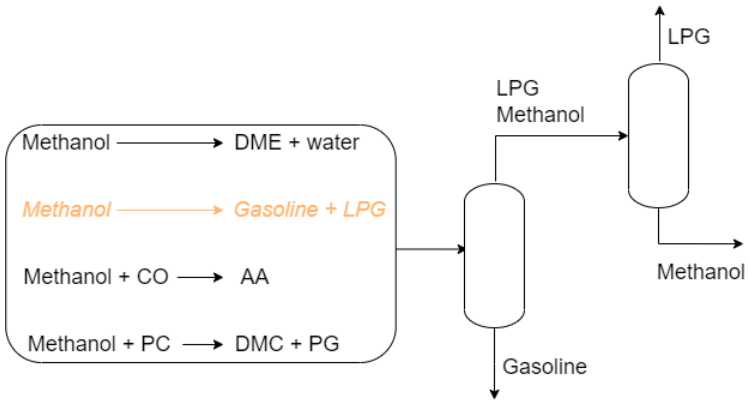

Figure 38. Optimal reaction pathway and configuration for methanol utilization.

Table 43. Process utility cost and carbon emissions for all the pathways' optimal process configurations of methanol utilization.

Reaction pathways	Process utility cost, $/h	Process carbon emissions, kg CO_2/h
R1	46.19	230.13
R2	17.74	87.79
R3	7.06	40.44
R4	99.09	725.46

5.3.3 BDO Production

This case study considers three two-step reaction pathways that use different raw materials, acetylene, propylene oxide, and maleic anhydride, for BDO production. The pathways and the associated conversion rates/selectivities are given in Table 44. We assume 100 kmol/h inlet flowrate for these three raw materials, and the co-reactant inlet flowrate are calculated based on reaction stoichiometry. The product purity is assumed to be 99 mol% with at least 90% recovery rate.

The objective of this case study is to find the best process route for BDO production with the lowest cost per unit product (refer to Equation 5.8). The optimal solution indicates that using acetylene as raw material for BDO production has the lowest cost. Table 45 presents the process cost for all the pathways based on their identified optimal process configurations. Because of high

conversion rate and selectivity in pathway R1 (refer to Table 44), this pathway has the lowest production cost, suggesting that using acetylene for BDO production may lead to higher process profit. Figure 39 plots the identified optimal process route for BDO production. Acetylene first reacts with formaldehyde to produce the intermediate product 1,4-butynediol. Then, the purified 1,4-butynediol, which has formaldehyde contaminant, reacts with hydrogen to produce the final product BDO. The BDO is purified by separating water and formaldehyde contaminant and then separating the remaining three components based on their boiling point sequence. Pointed out by Cukalovic and Stevens (2008), the largest share of the world BDO production is still based on pathway R1, the first developed pathway for BDO production. Additionally, a similar process flowsheet based on pathway R1 was presented in the literature (Teh et al., 2019). This verifies the effectiveness of the developed process route optimization algorithm for identifying the optimal pathway and associated process configuration for chemical production.

Table 44. Potential feasible pathways for the BDO production.

	Pathways
R1	$Acetylene + Formaldehyde \rightarrow 1{,}4-Butynediol$ Conversion rate: 0.97
	$1{,}4-Butynediol + H_2 \rightarrow BDO$ $1{,}4-Butynediol + H_2 \rightarrow 1-Butanol + Water$ Conversion rate: 0.97; Selectivity: 0.95
R2	$Propyelne\ oxide \rightarrow Ally\ alcohol$ $Propyelne\ oxide \rightarrow Propionaldehyde$ Conversion rate: 0.65; Selectivity: 0.94
	$Ally\ alcohol + CO + H_2 \rightarrow BDO$ $Ally\ alcohol + CO + H_2 \rightarrow 2-Methyl-1{,}3-Propanediol + Water$ Conversion rate: 0.93; Selectivity: 0.67 (Stahl and Alsters, 2016)
R3	$Maleic\ anhydride + Water \rightarrow Maleic\ acid$ Conversion rate: 1
	$Maleic\ acid + H_2 \rightarrow BDO + Water$ $Maleic\ acid + H_2 \rightarrow Tetrahydrofuran + Water$ $aleic\ acid + H_2 \rightarrow Gamma\ butyrolactone + Water$ Conversion rate: 0.97; Selectivity: 0.74 (Budge et al. 1995; Hepfer et al. 2006)

Table 45. Process utility cost and carbon emissions for all the pathways' optimal process configurations of BDO production.

Reaction pathways	Process utility cost, $/h	Process utility and raw material cost, $/h
R1	1.84	73.79
R2	4.07	137.22
R3	13.82	168.56

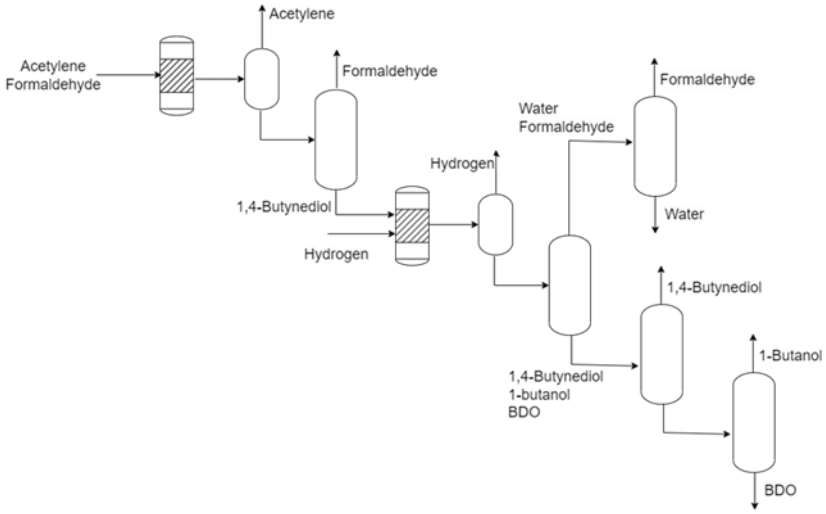

Figure 39. Optimal process route for BDO production.

5.4 Conclusions

In this study, a generalized MINLP model was developed to enable sustainable process selection by integrating reaction pathways and downstream separation network optimization. The model offers a comprehensive approach to identifying the optimal process route with the lowest cost or highest profit, given a specific product/raw material and the potential reaction pathways.

The effectiveness of the model was demonstrated through case studies involving one-step isobutylene and methanol utilization, as well as two-step BDO production. The results revealed valuable insights for process selection. For isobutylene utilization, the optimal process involved converting isobutylene into PA and separating the mixture based on the boiling point sequence,

ensuring both process profitability and sustainability. In the case of methanol utilization, gasoline emerged as the best product, and the configuration that prioritized gasoline separation exhibited the most promising process performance. In the two-step BDO production, the process route utilizing acetylene for BDO production with 1,4-butynediol as an intermediate product demonstrated the lowest cost among the considered routes. The corresponding optimal downstream separation strategy was first to separate the light contaminants and then separate the unreacted reactant and side-product based on the boiling point sequence.

The developed optimization framework serves as a valuable guide for sustainable process route selection, encompassing the optimization of raw materials/products and process configurations. Notably, for multistep reactions, this framework empowers the process industry to determine optimal sustainable and profitable processes for the upstream, intermediate, and downstream stages, thus achieving global optimization for the entire process system.

Chapter 6 – **Conclusions and Future Work**

6.1 Achievements

The main contribution of this work is the extension of the developed process synthesis algorithm to incorporate different reaction pathways and innovative separation techniques, enabling the identification of sustainable process routes for chemical production or raw material utilization. Unlike conventional process synthesis, which focuses on a fixed reaction pathway, utilizes conventional separation techniques, and faces challenges in determining the appropriate solvent for azeotrope mixture separation, this extended work can identify the best process route for both ideal and azeotrope mixture systems, encompassing various feasible potential pathways and innovative separation configurations.

Chapter 3 evaluates the performance of innovative separation techniques, such as hybrid membrane/adsorption distillation, for both simple and azeotrope mixtures. Specifically, a solvent evaluation method FSES is proposed and validated through DFO in four different azeotrope mixture systems. The results demonstrate that FSES provides a fast and efficient preliminary evaluation of solvent selection before conducting rigorous simulation and optimization. Building upon the identified optimal solvent, the study further applies DFO for designing hybrid extractive distillation for the separation of methanol/methyl acetate and benzene/cyclohexane azeotropes. Compared to conventional extractive distillation, the hybrid system significantly reduces solvent and energy usage, although its application is constrained by membrane properties. Furthermore, the hybrid distillation design is explored for simple mixture separation. The findings indicate that implementing hybrid distillation for an existing distillation column could enhance process thermal efficiency, resulting in improved distillation throughput or reduced energy costs. These results

suggest that integrating hybrid distillation into process synthesis can lead to more sustainable process configurations compared to relying solely on distillation.

In light of the exceptional process performance of hybrid distillation, Chapter 6 introduces a three-stage synthesis framework that incorporates reaction pathway selection and innovative separation techniques into process synthesis. Stage one involves reaction synthesis, generating potential feasible reaction pathways. Stage two focuses on separation synthesis, identifying sustainable process flowsheets. Lastly, stage three entails rigorous simulation to analyze the performance of the process flowsheets. This framework expands the conventional synthesis search space by considering different raw materials/products, reaction pathways, solvents, agent-based distillation, and innovative separation techniques, thereby enabling the discovery of sustainable process routes for chemical production or raw material utilization. The framework is applied to three new process designs and two process retrofitting case studies. For the new design case studies, various process alternatives generated based on different solvents, reaction pathways, and feasible separation techniques are ranked and evaluated. The results demonstrate that the three-stage framework provides an efficient method to identify the optimal process route for a given target chemical. In the retrofitting problems, the framework generates various feasible alternative separation techniques that can potentially replace energy-intensive bottleneck separation techniques. Compared to the base case process, the suggested retrofitting processes lead to energy savings ranging from 5% to 20%.

Chapter 5 explores the simultaneous optimization of reaction pathways and separation networks, determining the optimal pathway and sustainable separation configuration through rigorous optimization. An extended generalized separation network optimization model is developed and connected to a thermodynamic database to address raw material utilization and

chemical production problems. The optimization model is applied to three case studies, including both one-step and multi-step reaction and separation processes. With the input of multi-step reaction pathways along with their conversion rate and selectivity, the optimization model automatically determines the optimal distillation configurations for all the pathways, and the best process route is identified after comparing the performance of these optimal configurations. The case study results validate the effectiveness of the proposed three-stage framework and offer valuable guidance for the process industry in determining optimal, sustainable, and profitable process routes for the entire process system.

6.2 Future work

1. Extension of the method to handle uncertainty: All the tested raw material utilization case studies find the most profitable chemical product and its process configurations with a fixed chemical price. But the chemical price fluctuates with time, which may influence the decision of the optimal process route. The uncertainty of the chemical price should be considered in the synthesis problem to generate robust optimal solutions.

2. Integration of reaction network design with separation network optimization: The developed synthesis framework was tested in case studies to select the optimal reaction pathway and the corresponding separation flowsheet. In the process industry, raw materials/products are mainly produced from a reaction network, rather than a single sequential reaction pathway. In this case, one must determine the optimal separation and reaction networks, including selecting different reaction networks and optimizing the network configurations. This leads to a complicated reaction pathway network and separation network optimization problems. Gao et al. (2020) presented an optimization model to determine the optimal path for a medicine product based on a generated retrosynthesis reaction network. The developed simultaneous optimization method can be

integrated with a reaction network or a reaction synthesis tool to identify/design the optimal path for producing/utilizing conventional chemicals.

3. Extension of the method for catalyst design/selection: The developed synthesis model can be extended to guide the research of catalyst design and selection. The use of a catalyst may significantly influence the composition of the mixture for separation, which may influence the process route selection. For example, although using propylene carbonate is identified as the best process route for DMC production, it has difficulties producing high-purity DMC because of the impurity caused by the catalyst reaction. The developed method can incorporate different catalysts for a list of pathways. Thus, the optimal solution includes the optimal process route and the associated catalyst.

Chapter 7 – **References**

Agnihotri, R.B., Motard, R.L., 1980. Reaction path synthesis in industrial chemistry. ACS Publications.

Asprion, N., Kaibel, G., 2010. Dividing wall columns: Fundamentals and recent advances. Chem. Eng. Process. Process Intensif. 49, 139–146. https://doi.org/10.1016/j.cep.2010.01.013

Babi, D.K., Gani, R., 2014. Hybrid Distillation Schemes: Design, Analysis, and Application, Distillation: Fundamentals and Principles. Elsevier. https://doi.org/10.1016/B978-0-12-386547-2.00009-0

Bausa, J., Marquardt, W., 2000. Shortcut design methods for hybrid membrane/distillation processes for the separation of nonideal multicomponent mixtures. Ind. Eng. Chem. Res. 39, 1658–1672.

Beierling, T., Micovic, J., Lutze, P., Sadowski, G., 2014. Using complex layer melt crystallization models for the optimization of hybrid distillation/melt crystallization processes. Chem. Eng. Process. Process Intensif. 85, 10–23. https://doi.org/10.1016/j.cep.2014.07.011

Berry, D.A., Ng, K.M., 1997. Synthesis of Crystallization-Distillation Hybrid Separation Processes. AIChE J. 43, 1751–1762. https://doi.org/10.1002/aic.690430712

Bhargava, M., Sharma, A.P., 2019. Introduction to Dividing-Wall Columns. Chem. Eng. Prog. 30–34.

Bianchi, P., Williams, J.D., Kappe, C.O., 2020. Oscillatory flow reactors for synthetic chemistry applications. J. Flow Chem. 10, 475–490.

Bokade, V.V., Joshi, P.N., Niphadkar, P.S., 2014. Process for conversion of isobutylene to tertiary

butylamine.

Buchaly, C., Kreis, P., Górak, A., 2007. Hybrid separation processes—Combination of reactive distillation with membrane separation. Chem. Eng. Process. Process Intensif. 46, 790–799.

Budge, J.R., Attig, T.G., Pedersen, S.E., 1995. Process for the hydrogenation of maleic acid to 1, 4-butanediol.

Caballero, J.A., Grossmann, I.E., Keyvani, M., Lenz, E.S., 2009. Design of hybrid distillation−vapor membrane separation systems. Ind. Eng. Chem. Res. 48, 9151–9162.

Chabanon, E., Mangin, D., Charcosset, C., 2016. Membranes and crystallization processes: State of the art and prospects. J. Memb. Sci. 509, 57–67.

Charcosset, C., 1998. Purification of proteins by membrane chromatography. J. Chem. Technol. Biotechnol. Int. Res. Process. Environ. Clean Technol. 71, 95–110.

Charpentier, J.C., 2007. In the frame of globalization and sustainability, process intensification, a path to the future of chemical and process engineering (molecules into money). Chem. Eng. J. 134, 84–92. https://doi.org/10.1016/j.cej.2007.03.084

Chavewanmas, Y., Malakul, P., Gani, R., 2017. LCSoft–the Life Cycle Assessment Software: New developments and status, in: Computer Aided Chemical Engineering. Elsevier, pp. 2305–2310.

Cheng, S.H., Liu, Y.A., 1988. Studies in chemical process design and synthesis. 8. A simple heuristic method for the synthesis of initial sequences for sloppy multicomponent separations. Ind. Eng. Chem. Res. 27, 2304–2322.

Chenier, P.J., 2012. Survey of industrial chemistry. Springer Science & Business Media.

Cignitti, S., Rodriguez-Donis, I., Abildskov, J., You, X., Shcherbakova, N., Gerbaud, V., 2019. CAMD for entrainer screening of extractive distillation process based on new thermodynamic criteria. Chem. Eng. Res. Des. 147, 721–733.

Coley, C.W., Barzilay, R., Jaakkola, T.S., Green, W.H., Jensen, K.F., 2017. Prediction of Organic Reaction Outcomes Using Machine Learning. ACS Cent. Sci. 3, 434–443. https://doi.org/10.1021/acscentsci.7b00064

Coley, C.W., Green, W.H., Jensen, K.F., 2018. Machine learning in computer-aided synthesis planning. Acc. Chem. Res. 51, 1281–1289.

Corey, E.J., 1971. Centenary lecture. Computer-assisted analysis of complex synthetic problems. Q. Rev. Chem. Soc. 25, 455–482.

Corey, E.J., Howe, W.J., Pensak, D.A., 1974. Computer-assisted synthetic analysis. Methods for machine generation of synthetic intermediates involving multistep look-ahead. J. Am. Chem. Soc. 96, 7724–7737.

Costa, A., Nannicini, G., 2018. RBFOpt: an open-source library for black-box optimization with costly function evaluations. Math. Program. Comput. 10, 597–629.

Cukalovic, A., Stevens, C. V, 2008. Feasibility of production methods for succinic acid derivatives: a marriage of renewable resources and chemical technology. Biofuels, Bioprod. Biorefining 2, 505–529.

d'Anterroches, L., Gani, R., 2005. Group contribution based process flowsheet synthesis, design and modelling. Fluid Phase Equilib. 228, 141–146.

Deb, K., 2011. Multi-objective optimisation using evolutionary algorithms: an introduction, in:

Multi-Objective Evolutionary Optimisation for Product Design and Manufacturing. Springer, pp. 3–34.

Dejanović, I., Matijašević, L., Olujić, Ž., 2010. Dividing wall column-A breakthrough towards sustainable distilling. Chem. Eng. Process. Process Intensif. 49, 559–580. https://doi.org/10.1016/j.cep.2010.04.001

Deng, W., Shi, L., Yao, J., Zhang, Z., 2019. A review on transesterification of propylene carbonate and methanol for dimethyl carbonate synthesis. Carbon Resour. Convers. 2, 198–212.

Dong, G., Nagasawa, H., Yu, L., Wang, Q., Yamamoto, K., Ohshita, J., Kanezashi, M., Tsuru, T., 2020. Pervaporation removal of methanol from methanol/organic azeotropes using organosilica membranes: Experimental and modeling. J. Memb. Sci. 610, 118284.

Drioli, E., Stankiewicz, A.I., Macedonio, F., 2011. Membrane engineering in process intensification—An overview. J. Memb. Sci. 380, 1–8.

Duran, M.A., Grossmann, I.E., 1986. A mixed-integer nonlinear programming algorithm for process systems synthesis. AIChE J. 32, 592–606.

Eliceche, A.M., Daviou, M.C., Hoch, P.M., Uribe, I.O., 2002. Optimisation of azeotropic distillation columns combined with pervaporation membranes. Comput. Chem. Eng. 26, 563–573.

Floquet, P., Pibouleau, L., Aly, S., Domenech, S., 1994. Fuzzy heuristic approach for sharp separation sequence synthesis. Comput. Chem. Eng. 18, 785–795.

Floudas, C.A., Ciric, A.R., Grossmann, I.E., 1986. Automatic synthesis of optimum heat exchanger network configurations. AIChE J. 32, 276–290.

https://doi.org/10.1002/aic.690320215

Fox, J.A., Hildebrandt, D., Glasser, D., Patel, B., 2013. A graphical approach to process synthesis and its application to steam reforming. AIChE J. 59, 3714–3729.

Franke, M.B., Nowotny, N., Ndocko, E.N., Górak, A., Strube, J., 2008. Design and optimization of a hybrid distillation/melt crystallization process. AIChE J. 54, 2925–2942.

Gabruś, E., Nastaj, J., Tabero, P., Aleksandrzak, T., 2015. Experimental studies on 3A and 4A zeolite molecular sieves regeneration in TSA process: Aliphatic alcohols dewatering–water desorption. Chem. Eng. J. 259, 232–242.

Gadalla, M., Jobson, M., Smith, R., 2003. Increase capacity and decrease energy for existing refinery distillation columns. Chem Eng Prog 99, 44–50.

Gani, R., Bek-Pedersen, E., 2000. Simple new algorithm for distillation column design. AIChE J. 46, 1271–1274.

Gao, H., Coley, C.W., Struble, T.J., Li, L., Qian, Y., Green, W.H., Jensen, K.F., 2020. Combining retrosynthesis and mixed-integer optimization for minimizing the chemical inventory needed to realize a WHO essential medicines list. React. Chem. Eng. 5, 367–376.

García-Herreros, P., Gómez, J.M., Gil, I.D., Rodríguez, G., 2011. Optimization of the design and operation of an extractive distillation system for the production of fuel grade ethanol using glycerol as entrainer. Ind. Eng. Chem. Res. 50, 3977–3985.

Gelernter, H.L., Sanders, A.F., Larsen, D.L., Agarwal, K.K., Boivie, R.H., Spritzer, G.A., Searleman, J.E., 1977. Empirical explorations of SYNCHEM. Science (80-.). 197, 1041–1049.

Gerbaud, V., Rodriguez-Donis, I., Hegely, L., Lang, P., Denes, F., You, X., 2019. Review of extractive distillation. Process design, operation, optimization and control. Chem. Eng. Res. Des. 141, 229–271.

Ghosh, T.K., Lin, H. Da, Hines, A.L., 1993. Hybrid Adsorption-Distillation Process for Separating Propane and Propylene. Ind. Eng. Chem. Res. 32, 2390–2399. https://doi.org/10.1021/ie00022a024

Govind, R., Powers, G.J., 1981. Studies in reaction path synthesis. AIChE J. 27, 429–442.

Grossmann, I.E., 2002. Review of nonlinear mixed-integer and disjunctive programming techniques. Optim. Eng. 3, 227–252.

Grossmann, I.E., 1990. Mixed-integer nonlinear programming techniques for the synthesis of engineering systems. Res. Eng. Des. 1, 205–228. https://doi.org/10.1007/BF01581212

Grossmann, I.E., Daichendt, M.M., 1996. New trends in optimization-based approaches to process synthesis. Comput. Chem. Eng. 20, 665–683. https://doi.org/10.1016/0098-1354(95)00201-4

Harmsen, G.J., 2007. Reactive distillation: The front-runner of industrial process intensification. A full review of commercial applications, research, scale-up, design and operation. Chem. Eng. Process. Process Intensif. 46, 774–780. https://doi.org/10.1016/j.cep.2007.06.005

Hassan, M.M., Ruthven, D.M., Raghavan, N.S., 1986. Air separation by pressure swing adsorption on a carbon molecular sieve. Chem. Eng. Sci. 41, 1333–1343.

Hendrickson, J.B., 1975a. Systematic synthesis design. III. scope of the problem. J. Am. Chem. Soc. 97, 5763–5784.

Hendrickson, J.B., 1975b. Systematic synthesis design. IV. Numerical codification of construction

reactions. J. Am. Chem. Soc. 97, 5784–5800.

Hendrickson, J.B., 1971. Systematic characterization of structures and reactions for use in organic synthesis. J. Am. Chem. Soc. 93, 6847–6854.

Hendry, J.E., Rudd, D.F., Seader, J.D., 1973. Synthesis in the design of chemical processes. AIChE J. 19, 1–15.

Hepfer, R.P., Miller, C.T., Norenberg, G.A., Attig, T.G., Budge, J.R., 2006. Two-stage process for the hydrogenation of maleic acid to 1, 4-butanediol.

Hohmann Jr, E.C., 1971. Optimum networks for heat exchange. University of Southern California.

Hostrup, M., Gani, R., Kravanja, Z., Sorsak, A., Grossmann, I., 2001. Integration of thermodynamic insights and MINLP optimization for the synthesis, design and analysis of process flowsheets. Comput. Chem. Eng. 25, 73–83.

Ivonne, R.D., Vincent, G., Xavier, J., 2001. Heterogeneous entrainer selection for the separation of azeotropic and close boiling temperature mixtures by heterogeneous batch distillation. Ind. Eng. Chem. Res. 40, 4935–4950.

Jaksland, C.A., Gani, R., Lien, K.M., 1995. Separation process design and synthesis based on thermodynamic insights. Chem. Eng. Sci. 50, 511–530.

Kalakul, S., Malakul, P., Siemanond, K., Gani, R., 2014. Integration of life cycle assessment software with tools for economic and sustainability analyses and process simulation for sustainable process design. J. Clean. Prod. 71, 98–109. https://doi.org/10.1016/j.jclepro.2014.01.022

Kalck, P., Le Berre, C., Serp, P., 2020. Recent advances in the methanol carbonylation reaction

into acetic acid. Coord. Chem. Rev. 402, 213078.

Kapteijn, F., Moulijn, J.A., 2022. Structured catalysts and reactors–Perspectives for demanding applications. Catal. Today 383, 5–14.

Kayala, M.A., Azencott, C.-A., Chen, J.H., Baldi, P., 2011. Learning to predict chemical reactions. J. Chem. Inf. Model. 51, 2209–2222.

Kayala, M.A., Baldi, P., 2012. ReactionPredictor: prediction of complex chemical reactions at the mechanistic level using machine learning. J. Chem. Inf. Model. 52, 2526–2540.

Khajuria, H., Pistikopoulos, E.N., 2013. Optimization and control of pressure swing adsorption processes under uncertainty. AIChE J. 59, 120–131.

Kiss, A.A., 2014. Distillation technology–still young and full of breakthrough opportunities. J. Chem. Technol. Biotechnol. 89, 479–498.

Kokossis, A.C., 1990. Optimization of complex reactor networks—I. Isothermal operation. Chem. Eng. Sci. 45, 595–614.

Kokossis, A.C., Floudas, C.A., 1994. Optimization of complex reactor networks-II. Nonisothermal operation. Chem. Eng. Sci. 49, 1037–1051. https://doi.org/10.1016/0009-2509(94)80010-3

Kongpanna, P., Pavarajarn, V., Gani, R., Assabumrungrat, S., 2015. Techno-economic evaluation of different CO2-based processes for dimethyl carbonate production. Chem. Eng. Res. Des. 93, 496–510.

Kookos, I.K., 2003. Optimal design of membrane/distillation column hybrid processes. Ind. Eng. Chem. Res. 42, 1731–1738.

Kossack, S., Kraemer, K., Gani, R., Marquardt, W., 2008. A systematic synthesis framework for

extractive distillation processes. Chem. Eng. Res. Des. 86, 781–792.

Kothare, M. V, 2006. Dynamics and control of integrated microchemical systems with application to micro-scale fuel processing. Comput. Chem. Eng. 30, 1725–1734.

Kumar, R., Golden, T.C., White, T.R., Rokicki, A., 1992. Novel adsorption distillation hybrid scheme for propane/propylene separation. Sep. Sci. Technol. 27, 2157–2170. https://doi.org/10.1080/01496399208019472

Lange, J., 2017. Don't forget product recovery in catalysis research—Check the distillation resistance. ChemSusChem 10, 245–252.

Liang, S., Cao, Y., Liu, X., Li, X., Zhao, Y., Wang, Yongkun, Wang, Yinglong, 2017. Insight into pressure-swing distillation from azeotropic phenomenon to dynamic control. Chem. Eng. Res. Des. 117, 318–335.

Lipnizki, F., Field, R.W., Ten, P.-K., 1999. Pervaporation-based hybrid process: a review of process design, applications and economics. J. Memb. Sci. 153, 183–210.

Liu, Y.A., Quantrille, T.E., Cheng, S.H., 1990. Studies in chemical process design and synthesis. 9. A unifying method for the synthesis of multicomponent separation sequences with sloppy product streams. Ind. Eng. Chem. Res. 29, 2227–2241.

Lu, L., Peng, F., Jiang, Z., Wang, J., 2006. Poly (vinyl alcohol)/chitosan blend membranes for pervaporation of benzene/cyclohexane mixtures. J. Appl. Polym. Sci. 101, 167–173.

Lu, M.D., Motard, R.L., 1985. Computer-aided total flowsheet synthesis. Comput. Chem. Eng. 9, 431–445. https://doi.org/10.1016/0098-1354(85)80021-1

Luis, P., Van der Bruggen, B., Van Gerven, T., 2011. Non-dispersive absorption for CO2 capture:

from the laboratory to industry. J. Chem. Technol. Biotechnol. 86, 769–775.

Lutze, P., Gani, R., Woodley, J.M., 2010. Process intensification: a perspective on process synthesis. Chem. Eng. Process. Process Intensif. 49, 547–558.

Luyben, W.L., 2017. Improving the conventional reactor/separation/recycle DME process. Comput. Chem. Eng. 106, 17–22.

Luyben, W.L., 2013. Comparison of extractive distillation and pressure-swing distillation for acetone/chloroform separation. Comput. Chem. Eng. 50, 1–7.

Malone, M.F., Doherty, M.F., 2000. Reactive distillation. Ind. Eng. Chem. Res. 39, 3953–3957.

Marín, P., Díez, F. V, Ordóñez, S., 2019. Reverse flow reactors as sustainable devices for performing exothermic reactions: Applications and engineering aspects. Chem. Eng. Process. Intensif. 135, 175–189.

Marquardt, W., Kossack, S., Kraemer, K., 2008. A framework for the systematic design of hybrid separation processes. Chinese J. Chem. Eng. 16, 333–342.

Medina-Herrera, N., Grossmann, I.E., Mannan, M.S., Jiménez-Gutiérrez, A., 2014. An approach for solvent selection in extractive distillation systems including safety considerations. Ind. Eng. Chem. Res. 53, 12023–12031.

Micovic, J., Beierling, T., Lutze, P., Sadowski, G., Górak, A., 2013. Design of hybrid distillation/melt crystallisation processes for separation of close boiling mixtures. Chem. Eng. Process. Process Intensif. 67, 16–24. https://doi.org/10.1016/j.cep.2012.07.012

Minceva, M., Rodrigues, A.E., 2002. Modeling and simulation of a simulated moving bed for the separation of p-xylene. Ind. Eng. Chem. Res. 41, 3454–3461.

Mizsey, P., Fonyo, Z., 1990. Toward a more realistic overall process synthesis—the combined approach. Comput. Chem. Eng. 14, 1213–1236.

Modi, A.K., Westerberg, A.W., 1992. Distillation column sequencing using marginal price. Ind. Eng. Chem. Res. 31, 839–848.

Moganti, S., Noble, R.D., Koval, C.A., 1994. Analysis of a membrane/distillation column hydrid process. J. Memb. Sci. 93, 31–44. https://doi.org/10.1016/0376-7388(94)85013-5

Moo-Young, M., 2019. Comprehensive biotechnology. Elsevier.

Mujiburohman, M., Sediawan, W.B., Sulistyo, H., 2006. A preliminary study: Distillation of isopropanol-water mixture using fixed adsorptive distillation method. Sep. Purif. Technol. 48, 85–92. https://doi.org/10.1016/j.seppur.2005.07.025

Mulia-Soto, J.F., Flores-Tlacuahuac, A., 2011. Modeling, simulation and control of an internally heat integrated pressure-swing distillation process for bioethanol separation. Comput. Chem. Eng. 35, 1532–1546.

Munoz, R., Montón, J.B., Burguet, M.C., De la Torre, J., 2006. Separation of isobutyl alcohol and isobutyl acetate by extractive distillation and pressure-swing distillation: Simulation and optimization. Sep. Purif. Technol. 50, 175–183.

Nadgir, V.M., Liu, Y.A., 1983. Studies in chemical process design and synthesis: Part V: A simple heuristic method for systematic synthesis of initial sequences for multicomponent separations. AIChE J. 29, 926–934.

Nannicini, G., 2021. On the implementation of a global optimization method for mixed-variable problems. Open J. Math. Optim. 2, 1–25.

Nath, R., Motard, R.L., 1981. Evolutionary synthesis of separation processes. AIChE J. 27, 578–587. https://doi.org/10.1002/aic.690270407

Nishida, N., Stephanopoulos, G., Westerberg, A.W., 1981. A review of process synthesis. AIChE J. 27, 321–351.

O'Connell, J.P., Eden, M.R., Tula, A.K., Gani, R., 2019. Retrofitting Distillation Columns with Membranes. Chem. Eng. Prog. 115, 41–49.

Okamoto, K., Kita, H., Horii, K., Kondo, K.T., 2001. Zeolite NaA membrane: preparation, single-gas permeation, and pervaporation and vapor permeation of water/organic liquid mixtures. Ind. Eng. Chem. Res. 40, 163–175.

Olajossy, A., Gawdzik, A., Budner, Z., Dula, J., 2003. Methane separation from coal mine methane gas by vacuum pressure swing adsorption. Chem. Eng. Res. Des. 81, 474–482.

Pajula, E., Seuranen, T., Koiranen, T., Hurme, M., 2001. Synthesis of separation processes by using case-based reasoning. Comput. Chem. Eng. 25, 775–782.

Pawliszyn, J., 2012. Comprehensive sampling and sample preparation: analytical techniques for scientists. Academic Press.

Peng, H., Couenne, F., Le Gorrec, Y., 2011. Robust control of a pressure swing adsorption process. IFAC Proc. Vol. 44, 7310–7315.

Pettersen, T., Lien, K.M., 1995. Design of hybrid distillation and vapor permeation processes. J. Memb. Sci. 102, 21–30.

Powell, J.B., 2017. Application of multiphase reaction engineering and process intensification to the challenges of sustainable future energy and chemicals. Chem. Eng. Sci. 157, 15–25.

https://doi.org/10.1016/j.ces.2016.09.007

Pramanik, B.K., Thangavadivel, K., Shu, L., Jegatheesan, V., 2016. A critical review of membrane crystallization for the purification of water and recovery of minerals. Rev. Environ. Sci. Biotechnol. 15, 411–439. https://doi.org/10.1007/s11157-016-9403-0

Pressly, T.G., Ng, K.M., 1998. A Break-Even Analysis of Distillation-Membrane Hybrids. AIChE J. 44, 93–105. https://doi.org/10.1002/aic.690440111

Qasim, F., Shin, J.S., Cho, S.J., Park, S.J., 2016. Optimizations and heat integrations on the separation of toluene and 1-butanol azeotropic mixture by pressure swing distillation. Sep. Sci. Technol. 51, 316–326.

Raman, R., Grossmann, I.E., 1994. Modelling and computational techniques for logic based integer programming. Comput. Chem. Eng. 18, 563–578.

Ritter, J.A., Wu, F., Ebner, A.D., 2012. New approach for modeling hybrid pressure swing adsorption-distillation processes. Ind. Eng. Chem. Res. 51, 9343–9355. https://doi.org/10.1021/ie300744n

Rodríguez-Donis, I., Gerbaud, V., Joulia, X., 2001. Entrainer selection rules for the separation of azeotropic and close-boiling-temperature mixtures by homogeneous batch distillation process. Ind. Eng. Chem. Res. 40, 2729–2741.

Ryu, J., Maravelias, C.T., 2021. A generalized distillation network synthesis model. Chem. Eng. Sci. 244, 116766.

Ryu, J., Maravelias, C.T., 2020. Computationally efficient optimization models for preliminary distillation column design and separation energy targeting. Comput. Chem. Eng. 143,

107072.

Salatin, T.D., Jorgensen, W.L., 1980. Computer-assisted mechanistic evaluation of organic reactions. 1. Overview. J. Org. Chem. 45, 2043–2051.

Satoh, H., Funatsu, K., 1995. SOPHIA, a knowledge base-guided reaction prediction system-utilization of a knowledge base derived from a reaction database. J. Chem. Inf. Comput. Sci. 35, 34–44.

Seader, J.D., Westerberg, A.W., 1977. A combined heuristic and evolutionary strategy for synthesis of simple separation sequences. AIChE J. 23, 951–954.

Segler, M.H.S., Waller, M.P., 2017a. Neural-symbolic machine learning for retrosynthesis and reaction prediction. Chem. Eur. J. 23, 5966–5971.

Segler, M.H.S., Waller, M.P., 2017b. Modelling chemical reasoning to predict and invent reactions. Chem. Eur. J. 23, 6118–6128.

Sempuga, B.C., Hausberger, B., Patel, B., Hildebrandt, D., Glasser, D., 2010. Classification of chemical processes: a graphical approach to process synthesis to improve reactive process work efficiency. Ind. Eng. Chem. Res. 49, 8227–8237.

Shah, M., Kiss, A.A., Zondervan, E., De Haan, A.B., 2012. A systematic framework for the feasibility and technical evaluation of reactive distillation processes. Chem. Eng. Process. Process Intensif. 60, 55–64. https://doi.org/10.1016/j.cep.2012.05.007

Sharma, M.M., Mahajani, S.M., 2002. Industrial applications of reactive distillation. React. Distill. 3, 1–29.

Shen, W., Dong, L., Wei, S., Li, J., Benyounes, H., You, X., Gerbaud, V., 2015. Systematic design

of an extractive distillation for maximum-boiling azeotropes with heavy entrainers. AIChE J. 61, 3898–3910.

Shi, T., Liu, Y., Yu, H., Yang, A., Sun, S., Shen, W., Lee, C.K.M., Ren, J., 2022. Improved design of heat-pump extractive distillation based on the process optimization and multi-criteria sustainability analysis. Comput. Chem. Eng. 156, 107552.

Siirola, J.J., Powers, G.J., Rudd, D.F., 1971. Synthesis of system designs: III. Toward a process concept generator. AIChE J. 17, 677–682.

Skiborowski, M., Harwardt, A., Marquardt, W., 2013. Conceptual Design of Distillation-Based Hybrid Separation Processes. Annu. Rev. Chem. Biomol. Eng. 4, 45–68. https://doi.org/10.1146/annurev-chembioeng-061010-114129

Sommer, S., Melin, T., 2005. Influence of operation parameters on the separation of mixtures by pervaporation and vapor permeation with inorganic membranes. Part 1: Dehydration of solvents. Chem. Eng. Sci. 60, 4509–4523.

Stahl, S.S., Alsters, P.L., 2016. Liquid phase aerobic oxidation catalysis: industrial applications and academic perspectives. John Wiley & Sons.

Stefanski, M., Fassler, P., 2002. Combining distillization and crystallization. Sulzer Tech. Rev. 84, 14–16.

Stepanski, M., Haller, U., 2000. Economic Recovery of meta-Xylene Melt crystallization produces meta-xylene with a purity of 99.5%. Sulzer Tech. Rev. 8–9.

SunSirs, China Commodity Data Group [WWW Document], n.d. URL https://www.sunsirs.com/uk/price.html (accessed 7.19.23).

Szitkai, Z., Lelkes, Z., Fonyo, Z., 2002. Optimization of hybrid ethanol dehydration systems. Chem. Eng. Process. Process Intensif. 41, 631–646.

Teh, S.Y., Chua, K.B., Hong, B.H., Ling, A.J.W., Andiappan, V., Foo, D.C.Y., Hassim, M.H., Ng, D.K.S., 2019. A hybrid multi-objective optimization framework for preliminary process design based on health, safety and environmental impact. Processes 7, 200.

Thömmes, J., Kula, M.-R., 1995. Membrane chromatography-an integrative concept in the downstream processing of proteins. Biotechnol. Prog. 11, 357–367.

Tian, Y., Demirel, S.E., Hasan, M.M.F., Pistikopoulos, E.N., 2018. An overview of process systems engineering approaches for process intensification: State of the art. Chem. Eng. Process. - Process Intensif. 133, 160–210. https://doi.org/10.1016/j.cep.2018.07.014

Tsirlin, A.M., Kazakov, V., Romanova, T.S., 2007. Optimal separation sequence for three-component mixtures. J. Phys. Chem. B 111, 3178–3182.

Tsirlin, A.M., Sukin, I.A., 2014. Attainability region of binary distillation and separation sequence of three-component mixture. Theor. Found. Chem. Eng. 48, 764–775. https://doi.org/10.1134/S0040579514060116

Tsirlin, A.M., Vyasileva, E.N., Romanova, T.S., 2009. Finding the thermodynamically optimal separation sequence for multicomponent mixtures and the optimum distribution of the heat- and mass-transfer surface areas. Theor. Found. Chem. Eng. 43, 238–244.

Tula, A.K., Babi, D.K., Bottlaender, J., Eden, M.R., Gani, R., 2017. A computer-aided software-tool for sustainable process synthesis-intensification. Comput. Chem. Eng. 105, 74–95. https://doi.org/10.1016/j.compchemeng.2017.01.001

Tula, A.K., Eden, M.R., Gani, R., 2019. Systematic Method and Tool for Sustainable Process Synthesis, Designanalysis and Innovation, in: Computer Aided Chemical Engineering. Elsevier, pp. 385–390.

Tula, A.K., Eden, M.R., Gani, R., 2015. Process synthesis, design and analysis using a process-group contribution method. Comput. Chem. Eng. 81, 245–259. https://doi.org/10.1016/j.compchemeng.2015.04.019

Turton, R., Bailie, R.C., Whiting, W.B., Shaeiwitz, J.A., 2008. Analysis, synthesis and design of chemical processes. Pearson Education.

Ugi, I., Marquarding, D., Klusacek, H., Gokel, G., Gillespie, P., 1970. Chemistry and logical structures. Angew. Chemie Int. Ed. English 9, 703–730.

Wei, J.N., Duvenaud, D., Aspuru-Guzik, A., 2016. Neural networks for the prediction of organic chemistry reactions. ACS Cent. Sci. 2, 725–732.

Westerberg, A.W., 2004. A retrospective on design and process synthesis. Comput. Chem. Eng. 28, 447–458. https://doi.org/10.1016/j.compchemeng.2003.09.029

Wipke, W.T., Ouchi, G.I., Krishnan, S., 1978. Simulation and evaluation of chemical synthesis—SECS: An application of artificial intelligence techniques. Artif. Intell. 11, 173–193.

Xu, S., Cremaschi, S., Eden, M.R., Tula, A.K., 2023a. An integrated framework for sustainable process design by hybrid and intensified equipment. Comput. Chem. Eng. 176, 108288.

Xu, S., Cremaschi, S., Eden, M.R., Tula, A.K., 2023b. Simultaneous selection and optimization of reaction pathways and downstream separation network, in: Computer Aided Chemical Engineering. Elsevier, pp. 475–480.

Xu, S., Cremaschi, S., Eden, M.R., Tula, A.K., 2022a. Integrated process synthesis and design of intensified/hybrid processes, in: Computer Aided Chemical Engineering. Elsevier, pp. 709–714.

Xu, S., Cremaschi, S., Eden, M.R., Tula, A.K., 2021. Simulation-based Derivative-free Optimization for Hybrid Separation Design, in: Computer Aided Chemical Engineering. Elsevier, pp. 173–178.

Xu, S., Crump, T., Cremaschi, S., Eden, M.R., Tula, A.K., 2022b. A Short-Cut Method for Synthesis of Solvent-based Separation Processes, in: Computer Aided Chemical Engineering. Elsevier, pp. 151–156.

Yee, T.F., Grossmann, I.E., 1990. Simultaneous optimization models for heat integration—II. Heat exchanger network synthesis. Comput. Chem. Eng. 14, 1165–1184.

Yee, T.F., Grossmann, I.E., Kravanja, Z., 1990. Simultaneous optimization models for heat integration—I. Area and energy targeting and modeling of multi-stream exchangers. Comput. Chem. Eng. 14, 1151–1164.

Yildirim, Ö., Kiss, A.A., Kenig, E.Y., 2011. Dividing wall columns in chemical process industry: A review on current activities. Sep. Purif. Technol. 80, 403–417. https://doi.org/10.1016/j.seppur.2011.05.009

Zhai, J., Liu, Y., Li, L., Zhu, Y., Zhong, W., Sun, L., 2015. Applications of dividing wall column technology to industrial-scale cumene production. Chem. Eng. Res. Des. 102, 138–149.

Zhou, D.-D., Chen, P., Wang, C., Wang, S.-S., Du, Y., Yan, H., Ye, Z.-M., He, C.-T., Huang, R.-K., Mo, Z.-W., 2019. Intermediate-sized molecular sieving of styrene from larger and smaller

analogues. Nat. Mater. 18, 994–998.

Appendix 1

8.1 Detailed DFO Model

$$min: TAC = \frac{0.1(0.1+1)^5}{(0.1+1)^5-1} \times \sum_j IC_j + 24 \times 300 \times \sum_j UC_j$$

Heat exchanger investment cost:

$$\mathrm{IC_{heat\ exchanger}} = 4.74 \times (59.628 \times \mathrm{A} + 4071.2)$$

$$\mathrm{A} = \frac{\mathrm{q}}{\mathrm{h} \times \mathrm{LMTD}}$$

$$\mathrm{LMTD} = \frac{(T_{out} - T_{utility,in}) - (T_{in} - T_{utility,out})}{\ln(\frac{T_{out} - T_{utility,in}}{T_{in} - T_{utility,out}})}$$

A: heat transfer area (m^2), $3.52 \leq A \leq 635$; q: heat duty (Kw); h: heat transfer coefficient (Kw/m2*K); T_{out}, T_{in} : outlet and inlet temperature of the heating/cooling stream (°C); $T_{utility,in}, T_{utility,out}$: inlet and outlet temperature of the utility stream (°C).

Table A1.1. Parameters for heat exchanger investment cost.

	Water	Low pressure steam	Medium pressure steam	High pressure steam
h	0.8	1.6	1.6	1.6
$T_{utility,in}$	20	125	175	250
$T_{utility,out}$	25	124	174	249

Heater investment cost:

$$\mathrm{IC_{heater}} = 4.74 \times (176.04 \times \mathrm{q}^{0.7628})$$

q: heat duty (Kw);

Pump investment cost:

$$\mathrm{IC_{pump}} = 4.74 \times (-0.7712 \times \mathrm{S}^2 + 795.92 \times \mathrm{S} + 8081.1)$$

$$\mathrm{S} = \frac{V}{P_{out} - P_{in}}$$

S: pump sizing parameter (m^3/s*Kpa), $6 \leq S \leq 70$; V: volume flowrate (m^3/s); P_{out}, P_{in}: outlet and inlet pressure of the pump (Kpa).

Compressor investment cost:

$$\mathrm{IC_{compressor}} = 4.74 \times (877.3 \times \mathrm{q}^{0.9435})$$

q: heat duty (Kw), $75 \leq q \leq 6000$;

Distillation column investment cost:

$$\mathrm{IC_{column\ shell}} = 4.74 \times (\mathrm{a} \times \mathrm{H}^2 + \mathrm{b} \times \mathrm{H} + \mathrm{c})$$

$$\mathrm{IC_{sieve\ tray}} = 4.74 \times (-32.7 \times \mathrm{D}^3 + 234.91 \times \mathrm{D}^2 - 66.321 \times \mathrm{D} + 293.53)$$

$$\mathrm{H} = 0.6 \times \mathrm{N}$$

H: height (m); D: diameter (m); N: column number of stages.

Table A1.2. Parameters for distillation column investment cost.

	$0 < D \leq 0.5$	$0.5 < D \leq 1$	$1 < D \leq 2$	$2 < D \leq 3$	$3 < D \leq 4$
a	15.401	13.929	3.011	-23.555	-4.972
b	1588.5	2028.4	3139.4	5119.4	5021.1
c	1495.5	1850.6	7166.9	10945	24285

Adsorption/membrane investment cost:

$$\mathrm{IC_{ad,mem}} = 4.74 \times \mathrm{Price} \times \mathrm{A}$$

$$\mathrm{A} = \frac{F}{J}$$

Price: price of the membrane/adsorbent (2500 \$/m^2 for zeolite-based membrane, 200 \$/m^2 for PVA based membrane, 10 \$/Kg for zeolite molecular sieve); F: membrane/adsorption mass flowrate (Kg/h); J: membrane permeability or adsorption capacity (kg/m^2*h or Kg/Kg), which is calculated based on the model from Section S1.

Utility cost:

$$\mathrm{UC_j} = \mathrm{Utility\ price} \times q_j$$

q: heat duty (GJ/h);

Table A1.3. Utility price for different types of utilities.

	Water	Low pressure steam	Medium pressure steam	High pressure steam	Natural gas	Electricity
Utility price, \$/GJ	0.354	7.78	8.22	9.83	6	16.8

Product purity: $x_{methanol} \geq x_{1,product}, x_{methyl\ acetate} > x_{2,product}$

8.2 Detailed Methanol/water Hybrid Distillation Retrofitting Optimization Model

$$min: TAC = \frac{0.1(0.1+1)^5}{(0.1+1)^5 - 1} \times IC + 24 \times 300 \times UC$$

$$max: Profit = 24 \times 300 \times 286 F_{retentate} W_m$$

$$s.t.\ \mathrm{UC} = -0.354 q_{condenser} + 7.78 q_{reboiler} + 16.8 q_{compressor}$$

$$\mathrm{IC} = 2500\mathrm{A} + 4.74 \times 877.3\mathrm{q}_{compressor}^{0.9435})$$

$$q_{compressor} = 7.19F_{permeate}$$

$$\mathrm{A} = \frac{W_w \mathrm{F_D} \times (1 - \mathrm{x_{top,switching}})}{j_w}$$

$$j_w, j_m, \beta_{\frac{\mathrm{w}}{\mathrm{m}}} = f(T_{in}, x_{top,switching}, p_{in}, p_p, y_p)$$

$$\beta_{\frac{\mathrm{w}}{\mathrm{m}}} = \frac{j_w / j_m}{\frac{(1 - x_{top,switching})W_w}{x_{top,switching}W_m}}$$

$$T_{in} = 100 \times \left(1 - \mathrm{x_{top,switching}}\right) + 65\mathrm{x_{top,switching}} + 273.15$$

$$F_{permeate} = \mathrm{F_D}\left[(1 - \mathrm{x_{top,switching}}) \times 0.999 + \mathrm{x_{top,switching}} \frac{0.999}{\beta_{\frac{\mathrm{w}}{\mathrm{m}}}}\right]$$

$$F_{rententate} = F_D - F_{permeate}$$

$$q_{condenser} = (F_D H_{1,g} + RF_D H_{1,L} - (1 + R)F_D H_{2,g}) \times \frac{1000 \times 1.055 \times 10^{-6}}{453.59}$$

$$q_{reboiler} = ((1 + R)F_D H_{2,g} + F_B H_{bottom,L} - RF_D H_{1,L} - H_{feed}F_{feed}) \times \frac{1000 \times 1.055 \times 10^{-6}}{453.59}$$

$$H_{1,g} = -3338.3\, x_{top,switching} + 20669$$

$$H_{2,g} = -3338.3\, x_{2,methanol} + 20669$$

$$H_{1,L} = -892.93\, x_{top,switching} + 3018.4$$

$$H_{bottom,L} = -892.93 \times (1 - x_{bottom,switching}) + 20669$$

$$x_{2,methanol} = \frac{F_D x_{top,switching} + RF_D x_{top,liquid}}{(1 + R)F_D}$$

$$x_{top,liquid} = f(x_{top,switching})$$

$$x_m = \frac{x_{top,switching}\left(1 - \frac{0.999}{\beta_{\frac{\mathrm{w}}{\mathrm{m}}}}\right)F_D}{F_{rententate}}$$

$$x_w = \frac{0.999\left(1 - x_{top,switching}\right)F_D + x_{bottom,swithching}F_B}{F_{rententate} + F_B}$$

$F_D, F_B, R, D_s, D_r = f(x_{top,switching}, x_{bottom,swithching}, F_{feed})$

$D_s, D_r \leq 1.85$

$x_m, x_w \geq 0.999$

$0.75 \leq x_{top,switching} \leq 0.975$

$0.9 \leq x_{top,switching} \leq 0.9995$

$1342 \leq F_{feed} \leq 2500$

IC is the total investment cost; UC is the utility cost \$/hr; $F_{retentate}$ is the methanol product flowrate (kmol/h); W_m, W_w is the molar mass of methanol and water; $q_{condenser}, q_{reboiler}, q_{compressor}$ are the heat duty of the condenser, reboiler, and compressor (GJ/hr); $F_{permeate}$ is the permeate flowrate (kmol/h); A is the membrane surface area (m^2); F_D, F_B are the distillate and bottom flowrate (kmol/h); $x_{top,switching}, x_{bottom,swithching}, F_{feed}$ are the three decision variables (top switching composition (mol%), bottom switching composition (mol%) and feed flowrate (kmol/h)); P_P, total pressure at permeate side (2 kpa); y_P, mole composition at permeate side (assumed to be 1 in here); j_w, j_m are the permeability of water and methanol (kg/m^2*h) ; T_{in}, feed temperature (K); P_{in}, feed pressure (101.325 Kpa); $\beta_{\frac{w}{m}}$, membrane selectivity; $f(T_{in}, x_{top,switching}, p_{in}, p_p, y_p)$ is the membrane model shown in Section S1.3; $H_{2,g}, H_{1,g}$ are the gas molar enthalpy at the second and first of the column (kJ/mol); $H_{1,L}, H_{bottom,L}$ are the liquid molar enthalpy at the first and bottom of the column (kJ/mol); H_{feed} is the enthalpy of the feed stream (2,808.56 Btu/lbmole); $x_{2,methanol}$ is the gas methanol composition at the second stage of the column; $x_{top,liquid}$ is the liquid phase methanol composition at the second stage of the column; $f(x_{top,switching})$ is the phase equilibrium model, which is based on the regression of the VLE data; x_m, x_w are the methanol and water product composition (mol%); F_D, F_B are the distillate and bottom flowrate (kmol/h); R is the column reflux ratio; D_s, D_r are the calculated column diameter

for the stripping and rectifying sections (m); $f(x_{top,switching}, x_{bottom,swithching}, F_{feed})$ is the short-cut distillation model.

Appendix 2

9.1 Acrylic Acid Production

Table A2.1. Generated process alternatives for acrylic acid production.

No.	Process alternatives	Process energy index, GJ
1	(dllmA/BC)(pvB/C)	44.04
2	(dlpvA/BC)(pvB/C)	44.04
3	(dladA/BC)(pvB/C)	44.04
4	(dllmA/BC)(dlpvB/C)	44.48
5	(dlpvA/BC)(dlpvB/C)	44.48
6	(dladA/BC)(dlpvB/C)	44.48
7	(dllmA/BC)(dladB/C)	44.48
8	(dlpvA/BC)(dladB/C)	44.48
9	(dladA/BC)(dladB/C)	44.48
10	(dllmA/BC)(dlB/C)	44.88
11	(dlpvA/BC)(dlB/C)	44.88
12	(dladA/BC)(dlB/C)	44.88
13	(dllmA/BC)(adB/C)	46.50
14	(dlpvA/BC)(adB/C)	46.50
15	(dladA/BC)(adB/C)	46.50
16	(dlA/BCS1)(dllmB/CS1)(dlgmC/S1)	75.27
17	(dlA/BCS1)(dllmB/CS1)(dllmC/S1)	75.27
18	(dlA/BCS1)(dllmB/CS1)(dlpvC/S1)	75.27
19	(dlA/BCS1)(dlpvB/CS1)(dlgmC/S1)	75.27
20	(dlA/BCS1)(dlpvB/CS1)(dllmC/S1)	75.27
21	(dlA/BCS1)(dlpvB/CS1)(dlpvC/S1)	75.27
22	(dlA/BCS2)(dllmB/CS2)(dlgmC/S2)	75.35
23	(dlA/BCS2)(dllmB/CS2)(dllmC/S2)	75.35
24	(dlA/BCS2)(dllmB/CS2)(dlpvC/S2)	75.35
25	(dlA/BCS2)(dlpvB/CS2)(dlgmC/S2)	75.35
26	(dlA/BCS2)(dlpvB/CS2)(dllmC/S2)	75.35
27	(dlA/BCS2)(dlpvB/CS2)(dlpvC/S2)	75.35
28	(dlA/BCS1)(dlB/CS1)(dlgmC/S1)	75.67
29	(dlA/BCS1)(dlB/CS1)(dllmC/S1)	75.67
30	(dlA/BCS1)(dlB/CS1)(dlpvC/S1)	75.67
31	(dlA/BCS2)(dlB/CS2)(dlgmC/S2)	75.75
32	(dlA/BCS2)(dlB/CS2)(dllmC/S2)	75.75
33	(dlA/BCS2)(dlB/CS2)(dlpvC/S2)	75.75
34	(dlA/BCS1)(dllmB/CS1)(dlC/S1)	76.29

35	(dlA/BCS1)(dlpvB/CS1)(dlC/S1)	76.29
36	(dlA/BCS2)(dllmB/CS2)(dlC/S2)	76.43
37	(dlA/BCS2)(dlpvB/CS2)(dlC/S2)	76.43
38	(dlA/BCS1)(dlB/CS1)(dlC/S1)	76.69
39	(dlA/BCS2)(dlB/CS2)(dlC/S2)	76.82
40	(dlA/BCS1)(dlBC/S1)(pvB/C)	76.84
41	(dlA/BCS2)(dlBC/S2)(pvB/C)	76.98
42	(dlA/BCS1)(dlBC/S1)(dlpvB/C)	77.29
43	(dlA/BCS1)(dlBC/S1)(dladB/C)	77.29
44	(dlA/BCS2)(dlBC/S2)(dlpvB/C)	77.42
45	(dlA/BCS2)(dlBC/S2)(dladB/C)	77.42
46	(dlA/BCS1)(dlBC/S1)(dlB/C)	77.68
47	(dlA/BCS2)(dlBC/S2)(dlB/C)	77.82
48	(dlA/BCS1)(dlBC/S1)(adB/C)	79.31
49	(dlA/BCS2)(dlBC/S2)(adB/C)	79.44
50	(dlA/BCS2)(dllmB/CS2)(lmC/S2)	81.65
51	(dlA/BCS2)(dlpvB/CS2)(lmC/S2)	81.65
52	(dlA/BCS2)(dlB/CS2)(lmC/S2)	82.05
53	(dlA/BCS1)(dllmB/CS1)(lmC/S1)	82.90
54	(dlA/BCS1)(dlpvB/CS1)(lmC/S1)	82.90
55	(dlA/BCS1)(dlB/CS1)(lmC/S1)	83.30
56	(dlA/BCS2)(dllmB/CS2)(pvC/S2)	84.12
57	(dlA/BCS2)(dlpvB/CS2)(pvC/S2)	84.12
58	(dlA/BCS2)(dlB/CS2)(pvC/S2)	84.51
59	(dlA/BCS1)(dllmB/CS1)(pvC/S1)	85.37
60	(dlA/BCS1)(dlpvB/CS1)(pvC/S1)	85.37
61	(dlA/BCS1)(dlB/CS1)(pvC/S1)	85.76
62	(dlA/BCS1)(dllmB/CS1)(gmC/S1)	111.95
63	(dlA/BCS1)(dlpvB/CS1)(gmC/S1)	111.95
64	(dlA/BCS1)(dlB/CS1)(gmC/S1)	112.35
65	(dlA/BCS2)(dllmB/CS2)(gmC/S2)	121.10
66	(dlA/BCS2)(dlpvB/CS2)(gmC/S2)	121.10
67	(dlA/BCS2)(dlB/CS2)(gmC/S2)	121.49
68	(IIS3A/S3ABC)(dllmS3/A)(dlS3A/BC)(pvB/C)	202.35
69	(IIS3A/S3ABC)(dlgmS3/A)(dlS3A/BC)(pvB/C)	202.35
70	(IIS3A/S3ABC)(dlpvS3/A)(dlS3A/BC)(pvB/C)	202.35
71	(IIS3A/S3ABC)(dladS3/A)(dlS3A/BC)(pvB/C)	202.35
72	(IIS3A/S3ABC)(dllmS3/A)(dlS3A/BC)(dlpvB/C)	202.80
73	(IIS3A/S3ABC)(dllmS3/A)(dlS3A/BC)(dladB/C)	202.80
74	(IIS3A/S3ABC)(dlgmS3/A)(dlS3A/BC)(dlpvB/C)	202.80
75	(IIS3A/S3ABC)(dlgmS3/A)(dlS3A/BC)(dladB/C)	202.80

76	(IIS3A/S3ABC)(dlpvS3/A)(dlS3A/BC)(dlpvB/C)	202.80
77	(IIS3A/S3ABC)(dlpvS3/A)(dlS3A/BC)(dladB/C)	202.80
78	(IIS3A/S3ABC)(dladS3/A)(dlS3A/BC)(dlpvB/C)	202.80
79	(IIS3A/S3ABC)(dladS3/A)(dlS3A/BC)(dladB/C)	202.80
80	(IIS3A/S3ABC)(lmS3/A)(dlS3A/BC)(pvB/C)	203.05
81	(IIS3A/S3ABC)(dllmS3/A)(dlS3A/BC)(dlB/C)	203.19
82	(IIS3A/S3ABC)(dlgmS3/A)(dlS3A/BC)(dlB/C)	203.19
83	(IIS3A/S3ABC)(dlpvS3/A)(dlS3A/BC)(dlB/C)	203.19
84	(IIS3A/S3ABC)(dladS3/A)(dlS3A/BC)(dlB/C)	203.19
85	(IIS3A/S3ABC)(dlS3/A)(dlS3A/BC)(pvB/C)	203.41
86	(IIS3A/S3ABC)(lmS3/A)(dlS3A/BC)(dlpvB/C)	203.50
87	(IIS3A/S3ABC)(lmS3/A)(dlS3A/BC)(dladB/C)	203.50
88	(IIS3A/S3ABC)(dlS3/A)(dlS3A/BC)(dlpvB/C)	203.85
89	(IIS3A/S3ABC)(dlS3/A)(dlS3A/BC)(dladB/C)	203.85
90	(IIS3A/S3ABC)(lmS3/A)(dlS3A/BC)(dlB/C)	203.89
91	(IIS3A/S3ABC)(dlS3/A)(dlS3A/BC)(dlB/C)	204.25
92	(IIS3A/S3ABC)(dllmS3/A)(dlS3A/BC)(adB/C)	204.82
93	(IIS3A/S3ABC)(dlgmS3/A)(dlS3A/BC)(adB/C)	204.82
94	(IIS3A/S3ABC)(dlpvS3/A)(dlS3A/BC)(adB/C)	204.82
95	(IIS3A/S3ABC)(dladS3/A)(dlS3A/BC)(adB/C)	204.82
96	(IIS3A/S3ABC)(lmS3/A)(dlS3A/BC)(adB/C)	205.52
97	(IIS3A/S3ABC)(dlS3/A)(dlS3A/BC)(adB/C)	205.87
98	(IIS3A/S3ABC)(pvS3/A)(dlS3A/BC)(pvB/C)	239.99
99	(IIS3A/S3ABC)(gmS3/A)(dlS3A/BC)(pvB/C)	240.40
100	(IIS3A/S3ABC)(adS3/A)(dlS3A/BC)(pvB/C)	240.40
101	(IIS3A/S3ABC)(pvS3/A)(dlS3A/BC)(dlpvB/C)	240.43
102	(IIS3A/S3ABC)(pvS3/A)(dlS3A/BC)(dladB/C)	240.43
103	(IIS3A/S3ABC)(pvS3/A)(dlS3A/BC)(dlB/C)	240.83
104	(IIS3A/S3ABC)(gmS3/A)(dlS3A/BC)(dlpvB/C)	240.85
105	(IIS3A/S3ABC)(gmS3/A)(dlS3A/BC)(dladB/C)	240.85
106	(IIS3A/S3ABC)(adS3/A)(dlS3A/BC)(dlpvB/C)	240.85
107	(IIS3A/S3ABC)(adS3/A)(dlS3A/BC)(dladB/C)	240.85
108	(IIS3A/S3ABC)(gmS3/A)(dlS3A/BC)(dlB/C)	241.25
109	(IIS3A/S3ABC)(adS3/A)(dlS3A/BC)(dlB/C)	241.25
110	(IIS3A/S3ABC)(pvS3/A)(dlS3A/BC)(adB/C)	242.45
111	(IIS3A/S3ABC)(gmS3/A)(dlS3A/BC)(adB/C)	242.87
112	(IIS3A/S3ABC)(adS3/A)(dlS3A/BC)(adB/C)	242.87

9.2 DMC Production

Table A2.2. Pure component properties in the DMC synthesis problem (reaction pathway 1).

Property	Methanol (A)	DMC (B)	Propylene glycol (C)	Propylene carbonate (D)	Aniline(S)
Boiling point (K)	337.85	363.40	460.75	514.85	457.15
Radius of gyration (Å)	1.55	3.25	3.15	3.41	3.44
Melting point (K)	175.47	273.15	213.15	223.95	267.13
Molar volume (m^3/Kmol)	0.04	0.08	0.07	0.09	0.09
Solubility parameter $(Mpa)^{0.5}$	29.59	20.24	29.52	26.26	24.12
Van der Walls volume (m^3/kmol)	0.02	0.05	0.05	0.05	0.06
Vapor pressure (KPa), 30 °C	20.87	1.92	0.03	0.01	0.10
Critical temperature (K)	512.64	548	626	778	699.00
Triple point pressure (Pa)	1.10E-6	0.018	9.17E-10	1.17E-08	0.00
Triple point temperature (K)	175.47	273.15	213.15	223.95	267.13
Kinetic diameter (Å)	3.8	-	-	-	5.79
Polarizability ($Å^3$)	3.21	7.56	7.55	8.55	12.16
Dipole moment (Debye)	1.7	0.9	3.63	4.55	1.53
Molecular weight (g/mol)	32	90	76.1	102.09	93.13

Table A2.3. Pure component properties in the DMC synthesis problem (reaction pathway 2).

Property	Methanol (A)	DMC (B)	Ethylene glycol (C)	Ethylene carbonate (D)	Aniline(S)
Boiling point (K)	337.85	363.40	470.45	511.15	457.15
Radius of gyration (Å)	1.55	3.25	2.56	2.87	3.44
Melting point (K)	175.47	273.15	260.15	309.55	267.13
Molar volume (m^3/Kmol)	0.04	0.08	0.06	0.07	0.09
Solubility parameter $(Mpa)^{0.5}$	29.59	20.24	33.70	30.04	24.12
Van der Walls volume (m^3/kmol)	0.02	0.05	0.04	0.04	0.06
Vapor pressure (KPa), 30 °C	20.87	1.92	0.02	0.004	0.10
Critical temperature (K)	512.64	548	719.7	790	699.00

Triple point pressure (Pa)	1.10E-6	0.018	2.45E-6	6.59E-5	0.00
Triple point temperature (K)	175.47	273.15	260.15	309.55	267.13
Kinetic diameter (Å)	3.8	-	-	-	5.79
Polarizability ($Å^3$)	3.21	7.56	5.71	6.6	12.16
Dipole moment (Debye)	1.7	0.9	2.31	4.51	1.53
Molecular weight (g/mol)	32	90	62	88	93.13

Table A2.4. Pure component properties in the DMC synthesis problem (reaction pathway 3).

Property	Methanol (A)	DMC (B)	Water (C)
Boiling point (K)	337.85	363.40	373.15
Radius of gyration (Å)	1.55	3.25	0.62
Melting point (K)	175.47	273.15	273.15
Molar volume (m^3/Kmol)	0.04	0.08	0.02
Solubility parameter $(Mpa)^{0.5}$	29.59	20.24	47.81
Van der Walls volume (m^3/kmol)	0.02	0.05	0.01
Vapor pressure (KPa), 30 °C	20.87	1.92	4.24
Critical temperature (K)	512.64	548	647.13
Triple point pressure (Pa)	1.10E-6	0.018	0.01
Triple point temperature (K)	175.47	273.15	273.16
Kinetic diameter (Å)	3.8	-	2.65
Polarizability ($Å^3$)	3.21	7.56	1.50
Dipole moment (Debye)	1.7	0.9	1.85
Molecular weight (g/mol)	32	90	18.02

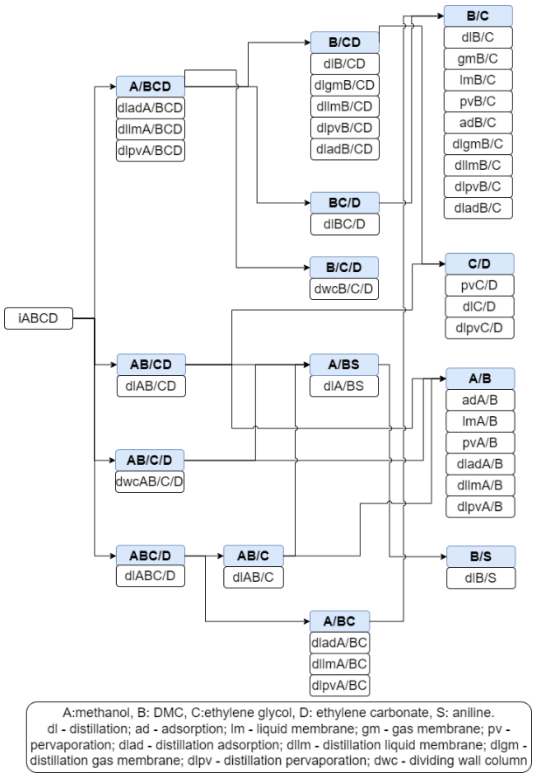

Figure A2.1. Separation superstructure for reaction pathway 2.

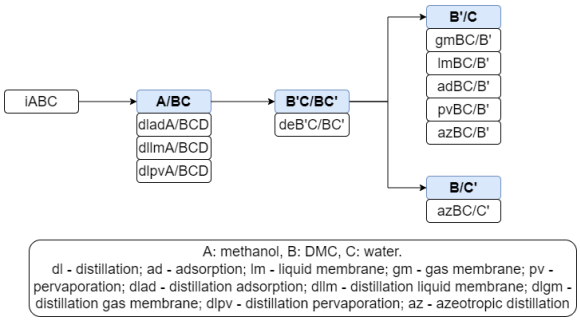

Figure A2.2. Separation superstructure for reaction pathway 3.

Table A2.5. Generated process alternatives for reaction pathway 1.

No.	Process alternatives	Process energy index, GJ
1	(dladA/BCD)(dladB/CD)(dladC/D)	6.78
2	(dladA/BCD)(dladB/CD)(dlpvC/D)	6.78
3	(dladA/BCD)(dlpvB/CD)(dladC/D)	6.78
4	(dladA/BCD)(dlpvB/CD)(dlpvC/D)	6.78
5	(dllmA/BCD)(dladB/CD)(dladC/D)	6.78

6	(dllmA/BCD)(dladB/CD)(dlpvC/D)	6.78
7	(dllmA/BCD)(dlpvB/CD)(dladC/D)	6.78
8	(dllmA/BCD)(dlpvB/CD)(dlpvC/D)	6.78
9	(dlpvA/BCD)(dladB/CD)(dladC/D)	6.78
10	(dlpvA/BCD)(dladB/CD)(dlpvC/D)	6.78
11	(dlpvA/BCD)(dlpvB/CD)(dladC/D)	6.78
12	(dlpvA/BCD)(dlpvB/CD)(dlpvC/D)	6.78
13	(dladA/BCD)(dladB/CD)(pvC/D)	6.92
14	(dladA/BCD)(dlpvB/CD)(pvC/D)	6.92
15	(dllmA/BCD)(dladB/CD)(pvC/D)	6.92
16	(dllmA/BCD)(dlpvB/CD)(pvC/D)	6.92
17	(dlpvA/BCD)(dladB/CD)(pvC/D)	6.92
18	(dlpvA/BCD)(dlpvB/CD)(pvC/D)	6.92
19	(dladA/BCD)(dladB/CD)(adC/D)	7.81
20	(dladA/BCD)(dlpvB/CD)(adC/D)	7.81
21	(dllmA/BCD)(dladB/CD)(adC/D)	7.81
22	(dllmA/BCD)(dlpvB/CD)(adC/D)	7.81
23	(dlpvA/BCD)(dladB/CD)(adC/D)	7.81
24	(dlpvA/BCD)(dlpvB/CD)(adC/D)	7.81
25	(dladA/BCD)(dlB/CD)(dladC/D)	7.87
26	(dladA/BCD)(dlB/CD)(dlpvC/D)	7.87
27	(dllmA/BCD)(dlB/CD)(dladC/D)	7.87
28	(dllmA/BCD)(dlB/CD)(dlpvC/D)	7.87
29	(dlpvA/BCD)(dlB/CD)(dladC/D)	7.87
30	(dlpvA/BCD)(dlB/CD)(dlpvC/D)	7.87
31	(dladA/BCD)(dlB/CD)(pvC/D)	8.01
32	(dllmA/BCD)(dlB/CD)(pvC/D)	8.01
33	(dlpvA/BCD)(dlB/CD)(pvC/D)	8.01
34	(dladA/BCD)(dladB/CD)(dlC/D)	8.44
35	(dladA/BCD)(dlpvB/CD)(dlC/D)	8.44
36	(dllmA/BCD)(dladB/CD)(dlC/D)	8.44
37	(dllmA/BCD)(dlpvB/CD)(dlC/D)	8.44
38	(dlpvA/BCD)(dladB/CD)(dlC/D)	8.44
39	(dlpvA/BCD)(dlpvB/CD)(dlC/D)	8.44
40	(dladA/BCD)(dlB/CD)(adC/D)	8.90
41	(dllmA/BCD)(dlB/CD)(adC/D)	8.90
42	(dlpvA/BCD)(dlB/CD)(adC/D)	8.90
43	(dladA/BCD)(dlB/CD)(dlC/D)	9.52
44	(dllmA/BCD)(dlB/CD)(dlC/D)	9.52
45	(dlpvA/BCD)(dlB/CD)(dlC/D)	9.52
46	(dladA/BCD)(dlBC/D)(dlB/C)	9.52

47	(dladA/BCD)(dlBC/D)(pvB/C)	9.52
48	(dladA/BCD)(dlBC/D)(adB/C)	9.52
49	(dladA/BCD)(dwcB/C/D)	9.52
50	(dllmA/BCD)(dwcB/C/D)	9.52
51	(dlpvA/BCD)(dwcB/C/D)	9.52
52	(dlAB/CD)(lmA/B)(dladC/D)	9.78
53	(dlAB/CD)(lmA/B)(dlpvC/D)	9.78
54	(dlAB/CD)(dllmA/B)(pvC/D)	9.83
55	(dlAB/CD)(dlpvA/B)(adC/D)	9.83
56	(dlAB/CD)(dlpvA/B)(pvC/D)	9.83
57	(dlAB/CD)(dlpvA/B)(dlC/D)	9.83
58	(dlAB/CD)(lmA/B)(pvC/D)	9.92
59	(dlAB/CD)(lmA/B)(adC/D)	10.81
60	(dlAB/CD)(adA/B)(dladC/D)	10.87
61	(dladA/BCD)(dlBC/D)(dlpvB/C)	11.16
62	(dllmA/BCD)(dlBC/D)(dlpvB/C)	11.16
63	(dlpvA/BCD)(dlBC/D)(dlpvB/C)	11.16
64	(dladA/BCD)(dlBC/D)(dladB/C)	11.16
65	(dllmA/BCD)(dlBC/D)(dladB/C)	11.16
66	(dlpvA/BCD)(dlBC/D)(dladB/C)	11.16
67	(dlAB/CD)(lmA/B)(dlC/D)	11.44
68	(dwcAB/C/D)(lmA/B)	11.44
69	(dlAB/CD)(dlA/BS)(dlB/S)(dlpvC/D)	11.61
70	(dlAB/CD)(pvA/B)(dladC/D)	11.77
71	(dlAB/CD)(pvA/B)(dlpvC/D)	11.77
72	(dlAB/CD)(pvA/B)(pvC/D)	11.91
73	(dllmA/BCD)(dlBC/D)(pvB/C)	11.91
74	(dlpvA/BCD)(dlBC/D)(pvB/C)	11.91
75	(dllmA/BCD)(dlBC/D)(dlB/C)	12.24
76	(dlpvA/BCD)(dlBC/D)(dlB/C)	12.24
77	(dlAB/CD)(dladA/B)(dladC/D)	12.31
78	(dlAB/CD)(dladA/B)(dlpvC/D)	12.31
79	(dlAB/CD)(dllmA/B)(dladC/D)	12.31
80	(dlAB/CD)(dllmA/B)(dlpvC/D)	12.31
81	(dlAB/CD)(dlpvA/B)(dladC/D)	12.31
82	(dlAB/CD)(dlpvA/B)(dlpvC/D)	12.31
83	(dlAB/CD)(dladA/B)(pvC/D)	12.45
84	(dlAB/CD)(pvA/B)(adC/D)	12.80
85	(dlAB/CD)(dladA/B)(adC/D)	13.35
86	(dlAB/CD)(dllmA/B)(adC/D)	13.35
87	(dlAB/CD)(adA/B)(dlpvC/D)	13.35

88	(dlAB/CD)(pvA/B)(dlC/D)	13.43
89	(dwcAB/C/D)(pvA/B)	13.43
90	(dlAB/CD)(adA/B)(pvC/D)	13.49
91	(dlAB/CD)(dladA/B)(dlC/D)	13.97
92	(dlAB/CD)(dllmA/B)(dlC/D)	13.97
93	(dwcAB/C/D)(dladA/B)	13.97
94	(dwcAB/C/D)(dllmA/B)	13.97
95	(dwcAB/C/D)(dlpvA/B)	13.97
96	(dllmA/BCD)(dlBC/D)(adB/C)	14.35
97	(dlpvA/BCD)(dlBC/D)(adB/C)	14.35
98	(dlAB/CD)(adA/B)(adC/D)	14.38
99	(dlAB/CD)(dlA/BS)(dlB/S)(adC/D)	14.43
100	(dlAB/CD)(dlA/BS)(dlB/S)(pvC/D)	14.43
101	(dlAB/CD)(dlA/BS)(dlB/S)(dlC/D)	14.43
102	(dlAB/CD)(dlA/BS)(dlB/S)(dladC/D)	14.43
103	(dlAB/CD)(adA/B)(dlC/D)	15.00
104	(dwcAB/C/D)(adA/B)	15.00
105	(dlABC/D)(dladA/BC)(dlpvB/C)	17.23
106	(dlABC/D)(dlpvA/BC)(dlpvB/C)	17.23
107	(dlABC/D)(dllmA/BC)(dlpvB/C)	17.23
108	(dlABC/D)(dladA/BC)(dladB/C)	17.23
109	(dlABC/D)(dlpvA/BC)(dladB/C)	17.23
110	(dlABC/D)(dllmA/BC)(dladB/C)	17.23
111	(dlABC/D)(dladA/BC)(pvB/C)	17.99
112	(dlABC/D)(dlpvA/BC)(pvB/C)	17.99
113	(dlABC/D)(dllmA/BC)(pvB/C)	17.99
114	(dlABC/D)(dladA/BC)(dlB/C)	18.32
115	(dlABC/D)(dlpvA/BC)(dlB/C)	18.32
116	(dlABC/D)(dllmA/BC)(dlB/C)	18.32
117	(dwcAB/C/D)(dlA/BS)(dlB/S)	18.57
118	(dlABC/D)(dlAB/C)(lmA/B)	18.60
119	(dlABC/D)(dladA/BC)(adB/C)	20.43
120	(dlABC/D)(dlpvA/BC)(adB/C)	20.43
121	(dlABC/D)(dllmA/BC)(adB/C)	20.43
122	(dlABC/D)(dlAB/C)(pvA/B)	20.59
123	(dlABC/D)(dlAB/C)(dladA/B)	21.13
124	(dlABC/D)(dlAB/C)(dllmA/B)	21.13
125	(dlABC/D)(dlAB/C)(dlpvA/B)	21.13
126	(dlABC/D)(dlAB/C)(adA/B)	22.17
127	(dlABC/D)(dlAB/C)(dlA/BS)(dlB/S)	22.91

Table A2.6. Generated process alternatives for reaction pathway 2.

1	(dladA/BCD)(dladB/CD)(pvC/D)	6.81
2	(dllmA/BCD)(dladB/CD)(pvC/D)	6.81
3	(dlpvA/BCD)(dladB/CD)(pvC/D)	6.81
4	(dladA/BCD)(dlgmB/CD)(pvC/D)	6.81
5	(dllmA/BCD)(dlgmB/CD)(pvC/D)	6.81
6	(dlpvA/BCD)(dlgmB/CD)(pvC/D)	6.81
7	(dladA/BCD)(dllmB/CD)(pvC/D)	6.81
8	(dllmA/BCD)(dllmB/CD)(pvC/D)	6.81
9	(dlpvA/BCD)(dllmB/CD)(pvC/D)	6.81
10	(dladA/BCD)(dlpvB/CD)(pvC/D)	6.81
11	(dllmA/BCD)(dlpvB/CD)(pvC/D)	6.81
12	(dlpvA/BCD)(dlpvB/CD)(pvC/D)	6.81
13	(dladA/BCD)(dladB/CD)(dlpvC/D)	6.84
14	(dllmA/BCD)(dladB/CD)(dlpvC/D)	6.84
15	(dlpvA/BCD)(dladB/CD)(dlpvC/D)	6.84
16	(dladA/BCD)(dlgmB/CD)(dlpvC/D)	6.84
17	(dllmA/BCD)(dlgmB/CD)(dlpvC/D)	6.84
18	(dlpvA/BCD)(dlgmB/CD)(dlpvC/D)	6.84
19	(dladA/BCD)(dllmB/CD)(dlpvC/D)	6.84
20	(dllmA/BCD)(dllmB/CD)(dlpvC/D)	6.84
21	(dlpvA/BCD)(dllmB/CD)(dlpvC/D)	6.84
22	(dladA/BCD)(dlpvB/CD)(dlpvC/D)	6.84
23	(dllmA/BCD)(dlpvB/CD)(dlpvC/D)	6.84
24	(dlpvA/BCD)(dlpvB/CD)(dlpvC/D)	6.84
25	(dladA/BCD)(dlB/CD)(pvC/D)	7.79
26	(dllmA/BCD)(dlB/CD)(pvC/D)	7.79
27	(dlpvA/BCD)(dlB/CD)(pvC/D)	7.79
28	(dladA/BCD)(dlB/CD)(dlpvC/D)	7.83
29	(dllmA/BCD)(dlB/CD)(dlpvC/D)	7.83
30	(dlpvA/BCD)(dlB/CD)(dlpvC/D)	7.83
31	(dladA/BCD)(dladB/CD)(dlC/D)	8.64
32	(dllmA/BCD)(dladB/CD)(dlC/D)	8.64
33	(dlpvA/BCD)(dladB/CD)(dlC/D)	8.64
34	(dladA/BCD)(dlgmB/CD)(dlC/D)	8.64
35	(dllmA/BCD)(dlgmB/CD)(dlC/D)	8.64
36	(dlpvA/BCD)(dlgmB/CD)(dlC/D)	8.64
37	(dladA/BCD)(dllmB/CD)(dlC/D)	8.64
38	(dllmA/BCD)(dllmB/CD)(dlC/D)	8.64
39	(dlpvA/BCD)(dllmB/CD)(dlC/D)	8.64

40	(dladA/BCD)(dlpvB/CD)(dlC/D)	8.64
41	(dllmA/BCD)(dlpvB/CD)(dlC/D)	8.64
42	(dlpvA/BCD)(dlpvB/CD)(dlC/D)	8.64
43	(dladA/BCD)(dlB/CD)(dlC/D)	9.63
44	(dllmA/BCD)(dlB/CD)(dlC/D)	9.63
45	(dlpvA/BCD)(dlB/CD)(dlC/D)	9.63
46	(dladA/BCD)(dwcB/C/D)	9.63
47	(dllmA/BCD)(dwcB/C/D)	9.63
48	(dlpvA/BCD)(dwcB/C/D)	9.63
49	(dlAB/CD)(lmA/B)(pvC/D)	9.71
50	(dlAB/CD)(lmA/B)(dlpvC/D)	9.74
51	(dladA/BCD)(dlBC/D)(lmB/C)	10.53
52	(dllmA/BCD)(dlBC/D)(lmB/C)	10.53
53	(dlpvA/BCD)(dlBC/D)(lmB/C)	10.53
54	(dladA/BCD)(dlBC/D)(dladB/C)	11.11
55	(dllmA/BCD)(dlBC/D)(dladB/C)	11.11
56	(dlpvA/BCD)(dlBC/D)(dladB/C)	11.11
57	(dladA/BCD)(dlBC/D)(dlgmB/C)	11.11
58	(dllmA/BCD)(dlBC/D)(dlgmB/C)	11.11
59	(dlpvA/BCD)(dlBC/D)(dlgmB/C)	11.11
60	(dladA/BCD)(dlBC/D)(dllmB/C)	11.11
61	(dllmA/BCD)(dlBC/D)(dllmB/C)	11.11
62	(dlpvA/BCD)(dlBC/D)(dllmB/C)	11.11
63	(dladA/BCD)(dlBC/D)(dlpvB/C)	11.11
64	(dllmA/BCD)(dlBC/D)(dlpvB/C)	11.11
65	(dlpvA/BCD)(dlBC/D)(dlpvB/C)	11.11
66	(dlAB/CD)(lmA/B)(dlC/D)	11.54
67	(dwcAB/C/D)(lmA/B)	11.54
68	(dlAB/CD)(pvA/B)(pvC/D)	11.70
69	(dlAB/CD)(pvA/B)(dlpvC/D)	11.73
70	(dladA/BCD)(dlBC/D)(dlB/C)	12.10
71	(dllmA/BCD)(dlBC/D)(dlB/C)	12.10
72	(dlpvA/BCD)(dlBC/D)(dlB/C)	12.10
73	(dladA/BCD)(dlBC/D)(pvB/C)	12.10
74	(dllmA/BCD)(dlBC/D)(pvB/C)	12.10
75	(dlpvA/BCD)(dlBC/D)(pvB/C)	12.10
76	(dlAB/CD)(dladA/B)(pvC/D)	12.24
77	(dlAB/CD)(dllmA/B)(pvC/D)	12.24
78	(dlAB/CD)(dlpvA/B)(pvC/D)	12.24
79	(dlAB/CD)(dladA/B)(dlpvC/D)	12.28
80	(dlAB/CD)(dllmA/B)(dlpvC/D)	12.28

81	(dlAB/CD)(dlpvA/B)(dlpvC/D)	12.28
82	(dlAB/CD)(adA/B)(pvC/D)	13.28
83	(dlAB/CD)(adA/B)(dlpvC/D)	13.31
84	(dlAB/CD)(pvA/B)(dlC/D)	13.53
85	(dwcAB/C/D)(pvA/B)	13.53
86	(dlAB/CD)(dladA/B)(dlC/D)	14.07
87	(dlAB/CD)(dllmA/B)(dlC/D)	14.07
88	(dlAB/CD)(dlpvA/B)(dlC/D)	14.07
89	(dwcAB/C/D)(dladA/B)	14.07
90	(dwcAB/C/D)(dllmA/B)	14.07
91	(dwcAB/C/D)(dlpvA/B)	14.07
92	(dladA/BCD)(dlBC/D)(adB/C)	14.61
93	(dllmA/BCD)(dlBC/D)(adB/C)	14.61
94	(dlpvA/BCD)(dlBC/D)(adB/C)	14.61
95	(dladA/BCD)(dlBC/D)(gmB/C)	14.61
96	(dllmA/BCD)(dlBC/D)(gmB/C)	14.61
97	(dlpvA/BCD)(dlBC/D)(gmB/C)	14.61
98	(dwcAB/C/D)(adA/B)	15.11
99	(dlAB/CD)(adA/B)(dlC/D)	15.11
100	(dlABC/D)(dladA/BC)(lmB/C)	16.45
101	(dlABC/D)(dllmA/BC)(lmB/C)	16.45
102	(dlABC/D)(dlpvA/BC)(lmB/C)	16.45
103	(dlAB/CD)(dlA/BS)(dlB/S)(pvC/D)	16.84
104	(dlAB/CD)(dlA/BS)(dlB/S)(dlpvC/D)	16.88
105	(dlABC/D)(dladA/BC)(dladB/C)	17.04
106	(dlABC/D)(dllmA/BC)(dladB/C)	17.04
107	(dlABC/D)(dlpvA/BC)(dladB/C)	17.04
108	(dlABC/D)(dladA/BC)(dlgmB/C)	17.04
109	(dlABC/D)(dllmA/BC)(dlgmB/C)	17.04
110	(dlABC/D)(dlpvA/BC)(dlgmB/C)	17.04
111	(dlABC/D)(dladA/BC)(dllmB/C)	17.04
112	(dlABC/D)(dllmA/BC)(dllmB/C)	17.04
113	(dlABC/D)(dlpvA/BC)(dllmB/C)	17.04
114	(dlABC/D)(dladA/BC)(dlpvB/C)	17.04
115	(dlABC/D)(dllmA/BC)(dlpvB/C)	17.04
116	(dlABC/D)(dlpvA/BC)(dlpvB/C)	17.04
117	(dlABC/D)(dladA/BC)(dlB/C)	18.03
118	(dlABC/D)(dllmA/BC)(dlB/C)	18.03
119	(dlABC/D)(dlpvA/BC)(dlB/C)	18.03
120	(dlABC/D)(dladA/BC)(pvB/C)	18.03
121	(dlABC/D)(dllmA/BC)(pvB/C)	18.03

122	(dlABC/D)(dlpvA/BC)(pvB/C)	18.03
123	(dlABC/D)(dlAB/C)(lmA/B)	18.46
124	(dlAB/CD)(dlA/BS)(dlB/S)(dlC/D)	18.67
125	(dwcAB/C/D)(dlA/BS)(dlB/S)	18.67
126	(dlABC/D)(adA/BC)(lmB/C)	20.12
127	(dlABC/D)(dlAB/C)(pvA/B)	20.45
128	(dlABC/D)(dladA/BC)(adB/C)	20.54
129	(dlABC/D)(dllmA/BC)(adB/C)	20.54
130	(dlABC/D)(dlpvA/BC)(adB/C)	20.54
131	(dlABC/D)(dladA/BC)(gmB/C)	20.54
132	(dlABC/D)(dllmA/BC)(gmB/C)	20.54
133	(dlABC/D)(dlpvA/BC)(gmB/C)	20.54
134	(dlABC/D)(adA/BC)(dladB/C)	20.71
135	(dlABC/D)(adA/BC)(dlgmB/C)	20.71
136	(dlABC/D)(adA/BC)(dllmB/C)	20.71
137	(dlABC/D)(adA/BC)(dlpvB/C)	20.71
138	(dlABC/D)(dlAB/C)(dladA/B)	20.99
139	(dlABC/D)(dlAB/C)(dllmA/B)	20.99
140	(dlABC/D)(dlAB/C)(dlpvA/B)	20.99
141	(dlABC/D)(adA/BC)(dlB/C)	21.70
142	(dlABC/D)(adA/BC)(pvB/C)	21.70
143	(dlABC/D)(dlAB/C)(adA/B)	22.02
144	(dlABC/D)(adA/BC)(adB/C)	24.21
145	(dlABC/D)(adA/BC)(gmB/C)	24.21
146	(dlABC/D)(dlAB/C)(dlA/BS)(dlB/S)	25.59

Table A2.7. Generated process alternatives for reaction pathway 3.

No.	Process alternatives	Process energy index, GJ
1	(dllmA/BC)(deB'C/BC')(lmBC/B')(azBC/C')	3.42
2	(dladA/BC)(deB'C/BC')(lmBC/B')(azBC/C')	3.42
3	(dlpvA/BC)(deB'C/BC')(lmBC/B')(azBC/C')	3.42
4	(dllmA/BC)(deB'C/BC')(pvBC/B')(azBC/C')	3.77
5	(dladA/BC)(deB'C/BC')(pvBC/B')(azBC/C')	3.77
6	(dlpvA/BC)(deB'C/BC')(pvBC/B')(azBC/C')	3.77
7	(dllmA/BC)(deB'C/BC')(gmBC/B')(azBC/C')	5.31
8	(dllmA/BC)(deB'C/BC')(adBC/B')(azBC/C')	5.31
9	(dladA/BC)(deB'C/BC')(gmBC/B')(azBC/C')	5.31
10	(dladA/BC)(deB'C/BC')(adBC/B')(azBC/C')	5.31
11	(dlpvA/BC)(deB'C/BC')(gmBC/B')(azBC/C')	5.31
12	(dlpvA/BC)(deB'C/BC')(adBC/B')(azBC/C')	5.31

13	(dllmA/BC)(deB'C/BC')(azBC/B')(azBC/C')	29.83
14	(dladA/BC)(deB'C/BC')(azBC/B')(azBC/C')	29.83
15	(dlpvA/BC)(deB'C/BC')(azBC/B')(azBC/C')	29.83

9.3 Isobutylene Utilization

Table A2.8. Pure component properties in the isobutylene utilization problem (reaction pathway 1).

Property	Isobutylene (A)	Water (B)	Pivalic acid (C)
Boiling point (K)	266.25	373.15	436.95
Radius of gyration (Å)	2.88	0.62	3.35
Melting point (K)	132.81	273.15	309.08
Molar volume (m^3/Kmol)	0.10	0.02	0.11
Solubility parameter $(Mpa)^{0.5}$	13.66	47.81	22.94
Van der Walls volume (m^3/kmol)	0.04	0.01	0.06
Vapor pressure (KPa), 30 °C	352.59	4.24	0.14
Critical temperature (K)	417.90	647.13	632.00
Triple point pressure (Pa)	0.00	0.01	0.00
Triple point temperature (K)	132.81	273.16	309.08
Kinetic diameter (Å)	4.84	2.65	-
Polarizability ($Å^3$)	8.00	1.50	10.95
Dipole moment (Debye)	0.50	1.85	1.70
Molecular weight (g/mol)	56.11	18.02	102.13

Table A2.9. Pure component properties in the isobutylene utilization problem (reaction pathway 2).

Property	Formaldehyde (A)	Isobutylene (B)	Prenol (C)
Boiling point (K)	254.05	266.25	413.15
Radius of gyration (Å)	1.22	2.88	-
Melting point (K)	181.15	132.81	213.85
Molar volume (m^3/Kmol)	0.04	0.10	-
Solubility parameter $(Mpa)^{0.5}$	23.82	13.66	-
Van der Walls volume (m^3/kmol)	0.02	0.04	-
Vapor pressure (KPa), 30 °C	609.74	352.59	0.32
Critical temperature (K)	408.00	417.90	-
Triple point pressure (Pa)	0.01	0.00	-
Triple point temperature (K)	181.15	132.81	-
Kinetic diameter (Å)	3.73	4.84	-
Polarizability ($Å^3$)	2.58	8.00	10.38
Dipole moment (Debye)	2.33	0.50	-
Molecular weight (g/mol)	30.03	56.11	86.13

Table A2.10. Pure component properties in the isobutylene utilization problem (reaction pathway 3).

Property	Ammonia (A)	Isobutylene (B)	tert-Butylamine (C)

Boiling point (K)	239.72	266.25	317.55
Radius of gyration (Å)	0.85	2.88	3.05
Melting point (K)	195.41	132.81	206.19
Molar volume (m^3/Kmol)	0.02	0.10	0.11
Solubility parameter $(Mpa)^{0.5}$	29.22	13.66	15.74
Van der Walls volume (m^3/kmol)	0.01	0.04	0.05
Vapor pressure (KPa), 30 °C	1,173.93	352.59	60.21
Critical temperature (K)	405.65	417.90	483.90
Triple point pressure (Pa)	0.06	0.00	0.00
Triple point temperature (K)	195.41	132.81	206.19
Kinetic diameter (Å)	2.60	4.84	-
Polarizability ($Å^3$)	1.99	8.00	9.38
Dipole moment (Debye)	1.47	0.50	1.29
Molecular weight (g/mol)	17.03	56.11	73.14

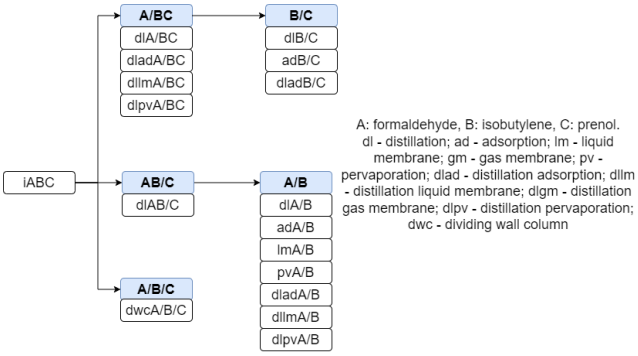

Figure A2.3. Separation superstructure for reaction pathway 2.

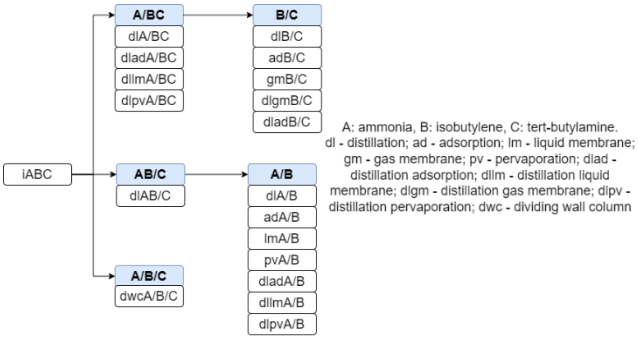

Figure A2.4. Separation superstructure for reaction pathway 3.

Table A2.11. Generated process alternatives for reaction pathway 1.

No.	Process alternatives	Process energy index, GJ
1	(dladA/BC)(lmB/C)	0.99
2	(dlgmA/BC)(lmB/C)	0.99
3	(dlpvA/BC)(lmB/C)	0.99
4	(dladA/BC)(dllmB/C)	1.52
5	(dladA/BC)(dladB/C)	1.52
6	(dladA/BC)(dlpvB/C)	1.52
7	(dlgmA/BC)(dllmB/C)	1.52
8	(dlgmA/BC)(dladB/C)	1.52
9	(dlgmA/BC)(dlpvB/C)	1.52
10	(dlpvA/BC)(dllmB/C)	1.52
11	(dlpvA/BC)(dladB/C)	1.52
12	(dlpvA/BC)(dlpvB/C)	1.52
13	(dlA/BC)(lmB/C)	1.65
14	(dladA/BC)(dlB/C)	1.88
15	(dlgmA/BC)(dlB/C)	1.88
16	(dlpvA/BC)(dlB/C)	1.88
17	(dlA/BC)(dllmB/C)	2.18
18	(dlA/BC)(dladB/C)	2.18
19	(dlA/BC)(dlpvB/C)	2.18
20	(dlA/BC)(dlB/C)	2.54
21	(dwcA/B/C)	2.54
22	(dlAB/C)(lmA/B)	3.65
23	(dlAB/C)(dlgmA/B)	4.64
24	(dlAB/C)(dllmA/B)	4.64
25	(dlAB/C)(dladA/B)	4.64
26	(dlAB/C)(dlpvA/B)	4.64
27	(dlAB/C)(dlA/B)	5.30
28	(dlAB/C)(pvA/B)	6.11
29	(dlAB/C)(gmA/B)	7.34
30	(dlAB/C)(adA/B)	7.34
31	(dladA/BC)(adB/C)	8.89
32	(dladA/BC)(pvB/C)	8.89
33	(dlgmA/BC)(adB/C)	8.89
34	(dlgmA/BC)(pvB/C)	8.89
35	(dlpvA/BC)(adB/C)	8.89
36	(dlpvA/BC)(pvB/C)	8.89
37	(dlA/BC)(adB/C)	9.55
38	(dlA/BC)(pvB/C)	9.55

Table A2.12. Generated process alternatives for reaction pathway 2.

No.	Process alternatives	Process energy index, GJ
1	(dlAB/C)(lmA/B)	1.84
2	(dlAB/C)(pvA/B)	2.91
3	(dlAB/C)(adA/B)	4.13
4	(dladA/BC)(dladB/C)	5.36
5	(dllmA/BC)(dladB/C)	5.36
6	(dlpvA/BC)(dladB/C)	5.36
7	(dladA/BC)(dlB/C)	5.84
8	(dllmA/BC)(dlB/C)	5.84
9	(dlpvA/BC)(dlB/C)	5.84
10	(dlAB/C)(dllmA/B)	6.48
11	(dlAB/C)(dladA/B)	6.48
12	(dlAB/C)(dlpvA/B)	6.48
13	(dlA/BC)(dladB/C)	8.45
14	(dlA/BC)(dlB/C)	8.93
15	(dwcA/B/C)	8.93
16	(dlAB/C)(dlA/B)	9.57
17	(dladA/BC)(adB/C)	14.79
18	(dllmA/BC)(adB/C)	14.79
19	(dlpvA/BC)(adB/C)	14.79
20	(dlA/BC)(adB/C)	17.88

Table A2.13. Generated process alternatives for reaction pathway 3.

No.	Process alternatives	Process energy index, GJ
1	(dladA/BC)(dlgmB/C)	3.27
2	(dladA/BC)(dladB/C)	3.27
3	(dllmA/BC)(dlgmB/C)	3.27
4	(dllmA/BC)(dladB/C)	3.27
5	(dlpvA/BC)(dlgmB/C)	3.27
6	(dlpvA/BC)(dladB/C)	3.27
7	(dlA/BC)(dlgmB/C)	4.08
8	(dlA/BC)(dladB/C)	4.08
9	(dlAB/C)(lmA/B)	4.48
10	(dladA/BC)(gmB/C)	4.61
11	(dladA/BC)(adB/C)	4.61
12	(dllmA/BC)(gmB/C)	4.61
13	(dllmA/BC)(adB/C)	4.61
14	(dlpvA/BC)(gmB/C)	4.61
15	(dlpvA/BC)(adB/C)	4.61
16	(dladA/BC)(dlB/C)	4.65

17	(dllmA/BC)(dlB/C)	4.65
18	(dlpvA/BC)(dlB/C)	4.65
19	(dlA/BC)(gmB/C)	5.42
20	(dlA/BC)(adB/C)	5.42
21	(dlA/BC)(dlB/C)	5.45
22	(dwcA/B/C)	5.45
23	(dlAB/C)(pvA/B)	5.47
24	(dlAB/C)(dllmA/B)	5.69
25	(dlAB/C)(dladA/B)	5.69
26	(dlAB/C)(dlpvA/B)	5.69
27	(dlAB/C)(dlA/B)	6.50
28	(dlAB/C)(adA/B)	6.70

9.4 Cumene Production

Table A2.14. Pure component properties in the cuemene production problem.

Property	Propylene (A)	Propane (B)	Benzene (C)	Cumene (D)	1,4-Diisopropylbenzene (E)
Boiling point (K)	225.46	231.11	353.15	425.56	483.65
Radius of gyration (Å)	2.25	2.43	3.00	4.32	5.18
Melting point (K)	87.89	85.47	278.65	177.14	256.08
Molar volume (m^3/Kmol)	0.19	0.20	0.09	0.43	0.60
Solubility parameter $(Mpa)^{0.5}$	13.15	13.10	18.73	17.44	16.93
Van der Walls volume (m^3/kmol)	0.03	0.04	0.05	0.08	0.10
Vapor pressure (KPa), 30 °C	1308.31	1083.34	15.89	0.82	0.05
Critical temperature (K)	365.57	369.83	562.05	631.10	689.00
Triple point pressure (Pa)	0.00	0.00	4762.28	0.00	0.70
Triple point temperature (K)	87.89	85.47	278.68	177.14	256.08
Kinetic diameter (Å)	4.50	4.30	5.85	6.80	7.10
Polarizability ($Å^3$)	6.36	6.26	10.44	14.82	-
Dipole moment (Debye)	0.40	0.00	0.00	0.65	0.00
Molecular weight (g/mol)	42.08	44.10	78.00	120.19	162.28

9.4 Styrene Production

Table A2.15. Pure component properties in the styrene production problem.

Property	Benzene (A)	Toluene (B)	Ethylbenzene (D)	Styrene (E)
Boiling point (K)	353.15	383.75	409.35	418.31
Radius of gyration (Å)	3.00	3.47	3.90	3.81
Melting point (K)	278.65	178.25	178.20	242.54
Molar volume (m^3/Kmol)	0.09	0.11	0.37	0.35
Solubility parameter $(Mpa)^{0.5}$	18.73	18.32	17.98	19.02
Van der Walls volume (m^3/kmol)	0.05	0.06	0.07	0.07
Vapor pressure (KPa), 30 °C	15.89	4.87	1.69	1.14
Critical temperature (K)	562.05	591.75	617.20	636.00
Triple point pressure (Pa)	4762.28	0.04	0.00	10.60
Triple point temperature (K)	278.68	178.18	178.15	242.54
Kinetic diameter (Å)	5.85	5.85	6.20	6.00
Polarizability ($Å^3$)	10.44	12.40	14.20	14.41
Dipole moment (Debye)	0.00	0.40	0.60	0.13
Molecular weight (g/mol)	78.00	92.00	106.17	104.15